POLITECNICO DI MILANO

Dipartimento di Ingegneria Idraulica, Ambientale,
Infrastrutture viarie, e Rilevamento

WELL-BALANCED SCHEMES FOR SHALLOW WATER EQUATIONS

Supervisor:
Dr. Stefano Mambretti
Co-supervisor:
Dr. Riadh Ata

Author:
Sara Pavan, Matr. 751012

Academic year: 2010-2011

Abstract

Natural hazards related to floodplains and levee failures are phenomena that are increasingly recurring in the world and that concern a large part of the fluvial communities. They can provoke devastating effects on human life and also have strong economical consequences, thus their prediction and mitigation is of great interest to communities.
These kinds of risk can be well modelled with the Saint Venant equations (also called shallow water equations), where the horizontal scales are prevailing to the vertical scale. Numerical models are powerful instruments to solve this system of equations, that is formed by a set of non-linear partial differential equations of hyperbolic type. Such a system presents discontinuities as possible solutions that can be easily captured using a finite volume method. This explains why past efforts have usually focused on the resolution of the homogeneous part of the SWEs, showing relevant results in terms of shock-capturing and so flux calculation. Nevertheless this is not sufficient for the simulation of real case, where the bed elevation is irregular and complex. Indeed to take into account the bed source, a finite volume method needs a good numerical discretization of the source terms. In this way we can obtain a well-balanced scheme, capable of reproducing steady cases such as a lake at rest.
The focus of this work is on the development of appropriate well-balanced schemes, combining good solvers for the flux calculation with a source term discretization as good.
This has been done using four different schemes, with different numerical properties, for which a validation procedure have been accomplished through some well-established benchmarks. Finally, the assessment of the various numerical performance of every scheme is presented.

Abstract

I rischi naturali legati alle inondazioni e alle rotture di argini fluviali sono fenomeni che si verificano sempre più frequentemente in tutto il mondo, a causa dell'aumento di eventi estremi come ad esempio piogge intense e prolungate. Questi fenomeni oltre ad avere un importante impatto di tipo economico possono anche mettere in pericolo la vita umana, per questo la predizione e la mitigazione di tali rischi risulta di grande interesse.
I fenomeni citati possono essere formulati matematicamente attraverso le equazioni di Saint Venant (chiamate anche shallow water equations), in cui le scale orizzontali prevalgono rispetto a quella verticale. I modelli numerici rappresentano uno dei metodi più efficaci per la soluzione di questo sistema, formato da equazioni differenziali parziali, non lineari, di tipo iperbolico. Tra i vari metodi numerici, il metodo dei volumi finiti risulta essere particolarmente adatto per la soluzione delle shallow water equations, in quanto è in grado di ben intercettare le discontinuità che si presentano come possibili soluzioni del sistema. Nel passato, una grande attenzione è stata dedicata alla risoluzione della parte omogenea delle SWEs, al fine di ottenere un buon calcolo del flusso numerico e quindi schemi in grado di captare gli shock in modo più preciso possibile. Questo però risulta insufficiente per ottenere un buon schema, in grado di simulare casi reali caratterizzati da una topografia irregolare e complessa. Perciò la discretizzazione del termine sorgente realtivo alla geometria è di fondamentale importanza e permette di derivare schemi cosidetti well-balanced in quanto capaci di riprodurre anche gli stati stazionari, come ad esempio quello di un lago a riposo.
Il fulcro di questo lavoro consiste nello sviluppo di appropriati schemi well-balanced, attraverso la combinazione di diversi metodi per il calcolo del flusso numerico e per la discretizzazione dei termini sorgenti.
Ciò si concretizza in quattro schemi differenti, ognuno dei quali gode di proprietà numeriche diverse, che permette di valutarli sotto vari punti di vista. Risulta quindi fondamentale la procedura di validazione di questi schemi, che permette di compararli in casi di varie difficoltò e quindi di individuarne gli aspetti più o meno performanti.

Contents

List of Figures

List of Tables

Chapter 1

Introduction

1.1 Context

This project has been carried out at the Laboratoire d'Hydraulique de Saint-Venant(LHSV), a laboratory that is shared between three different bodies: the Ecole des Ponts et Chaussées, a French engineering school; Electricité de France, the French electric company and the CETMEF (Centre d'Etudes Techniques Maritimes Fluviales), a research center for fluvial and maritime studies.
The laboratory proposes research activities in the domain of fluid mechanic applied to hydraulic and to environment, it especially covers the fields of free surface flows in fluvial, maritime, coastal and port field. My project deals with the validation of the finite volume kernel of Telemac-2D, that is an open-source software used to simulate a wide range of shallow water flows. It is one of the most used codes in the world and it is based on a Saint-Venant model (called also shallow water equations which are an adapted and a simplified form of Navier-Stokes equations).
One of the attractive particularities of Telemac-2D, is the fact that it contains two different kernels: the first one is based on finite elements method (FEM) and the other one uses mainly finite volumes (FVM). Historically, the FEM kernel is the oldest, the most used and the most validated. The FVM kernel has been developed recently and needs an important validation step. This kernel includes four new different schemes which have different formulations, orders and numerical characteristics.

1.2 Objectives

Numerical methods are useful tools for studying physical problems that can be mathematically modeled by a set of partial differential equations. They represent a good alternative when there aren't analytical solutions and when the experimental way is too expensive.
In hydraulic engineering, numerical models are often used to manage the risk and to develop emergency plans in the case of catastrophic natural events, such as inundations, dam-breaks and levee failures. These kind of events have a large impact, indeed they can endanger human life, they can cause big damages that have an important economic weight. This is the reason why plan ahead and protection activities have a huge importance.
Steady and unsteady free surface flows can be modeled by the Saint Venant equations, that are a system of non-linear partial equations of hyperbolic type. The non-linearity of the system makes discontinuities (shocks) as possible solutions for the system. In order to consider a shock

at the correct speed, conservative methods must be used. So finite volume methods are really adapted to solve this system. In fact we know from the work of Lax and Wendroff, that conservative methods if convergent, converge to the weak solution of the conservation laws [14].
Starting from these considerations, the shock-capturing is an important objective in the validation process, that need to be assessed. Once the shock is captured, for higher order methods it's important to avoid spurious oscillations near shocks and to retain a good order of accuracy in smooth part of the flow.
Several propositions of great schemes that find solutions of the homogeneous system of Saint Venant equations capturing shocks have been made by the scientific community in the last twenty years. But a new and more difficult end has interested researchers in the last years : handling the geometric source terms. This is a relevant aspect because in the reality, river flows are often characterized by complex geometry and high roughness, that in numerical schemes can create difficulties and numerical errors. One of the most important aspect in the source term discretization is the well balance between fluxes and source terms in the steady case.
In this work we will deepen this topic, choosing a specific source term treatment in order to obtain well-balanced schemes. The chosen method, called Hydrostatic Reconstruction (HR), will be applied to the new schemes and then compared to another technique that is the DFB (Divergence Form Bed), which presents some particular advantages. In the validation process, specific test cases will be proposed to verify the source term discretization.

Keeping these goals in mind, we make the validation of all the newly added schemes in Telemac-2D by testing them on several benchmarks (i.e. official validation tests of Telemac-2D). This will involve the assessment of numerical performances of the code as shock-capturing, numerical diffusion, boundary conditions treatment, mass conservation, and topography effects.

1.3 Overview

This work is organized as follows.
In chapter 2 the assumptions for the Saint Venant equations are recalled and also the mathematical procedure to obtain them, starting from the general conservation equilibrium of mass and momentum for an incompressible medium. In this chapter is proposed an overview of numerical methods, focusing on the finite volume method, the one used in this work.
In chapter 3 we will present our finite volume approach in order to then focus the attention afterwards on the source term treatment, giving some examples taken from scientific literature.
In chapter 4 the four new schemes added in Telemac-2D are presented in detail. In the description, we will separately treat the flux calculation and the source term discretization for every scheme.
In chapter 5 series of test cases are proposed. Analytical and reference solutions are compared with those obtained with the four new schemes but also with those obtained with the three existing schemes of Telemac-2D.
In chapter 6 we will show the main results of this work and we will propose some possible future developments and researches.

Chapter 2

The Saint Venant equations

This chapter will introduce the Saint Venant equations recalling their fundamental hypothesis and their properties. In the second part of the chapter the most used numerical methods are presented. A particular attention will be given to the finite volume method, developed in this work.

2.1 Saint Venant equations

The study of many natural phenomena involving risk is an important butt for the human security and also the environmental protection. Examples of practical problems are the debris flow, the breaking of waves on shallow beaches, the roll waves in open channels, the flood waves in rivers, the surge and the dam break wave. Some of these phenomena are governed by the Saint Venant equations, also called shallow water equations.
For all this problems we consider a free surface flow which can be modelled with the Saint Venant equations under some hypothesis.
The equations are a time-dependent two-dimensional system of non-linear partial differential equations (PDEs) of hyperbolic type. This aspect brings to the system some typical properties that we're going to present in the next sections.

2.1.1 Basic hypothesis

Before the derivation of 2D Saint-Venant equations, that are the result of the integral over the vertical direction of the Navier Stokes equations, we must specify some important assumptions.

- the pressure distribution is hydrostatic (this results from assuming that the vertical acceleration of the water particles has a negligible effect on the pressure);
- the fluid is incompressible : $\rho = const$;
- the depth of water is small with respect to wave length or free-surface curvature
- the effects of boundary friction and turbulence can be accounted for through resistance laws analogous to those used for steady state flow
- the average channel bed slope is small so that the cosine of the angle it makes with the horizontal may be replaced by unity.

We list also the main mathematical notations used in this work.
Defined two vectors $\mathbf{A} = (a_1, a_2, a_3)$ and $\mathbf{B} = (b_1, b_2, b_3)$, the dot product of two vectors is the scalar quantity

$$\mathbf{A} \cdot \mathbf{B} \equiv a_1 b_1 + a_2 b_2 + a_3 b_3$$

Given a scalar quantity ϕ that depends on the spatial variables x, y, z, the gradient operator ∇ as applied to ϕ is the vector

$$grad\phi \equiv \nabla\phi = \left(\frac{\partial \phi}{\partial x}, \frac{\partial \phi}{\partial y}, \frac{\partial \phi}{\partial z} \right)$$

The symbol $\nabla \cdot (\mathbf{A})$ represents the divergence operator, also written as

$$div(\mathbf{A}) \equiv \nabla \cdot \mathbf{A} = \frac{\partial a_1}{\partial x} + \frac{\partial a_2}{\partial y} + \frac{\partial a_3}{\partial z}$$

2.1.2 2D Saint Venant equations

In this section we will deal with the derivation of the Saint Venant equations, also called shallow water equations (SWEs), for domains of variable bed elevation. This section is based on the work of Toro [21], to which we make reference above all for the numerical and mathematical passages.
We consider a flow of water with a free surface under gravity in a three-dimensional domain. In figure 2.1 we indicate our convention for spatial coordinates; x-y determine a horizontal plane whilst z defines the vertical direction, which we associate with the free surface elevation.
We assume that the bottom boundary, called also just bottom or bed, is defined by a function

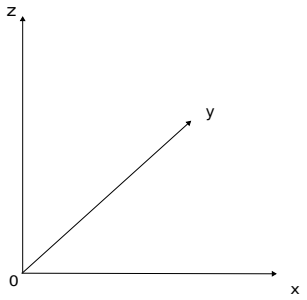

Figure 2.1: Convention for spatial coordinates

$$z = b(x, y) \tag{2.1}$$

and therefore the free surface is defined by

$$z = s(x, y, t) \equiv b(x, y) + h(x, y, t) \tag{2.2}$$

where $h(x, y, t)$ represents the water depth, the vertical distance between the bed and the free-surface position that is time-dependent. For a better comprehension we refer to the figure 2.2.

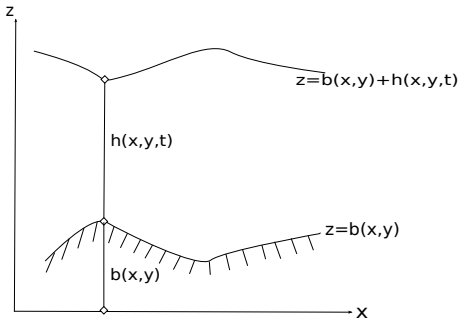

Figure 2.2: A free surface flow, for a fixed section y

We introduce now the governing equations, the general conservation of mass and momentum for a compressible material, written in differential conservation form:

$$\rho_t + \nabla \cdot (\rho \mathbf{V}) = 0 \tag{2.3}$$

and

$$\frac{\partial}{\partial t}(\rho \mathbf{V}) + \nabla \cdot [\rho \mathbf{V} \otimes \mathbf{V} + p\mathbf{I} - \Pi] = \rho \mathbf{g} \tag{2.4}$$

These equations state that the mass and the momentum $\rho\mathbf{V}$ are conserved. We distinguish independent variables from dependent variables. The independent variables are t for time and x, y, z for space. The dependent variables are ρ for the density, $\mathbf{V} = (u, v, w)$ for velocity, with u, v, w the x, y, z components of velocity, respectively; p is the pressure; $\mathbf{g} = (g_1, g_2, g_3)$ is a body force vector; the tensors involved are

$$\mathbf{V} \otimes \mathbf{V} = \begin{pmatrix} u^2 & uv & uw \\ vu & v^2 & vw \\ wu & wv & w^2 \end{pmatrix},$$

$$\mathbf{I} = \begin{pmatrix} 1 & 0 & 0 \\ 0 & 1 & 0 \\ 0 & 0 & 1 \end{pmatrix},$$

$$\Pi = \begin{bmatrix} \tau^{xx} & \tau^{xy} & \tau^{xz} \\ \tau^{yx} & \tau^{yy} & \tau^{yz} \\ \tau^{zx} & \tau^{zy} & \tau^{zz} \end{bmatrix}$$

Π represents the viscous stress tensor and may be defined using the Newtonian approximation, but for the moment we shall neglect viscous stresses.

The corresponding integral form of the conservation laws (2.3) and (2.4), is given respectively by

$$\frac{\partial}{\partial t}\iiint_V \rho \,\mathrm{d}V = -\iint_\Omega \mathbf{n}\cdot(\rho\mathbf{V})\,\mathrm{d}\Omega \tag{2.5}$$

and

$$\frac{\partial}{\partial t}\iiint_V (\rho\mathbf{V})\,\mathrm{d}V = -\iint_\Omega [\mathbf{V}(\mathbf{n}\cdot\rho\mathbf{V} + p\mathbf{n} - \mathbf{n}\cdot\Pi)]\,\mathrm{d}\Omega + \iiint_V \rho\mathbf{g}\,\mathrm{d}V, \tag{2.6}$$

where V is an arbitrary control volume of an element of fluid in three-dimensional space and Ω is its boundary. From a computational point of view, V will be a finite volume or a computational cell.

It results convenient to express the equations in terms of the primitive or physical variables ρ, u, v, w and p. If, for the moment, we neglect the viscous effect but we retain body force via a source term vector, we will obtain:

$$\begin{array}{lcl} \rho_t + u\rho_x + v\rho_y + w\rho_z + \rho(u_x + v_y + w_z) &=& 0, \\ u_t + uu_x + vu_y + wu_z + \frac{1}{\rho}p_x &=& g_1, \\ v_t + uv_x + vv_y + wv_z + \frac{1}{\rho}p_y &=& g_2, \\ v_t + uw_x + vw_y + ww_z + \frac{1}{\rho}p_z &=& g_3, \end{array} \tag{2.7}$$

Then we assume the density of the fluid constant, as said in section 2.1.1, so we can simplify to

$$u_x + v_y + w_z = 0, \tag{2.8}$$

$$u_t + uu_x + vu_y + wu_z = -\frac{1}{\rho}p_x, \tag{2.9}$$

$$v_t + uv_x + vv_y + wv_z = -\frac{1}{\rho}p_y, \tag{2.10}$$

$$w_t + uw_x + vw_y + ww_z = -\frac{1}{\rho}p_z - g, \tag{2.11}$$

We note that the body force vector is $\mathbf{g} = (0, 0, -g)$, where g is the gravity acceleration, taken as $g = 9.8m/s^2$, a constant.

To obtain the solution for the four unknowns values u, v, w, p, in principle, we need the initial and the boundary conditions on the bottom and the free surface, but the initial boundary value problem for equations (2.8)-(2.11) is computationally challenging. The main difficulty is the evaluation to the free surface that is a boundary, but his position remains unknown and therefore the domain on which equations are to be solved is not known a priori. To simplify the problem we assume that the depth of the water is small with respect to wave length or free-surface curvature, for example. This assumption gives rise to non-linear initial values problems that are analogous to those associated with wave propagation in compressible materials.

We discuss now boundary conditions for the full problem (2.8)-(2.11). We assume that a boundary is given by the surface

$$\psi(x, y, z, t) = 0 \tag{2.12}$$

For the free surface we have

$$\text{Free surface:} \quad \psi(x, y, z, t) \equiv z - s(x, y, t) = 0 \tag{2.13}$$

and for the bottom we have:

$$\text{Bottom or bed:} \quad \psi(x, y, z, t) \equiv z - b(x, y) = 0 \tag{2.14}$$

Two boundary conditions are imposed on the free surface $s(x, y, t)$, with ψ given by (2.13), namely the kinematic condition

$$\frac{\mathrm{d}}{\mathrm{d}t}\psi(x, y, z, t) = \psi_t + u\psi_x + v\psi_y + w\psi_z = 0 \tag{2.15}$$

and the dynamical condition

$$p(x, y, z, t)|_{z=s(x,y)} = p_{atm} = 0 \tag{2.16}$$

where p_{atm} is the atmospheric pressure, which for convenience is taken here to be identically zero.
For the bottom boundary $b(x, y)$, condition (2.15) also applies, with ψ given by (2.14).
For the derivation of the shallow water equations, we assume that the vertical component of acceleration is negligible, so

$$\frac{\mathrm{d}w}{\mathrm{d}t} = w_t + uw_x + vw_y + ww_z = 0 \tag{2.17}$$

Therefore the equation (2.11) becomes

$$p_z = -\rho g \tag{2.18}$$

Given the dynamical condition (2.16) ($p_{atm} = 0$), we obtain

$$p = \rho g(s - z) \tag{2.19}$$

Its differentiation with respect to x and y gives

$$p_x = \rho g s_x, \qquad p_x = \rho g s_y \tag{2.20}$$

We note that both p_x and p_y are independent of z and thus the x and y components of acceleration of water particles $\mathrm{d}u/\,\mathrm{d}t$ and $\mathrm{d}v/\,\mathrm{d}t$ are independent of z. Hence the x and y velocity components u and v are also independent of z that is $u_z = v_z = 0$. Therefore, thanks to the above conditions and making use of (2.20) in (2.9) and (2.10), we obtain

$$u_t + uu_x + vu_y = -gs_x \tag{2.21}$$

and

$$v_t + uv_x + vv_y = -gs_y \tag{2.22}$$

We integrate now the continuity equation (2.8) with respect to z, the vertical coordinate, between the bottom $z = b(x, y)$ and the free surface $z = s(x, y, t)$. That is

$$\int_b^s (u_x + v_y + w_z)\,\mathrm{d}z = 0 \tag{2.23}$$

which leads to

$$w|_{z=s} - w|_{z=b} + \int_b^s u_x\,\mathrm{d}z + \int_b^s v_y\,\mathrm{d}z \tag{2.24}$$

Then we apply boundary conditions in order to determine the first two terms in equation (2.24). Expanding (2.15) as applied to the free surface (2.13) gives

$$(s_t + us_x + vs_y - w)|_{z=s} = 0 \tag{2.25}$$

Expanding (2.15) as applied to the free surface (2.14) gives

$$(ub_x + vb_y - w)|_{z=b} = 0 \tag{2.26}$$

From equation (2.25) we obtain

$$w|_{z=s} = (s_t + us_x + vs_y)|_{z=s} \tag{2.27}$$

and from equation (2.26) we obtain

$$w|_{z=b} = ((ub_x + vb_y)|_{z=b} \tag{2.28}$$

Making substitution of (2.27) and (2.28) in (2.24), we have

$$(s_t + us_x + vs_y)|_{z=s} - (ub_x + vb_y)|_{z=b} + \int_b^s u_x \,\mathrm{d}z + \int_b^s v_y \,\mathrm{d}z = 0 \tag{2.29}$$

To simplify this last equation, we use Leibniz's formula on the last two integral terms in (2.29), which finally leads

$$s_t + \frac{\partial}{\partial x}\int_b^s u \,\mathrm{d}z + \frac{\partial}{\partial y}\int_b^s v \,\mathrm{d}z = 0 \tag{2.30}$$

Recall that both u nd v are independent of z; also $s = b + h$ and $b_t = 0$. Equation (2.30) becomes:

$$h_t + (hu)_x + (hv)_y = 0 \tag{2.31}$$

Equation (2.31) represents the law of conservation mass written in differential conservation form.
We want write also the momentum equations (2.10) and (2.11) in differential conservation law form, so we add equation (2.31), premultiplied by u to equation (2.21), premultiplied by h. We make use of a relation that does assume differentiability of water depth h:

$$h\frac{\partial h}{\partial x} = \frac{\partial}{\partial x}\left(\frac{1}{2}h^2\right) \tag{2.32}$$

to obtain

$$(hu)_t + (hu^2 + \frac{1}{2}gh^2)_x + (huv)_y = -ghb_x \tag{2.33}$$

Similary, for the y momentum we obtain

$$(hv)_t + (huv)_x + (hv^2 + \frac{1}{2}gh^2)_y = -ghb_y \tag{2.34}$$

All three partial differential equations can be written in differential conservation law form as a single vector equation

$$\mathbf{U}_t + \mathbf{G}(\mathbf{U})_x + \mathbf{H}(\mathbf{U})_y = \mathbf{S}(\mathbf{U}), \tag{2.35}$$

with

$$\mathbf{U} = \begin{bmatrix} h \\ hu \\ hv \end{bmatrix}, \mathbf{G}(\mathbf{U}) = \begin{bmatrix} hu \\ hu^2 + \frac{1}{2}gh^2 \\ huv \end{bmatrix},$$

$$\mathbf{H}(\mathbf{U}) = \begin{bmatrix} hv \\ huv \\ hv^2 + \frac{1}{2}gh^2 \end{bmatrix} \mathbf{S}(\mathbf{U}) = \begin{bmatrix} s_1 \\ s_2 \\ s_3 \end{bmatrix}$$

where $\mathbf{U}$ is the vector of conserved variables, $\mathbf{G}(\mathbf{U})$ and $\mathbf{H}(\mathbf{U})$ are flux vectors and $\mathbf{S}(\mathbf{U})$ is the source term vector. For many applications there will be additional terms in the source term vector (such as the friction, the Coriolis force...) but we will analyze it in the next chapter.
The solution of the system (2.35) allows to know the variation of the variables h, u, v with time, over all the domain. This type of equations can be hardly analytically solved, so we must use numerical methods to approximate the solution.

2.1.3 Properties of the system

The system (2.35) is widely studied in the literature. We recall here the main properties [3]:

- The system is strictly hyperbolic for all $h > 0$ and loses this hyperbolicity for $h = 0$. This means that water depth can vanish and dry regions may appear in the domain.
- The system admits an entropy ($\tilde{\eta}$) inequality related to physical energy (η)[5]:

$$\frac{\partial \tilde{\eta}(U)}{\partial t} + \frac{\partial \tilde{G}(U)}{\partial x} \leq 0 \tag{2.36}$$

  where
  $\eta(U) = hu^2/2 + gh^2/2, \qquad G(U) = \left(hu^2/2 + gh^2\right) u$
  $\tilde{\eta}(U,z) = \eta(U) + hgz, \qquad \tilde{G}(U,z) = G(U) + hgzu$

- The system admits non trivial steady states, such as the lake at rest ($h + z = const$ if $u = 0$). We will discuss these states later when dealing with the discretization of geometric source terms.

2.2 Numerical methods

This section is dedicated to the presentation of the different conventional approaches used to solve the Saint Venant equations or, more generally, a system of non-linear and hyperbolic PDEs.

2.2.1 Finite difference method

The finite differences method (FDM) is the first technique used to solve a system of differential equations. Indeed the first application of the FDM to obtain the numerical solution of the differential equations comes from Eulero (1768). The fundamental ideas of the theory, essentially based on the properties of the Taylor series and on the derivative definition, were lately presented by Courant, Freidrichs and Levy in 1928. Nevertheless, its potentiality were experimented and recognized only with the introduction of the modern computer methods.
The major idea consists in the substitution of the continuous functions, of continuous variables, that appear in the differential equations, with functions of discrete variables, defined only in a certain number of points. These points make up a computational grid. In this way the solution is discrete too and it means that we have a series of relations that give the values of h, hu, hv for a series of specific time steps.
To do this, some particular operators are necessary to substitute the total (or partial) derivatives that appear in the equations. To semplify, we can refer to the definition of derivative of a continuous function $y(x)$

$$\frac{\mathrm{d}y}{\mathrm{d}x} = \lim_{\Delta x \to 0} \frac{y(x + \Delta x) - y(x)}{\Delta x} \tag{2.37}$$

If Δx is small but finite, then the right hand side of the equation (2.37) represents an approximation of the exact value of the derivative $\mathrm{d}y/\,\mathrm{d}x$. This approximation can be improved reducing Δx but introducing an error of truncation that tends to zero when Δx tends to zero. The techniques to approximate a derivative of a function are various. If we consider three consecutive points in a uniform computational grid, we can define three kind of differences: central, upwind and downwind differences.
The main advantage of the method is the conceptual simplicity application and also the good precision that we can get. On the other hand it needs a regular and structured mesh and so its application remains limited to simple geometries. Moreover the method is not always conservative. The finite difference schemes can be explicit or implicit. In explicit schemes the unknowns are determined writing the SVEs so as to obtain an only unknown for every equation. In this way it is possible to solve the problem step by step, for example using a forward method in time and in space. On the other hand this method is proved to be unstable because the errors that are unavoidably introduced with the approximation of a derivative, are amplified with the proceeding of calculation. To overcome this problem there are other explicit schemes that are stable under a certain condition, also called Courant, Freidrichs and Levy condition that we will deepened in next sections.
The implicit schemes allow the numerical integration of the SVEs thanks to a non-linear system in which the number of unknowns is bigger than that of equations for every point. This entails that to know the values over a point (or in a section) it is necessary solving all the system in all points for a given time, that involves a waste in computational terms. The advantage of these kinds of method is the unconditional stability.

2.2.2 Finite element method

The finite elements method (FEM) chuckled up in the last decades a big success in various fields of engineering and it has been object of study in the hydraulic domain.
The characteristic of this method is the replacement of an initial continuous problem to a variational formulation. To do this we must create a mesh made up with finite elements that have a codified form (triangles or quadrilaterals in 2D domains or tetrahedrons and exahedrals in 3D domains). Over each elements the solution of the problem is expressed by the linear combination of functions called shape functions.
We take in consideration the differential equation

$$L_D y(\mathbf{x}) = f(\mathbf{x}) \tag{2.38}$$

where $\mathbf{x} = (x, y, z)$ is the position vector that identifies the generic point P compared to a Cartesian reference system of axis x, y, z. $y(\mathbf{x})$ is the dependent variable of the differential problem, $f(x, y, z)$ is an assigned function and L_D represents a generic differential operator. This equation identifies a PDE with solution y, founded in the integration domain D and subject to specific boundary condition on ∂D. We can consider y_n, as an approximate numerical solution of y written as

$$y_n(\mathbf{x}) = y_0(\mathbf{x}) + \sum_{i=1}^{N} a_i \xi_i(\mathbf{x}) \tag{2.39}$$

where $y_0(\mathbf{x})$ is a function normally introduced to satisfy the boundary conditions and $\xi(\mathbf{x})$ are known functions (shape functions), linearly combined with the N unknown coefficients, a_i.
Replacing (2.39) in (2.38), the last one will not be exactly satisfied, indeed it generates a residual

$$R(\mathbf{x}) = L_D y_n - f_n \tag{2.40}$$

The coefficients a_i are determined from the N equations obtained imposing the conditions

$$\int_D (L_D y_n - f_n) w_i \, \mathrm{d}D = 0 \tag{2.41}$$

where $w_i(\mathbf{x})$ are the N weight function, linearly independent and happily specified. Finally the choice of the weights w_i is related to the applied method.
We remark that the FEM is strictly linked to the FDM; specially the FEM can be compared to the implicit schemes of the FDMs. But this method can be applied when the geometry is complex or very variable and its formulation is based on strong mathematical fundamentals. In additional, the triangular elements offer a very good discretization of the ground and this discretization can be refined in the zone the most critical in order to obtain an accurate solution. The disadvantage is that this method is non conservative [28].

2.2.3 Finite volumes methods

The finite volumes methods (FVM) was developed thanks to the Godunov scheme (1959) and the Roe scheme (1981). These two schemes are based on the resolution of the Riemann problem. The first one proposes an exact solution of the Riemann problem, the second one suggests to replace the exact non-linear Riemann problem with a approximated linear problem. Later, Harten, Lax and van Leer (1983), presented a scheme family based on the approximate Riemann problem.
In this method, the domain is divided into a finite number of control volumes that cover all the computational domain. Over every control volume or cell the conservation laws are applied to determine the different variables associated to certain points (or nodes) that don't necessarily correspond to the points of the mesh. We have various choices to define the control volumes and the nodes (cell-centred, cell-vertex, node-vertex...), that we're going to present in the next paragraph. Also the mesh can be very variable, that means structured or non-structured, in order to give flexibility to the method.
The mesh corresponds to a discrete representation of the physical domain that we want describe. In the FVM it is very important to make a difference between an element and a control volume. We call element a surface or a 3D volume created by points, that serves only for the construction of the mesh and allows to spatially discretize the geometry. We call control volume a surface or a volume in which we apply the conservation equations in order to calculate the unknown variables. Normally we can find two types of mesh:

- a structured mesh (FD type)
- an unstructured mesh (FE type)

A finite volume method applied to a structured mesh brings to use numerical schemes that are easier than those used for an unstructured mesh. Even when we use an implicit scheme, a structured mesh makes the matrix system to solve easier, so it is efficient also for the computational time. In spite of these positive aspects, the representation of complex domains are difficult. Some examples of structured mesh are the Cartesian grid, that can be regular (same distance between neighbour points) or irregular in the space. Every point is identified by two or three index (i, j, k) that ease the location of the neighbor of a node. This aspect simplifies the programming and allows to obtain matrix with regular structure that can be exploited for the effective resolution with implicit schemes. Other examples of structured mesh are the curvilinear grid (body fitting), the mesh with non-congruent interfaces, composite mesh (Chimera grid) [28].

The category of unstructured mesh offers more flexibility for the construction of complex geometries. Indeed it is always possible to automatically create meshes made up with triangles in 2D (tetrahedrons in 3D), even if the domain is very complex. In practice we prefer using also quadrilaterals et hexahedrals to have a better precision in calculation.

We conclude that the construction of unstructured meshes is in general easier and faster. It's also very practical because it allows to refine a specific part of the mesh. Additionally we can create or eliminate some nodes/elements during the calculation. On the other hand the data structure associated to the nodes is more complex because it's necessary specify the localization of nodes, the connectivity with their neighbours...that implies more memory and a specific treatment in the solvers. In this way the performances decreases, if compared to a structured mesh.

The definition of the control volume is important because it affects the flux calculation (as we will see in the next paragraphs) from which precision depends. We describe here two kinds of scheme: the "cell-centred" and the "vertex-centred". In the first one, the variables associated to the fluid are stocked in the center of the mesh elements (primal mesh) and the control volumes correspond to the elements of the mesh. The unknown variables correspond to an averaged value over the control volume.

This description is the most used in the literature. Its main advantage is the fact that it allows an immediate use of any kind of mesh without any additional preprocessing. Nevertheless, this description could be very sensitive to the mesh quality and results may be poorly affected in presence of elements with high aspect ratio [28].

In a vertex-centred description, the unknown values are associated to the apex of the mesh elements and so the control volume is made around these nodes. The control volumes construction is made with the center of mass of every mesh element. We can find three kind of construction, that are often used:

- Centroid dual mesh: we connect the gravity centers with a straight segment (used in Telemac-2D)
- Median dual mesh: also called INRIA formulation. An intermediate point is created in the middle of the segments that link the nodes of the unknown variables. The control volume is made linking the gravity centers with these intermediate points with straight lines.
- Dirichlet: based on the Voronoi diagram [2], it allows to obtain convex control volumes that have interesting characteristics. On the other hand, its construction is complicated. Although this description induces an extra preprocessing, it has the advantage to be much less sensitive to the mesh quality. Moreover, it is more adapted to the finite volume averaging philosophy.

We take into consideration the two-dimensional shallow water equations written in differential conservation law form:

$$\mathbf{U_t} + \mathbf{F}(\mathbf{U})_\mathbf{x} + \mathbf{G}(\mathbf{U})_\mathbf{y} = \mathbf{S}(\mathbf{U}) \tag{2.42}$$

with

$$\mathbf{U} = \begin{bmatrix} h \\ hu \\ hv \end{bmatrix}, \mathbf{G} = \begin{bmatrix} hu \\ hu^2 + \frac{1}{2}gh^2 \\ huv \end{bmatrix}, \mathbf{H} = \begin{bmatrix} hv \\ huv \\ hv^2 + \frac{1}{2}gh^2 \end{bmatrix}, \mathbf{S} = \begin{bmatrix} s_1 \\ s_2 \\ s_3 \end{bmatrix}, \tag{2.43}$$

In the presence of discontinuities we must consider the integral form, that, excluding the source term vector, is

$$\frac{d}{\mathrm{d}t} \int \int_V \mathbf{U} \, \mathrm{d}V = - \int_\Omega \mathcal{H} \cdot \mathbf{n} \, \mathrm{d}\Omega, \tag{2.44}$$

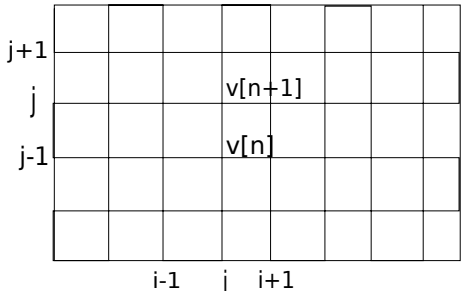

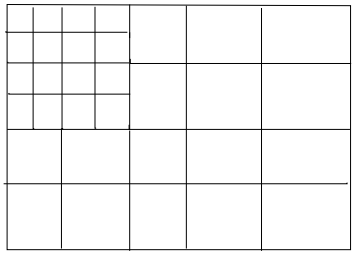

(a) Irregular cartesian grid and mesh with non-congruent interfaces

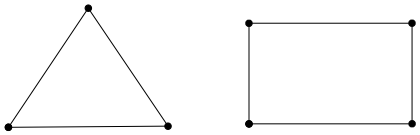

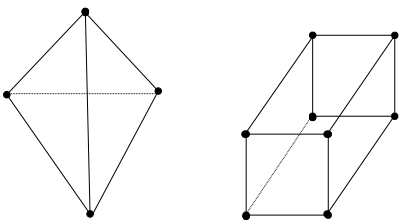

(b) 2d and 3d elements for unstructured meshes

Figure 2.3: Types of meshes and elements

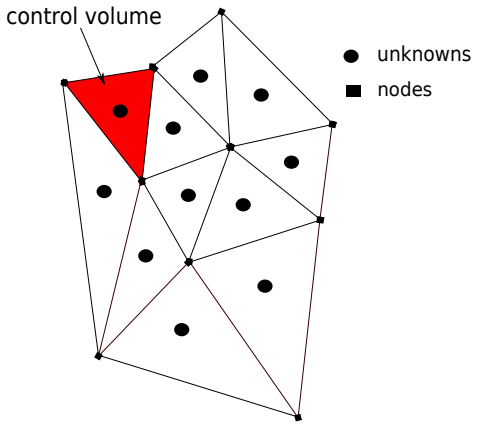

Figure 2.4: A cell-centred scheme

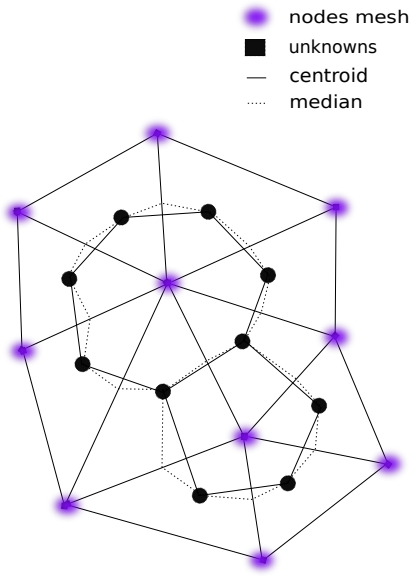

Figure 2.5: Vertex-centered schemes

where V represents a control volume, Ω is the boundary of V, $\mathcal{H} = (\mathbf{F}, \mathbf{G})$ is the tensor of fluxes, $\mathbf{n} = [n_1, n_2]$ is the outward unit vector normal to the surface Ω, $\mathrm{d}\Omega$ is an area element and $\mathcal{H} \cdot \mathbf{n}\,\mathrm{d}\Omega$ is the flux component normal to the boundary Ω.

The cell average for a control volume V in two-dimensional space, is

$$\widehat{\mathbf{U}} = \frac{1}{|V|} \int \int_V \mathbf{U} \, \mathrm{d}V, \tag{2.45}$$

where $|V|$ represents the area in the two-dimensional domain. So (2.44) becomes

$$\frac{d}{\mathrm{d}t} \widehat{\mathbf{U}} = -\frac{1}{|V|} \sum_{s=1}^{N} \mathcal{F}_s, \tag{2.46}$$

with fluxes

$$\mathcal{F}_s = \int_{A_s}^{A_{s+1}} [n_1 \mathbf{G}(\mathbf{U}) + n_2 \mathbf{H}(\mathbf{U})] \, \mathrm{d}\Omega \tag{2.47}$$

Considering a structured mesh, the volume V is discretized in smaller cells, labeled $I_{i,j}$. We replace now the time derivative by a forward in time approximation, in order to obtain the fully discrete schemes

$$\mathbf{U}_{i,j}^{n+1} = \mathbf{U}_{i,j}^{n} - \frac{\Delta t}{|I_{i,j}|} \sum_{s=1}^{N} \mathcal{F}_s \tag{2.48}$$

where $|I_{i,j}|$ is the area of the cell $I_{i,j}$.
Overtly we consider a case in wich the cells $I_{i,j}$, $\forall i, j$ are Cartesian cells of area $\Delta x \times \Delta y$; thus the expression (2.48) develops in

$$\mathbf{U}_{i,j}^{n+1} = \mathbf{U}_{i,j}^{n} - \frac{\Delta t}{\Delta x} [\mathbf{G}_{i+\frac{1}{2},j} - \mathbf{G}_{i-\frac{1}{2},j}] - \frac{\Delta t}{\Delta y} [\mathbf{H}_{i,j+\frac{1}{2}} - \mathbf{H}_{i,j-\frac{1}{2}}] \tag{2.49}$$

We note that a conservative method is completely defined once the fluxes contained in F_s, in particular the intercell flux (between cells i and i+1), have been specified.
A characteristic of conservative methods is the telescopic property, that says that the intercell fluxes, such as $\mathbf{G}_{i+\frac{1}{2},j}$ and $\mathbf{H}_{i,j+\frac{1}{2}}$, used to update the cell average $\mathbf{U}_{i,j}^{n}$, must be identical to the intercell flux $\mathbf{G}_{i-\frac{1}{2},j}$ and $\mathbf{H}_{i,j-\frac{1}{2}}$ used to update the cell average $\mathbf{U}_{i+1,j}^{n}$. So the sum of the flux at the boundary between the cell i and i+1 is erased when we sum $\mathbf{U}_{i,j}^{n}$ and $\mathbf{U}_{i+1,j}^{n}$ [21].
Another property that a good numerical method must satisfy is the consistency. This means that if all the arguments of the numerical flux are equal to a constant value $\widehat{\mathbf{U}}$, then the value of the numerical flux at $\widehat{\mathbf{U}}$ must coincide with the value of the physical (exact) flux at $\widehat{\mathbf{U}}$.
Finally we need also the convergence property. We refer to the Lax-Wendroff theorem that affirms that if the method, written in conservative form as (2.49) is convergent, then it converges to a weak solution of the (2.42), excluding the source term vector. At the same time an entropy condition is necessary to find a physically meaningful solution between the weak solutions.
To sum up, convergence and entropy allow to find a physical unique solution.
In this paragraph we have considered just the homogeneous part of the SWEs, but in the next chapter we will take into account also the source term, that is really essential for the Saint-Venant equations. Indeed the nature of the phenomena is strictly dependent by the source terms and their discretization.
The advantage in the FVM is that the spatial discretization is directly made over the physic domain. So there isn't any transformation between the different coordinate systems, as for example there is in the FEM, where a transformation from the real element to the reference element (of which the shape functions are known) is made. In addiction to this, the FVM can be used for structured or non-structured mesh, while this is not the case for the FEM.
Moreover the formulation for the FVM is based on a discretization of the conservation laws, that are naturally satisfied by the numerical scheme on the control volumes. This property is very

important when we treat shocks because it permits to guarantee that the Rankine-Hugoniot relations will be satisfied by the method.
Its simplicity of implementation and its flexibility make it one of the most used tachnique in Fluid Mechanic.

2.2.4 Numerical instabilities and numerical diffusion

The numerical methods represent a powerful way to approximate the solution of a system of PDEs but they need specific tricks to avoid numerical instabilities and to reduce numerical diffusion at the same time.
Oscillations appear in the solution in proximity of strong gradients of the dependent variables of the system. The numerical diffusion exhibits moreover in the critical points, as shocks but also in rarefaction waves. Normally higher order methods have less numerical diffusion than lower order methods.

We start taking as example a first order method, where the order is given by the value of s, linked to the error ([16]):

$$||E^n|| = C(\Delta x)^s + \text{high order terms} \tag{2.50}$$

when $\Delta x \to 0$, where C is some constant that depends on the particular solution being computed (and the time T). In these methods a numerical diffusion is present in the solutions and it is naturally linked to the low order of accuracy, that can't reach a better solution. To get a first order of accuracy the data are supposed to be constant in the domain of integration (see as the control volume) and this brutal assumption creates a numerical diffusion.
On the other hand, there are some particular schemes where a dissipative term is expressly introduced in order to avoid instability. The instability can be visualized as an oscillation of the solution that increases with time. This is the case for the simple centred schemes that are unstables and need the add of a dissipative term, that can be interpreted as a viscosity and that has the task to upwind the scheme making it stable. There are different formulation of this dissipative term that varies according to the flux calculation. Two possibilities of dissipative term will be treated in section 4.1.2 for the flux calculation in the Zokagoa and Tchamen scheme.
Other instabilities can spring up when we extend the accuracy from the first order to the second one. Indeed, in this case we have a better accuracy for smooth solutions (that means less diffusivity), but there are oscillations in presence of discontinuities. The main idea is avoiding oscillations near the shock and keeping a good accuracy in smooth parts of the solution. To do this we need to measure the oscillations, through the notion of total variation of a function ([16]). For a grid function Q we define

$$TV(Q) = \sum_{i=-\infty}^{\infty} |Q_i - Q_{i-1}| \tag{2.51}$$

and for an arbitrary function $q(x)$

$$TV(q) = sup \sum_{j=1}^{N} |q(\xi_j) - q(\xi_{j-1})| \tag{2.52}$$

where the supremum is taken over all subdivisions of the real line $-\infty = \xi_0 < \xi_1 < ... < \xi_N = \infty$.
If a method introduces oscillations, we will expect the total variation of Q^N increases with time.

So to avoid oscillations we must impose that the method do not increase the total variation. According to the LeVeque's definition [16] we can say that a two level method is called total variation diminishing (TVD) if, for any set of data Q^n, the values Q^{n+1} computed by the method satisfy

$$TV(Q^{n+1}) \leq TV(Q^n) \tag{2.53}$$

We remark that the TV doesn't necessarily decrease but it can remain constant in time. Additionally, if a method is TVD, then in particular data that is initially monotone, say

$$Q_i^n \geq Q_{i+1}^n, \qquad \text{for all} \qquad i \tag{2.54}$$

will remain monotone in all future time steps. So a discontinuity may become smeared in future time steps but cannot become oscillatory.
To achieve a second order accuracy, a piecewise constant reconstruction is not sufficient and we must construct a piecewise linear function from the cell average Q_i^n of the type:

$$\tilde{q}^n(x, t^n) = Q_i^n + \sigma_i^n(x - x_i) \qquad \text{for} \qquad x_{i-1/2} \leq x < x_{i+1/2} \tag{2.55}$$

where

$$x_i = \frac{1}{2}(x_{i-1/2} + x_{i+1/2}) = x_{i-1/2} + \frac{1}{2}\Delta x \tag{2.56}$$

is the center of the ith grid cell and σ_i^n is the slope on the ith cell. The choice of σ_i^n is important to satisfy the TVD property and to give second order accuracy for smooth solutions. We have several slope-limiter functions, as the Minmod or the Superbee limiter, but we will develop this topic in section 4.3.3. We add that the slope limiter methods can be written as flux differencing methods and so we will have the flux-limiter functions instead of slope-limiter function.

Chapter 3

Source term treatments

This chapter aims to analyze some approaches used to treat the numerical source term. In particular in this work we will focus our attention on the bed source term, neglecting for the moment the other possible terms.
We will present the best known methods that have been proposed in the last years by the scientific community. Among the several solutions proposed, we choose two specific techniques that we will apply to our models. In subsection 3.2.1 and 3.2.2, we will describe these techniques highlighting their advantages.
The first part of the chapter is dedicated to the description of the finite volume approach used in Telemac-2D in order to clarify what it means treating the source terms, in our case.

3.1 Finite volume approach

We recall the two-dimensional shallow-water equations:

$$\frac{\partial \mathbf{U}}{\partial t} + \frac{\partial \mathbf{G}(\mathbf{U})}{\partial x} + \frac{\partial \mathbf{H}(\mathbf{U})}{\partial y} = \mathbf{S}(\mathbf{U}) \qquad on \qquad \Omega \times [0, T_s] \tag{3.1}$$

where

$$\mathbf{U} = \begin{bmatrix} h \\ hu \\ hv \end{bmatrix}, \mathbf{G}(\mathbf{U}) = \begin{bmatrix} hu \\ hu^2 + \frac{1}{2}gh^2 \\ huv \end{bmatrix}, \mathbf{H}(\mathbf{U}) = \begin{bmatrix} hv \\ huv \\ hv^2 + \frac{1}{2}gh^2 \end{bmatrix}$$

$$\mathbf{S}(\mathbf{U}) = \begin{bmatrix} 0 \\ gh(S_{0_x} - S_{f_x}) \\ gh(S_{0_y} - S_{f_y}) \end{bmatrix}, \nabla z = \begin{bmatrix} S_{0_x} \\ S_{0_y} \end{bmatrix}, \mathbf{S_f} = \begin{bmatrix} S_{f_x} \\ S_{f_y} \end{bmatrix} = \begin{bmatrix} \frac{n^2 u\sqrt{u^2+v^2}}{h^{\frac{4}{3}}} \\ \frac{n^2 v\sqrt{u^2+v^2}}{h^{\frac{4}{3}}} \end{bmatrix}$$

where $h = \eta - z$ is the water depth, η is the free surface level, z is the bottom level, (u, v) are the averaged velocity components and g is the gravitational acceleration. n is the Manning roughness coefficient, S_f the friction vector and T_s the time duration.
We specify that in this work we will consider the source term formed just by the bathymetry and the friction, consequently we will neglect all other possible additional terms.
We present here the general framework of the finite volume approach that we're going to use for all the schemes described in this chapter. The entire domain Ω is subdivided into N subdomains called control volumes K_i associated to a vertex i. As explained in the previous chapter, two choices are possible when constructing the control volumes: we can choose a "cell-centered" or

a "vertex-centered" finite volume description. In our case we prefer to use a vertex centered approach, that involves a "dual mesh". Specifically the dual cell is obtained by joining the centers of mass of the triangles T_i surrounding the vertex i (see figure 3.1).
According to this approach, we will use the following notations (see figure 3.1)

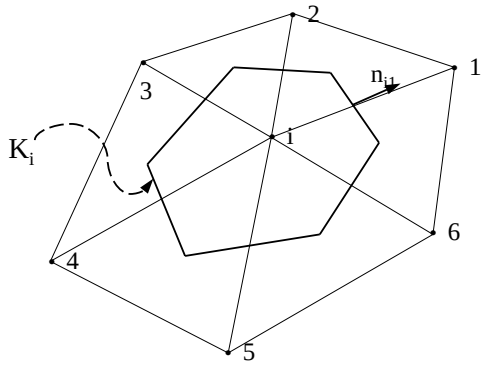

Figure 3.1: Vertex-centered approach used in this work.

- K_i is the control volume (cell) centered at the node i, and $|K_i|$ its area;
- Γ_{ij} the edge between the cell K_i and K_j;
- L_{ij} the length of Γ_{ij};
- $\mathbf{n}_{ij}$ the outward unit normal to the edge Γ_{ij};

For the vertex located at the boundary, the cell is completed by joining the center of mass of the triangle adjacent to the boundary with the middle of the boundary edge.
If we denote by Δt the time step and by $t^n = n\Delta t$, the application of Gauss theorem over equations 3.1 gives

$$\int_{K_i} \frac{\partial \mathbf{U}}{\partial t}\,\mathrm{d}V + \int_{\Gamma_i} (\mathbf{G}(\mathbf{U})n_x + \mathbf{H}(\mathbf{U})n_y)\,\mathrm{d}\Gamma = \int_{K_i} \mathbf{S}(\mathbf{U})\,\mathrm{d}V \tag{3.2}$$

also written as

$$\int_{K_i} \frac{\partial \mathbf{U}}{\partial t}\,\mathrm{d}V + \int_{\Gamma_i} \mathbf{F}(\mathbf{U})\cdot\mathbf{n}_i d\Gamma = \int_{K_i} \mathbf{S}(\mathbf{U})\,\mathrm{d}V \tag{3.3}$$

which gives the following finite volume discretization

$$\mathbf{U}_i^{n+1} = \mathbf{U}_i^n - \sum_{j=1}^{m_i} \sigma_{ij}\mathbf{F}(\mathbf{U}_i^n, \mathbf{U}_j^n, \mathbf{n}_{ij}) - \sigma_i \mathbf{F}(\mathbf{U}_i^n, \mathbf{U}_e^n, \mathbf{n}_i) + \Delta t \mathbf{S}_i^n \tag{3.4}$$

where $\mathbf{F} = (\mathbf{G}, \mathbf{H})^T$, $\mathbf{F}(\mathbf{U}_i, \mathbf{U}_j, \mathbf{n}_{ij})$ is the interpolation of the normal component of the flux $\mathbf{F}(\mathbf{U})\cdot\mathbf{n}_{ij}$ along the edge Γ_{ij}, and $\sigma_{ij} = \frac{\Delta t L_{ij}}{|K_i|}$, $\sigma_i = \frac{\Delta t L_i}{|K_i|}$, m_i is the number of edges in the

cell and $\mathbf{U_e}$ is a fictive state used to weakly impose the boundary condition.
By considering the integration of (3.1) in the xt space, $V = K_i \times [t^n, t^{n+1}]$, equation (3.4) is obtained by assuming the following interpretations:

- $\mathbf{U}_i^n$ is the spatial integral average of the solution at time t^n:

$$\mathbf{U}_i^n = \frac{1}{|K_i|} \int_{K_i} \mathbf{U}(\mathbf{x}, t^n)\, \mathrm{d}\mathbf{x} \tag{3.5}$$

- $\mathbf{F}(\mathbf{U}_i, \mathbf{U}_j, \mathbf{n}_{ij})$ is generally obtained using a one-dimensional solver, since the problem can be reduced to a 1D problem at a local scale. Indeed, using the rotation invariance property between $\mathbf{G}$ and $\mathbf{H}$, we get $\mathbf{F}(\mathbf{U}) \cdot \mathbf{n}_{ij} = \mathbf{T}_n \mathbf{G}(\mathbf{T}_n^{-1}\mathbf{U})$, where $\mathbf{T}_n$ is the rotation matrix given by

$$\mathbf{T}_n = \begin{bmatrix} 1 & 0 & 0 \\ 0 & \mathbf{n}_x & \mathbf{n}_y \\ 0 & -\mathbf{n}_y & \mathbf{n}_x \end{bmatrix} \tag{3.6}$$

  Thus, the 2D problem is transformed naturally to a 1D Riemann problem in the direction of the normal vector $\mathbf{n}_{ij}$ and with a left and right states.

- $\mathbf{S}_i$ is the volume-integral average in V:

$$\mathbf{S}_i^n = \frac{1}{|K_i|} \frac{1}{\Delta t} \int_{t^n}^{t^n + \Delta t} \int_{K_i} \mathbf{S}(\mathbf{U}_i(x,t))\, \mathrm{d}x\, \mathrm{d}t \tag{3.7}$$

To have a finite volume method, it is enough to prescribe a numerical flux $\mathbf{F}$ and a numerical source term $\mathbf{S_i}$.

3.2 Source term treatment

The irregular topography of regions subject to flooding can strongly affect flow dynamics, giving rise to the formation of hydraulic jumps, shocks and reflections. In order to capture these phenomena in numerical simulations, the treatment of the bed slope source term is important when accurate results both in the case of steady and unsteady flows must be obtained.
A huge effort has recently been undertaken by the scientific community in order to develop consistent numerical treatments of source terms due to bed slope. In particular, this effort has focused on the exact balance between the momentum flux and the source term in the case of quiescent flow. Indeed, in this case the bed slope source term must exactly satisfy the balance with the flux gradients, otherwise variations of the solution in time could appear. The capability of replicating the exact solution for the stationary flow problem is known as the C-property, introduced by Bermudez and Vazquez-Cendon [6]. They proposed a complex approach, that gives satisfactory results and that concerns the upwinding of the source terms, in a manner similar to that adopted for the construction of numerical fluxes for solving homogeneous conservation laws. This approach was later extended to a wide range of problems by Garcia-Navarro and Vazquez-Cendon [11]. This technique was also successively generalized to a finite volume high order TVD version of Roe's scheme and to an arbitrary polygonal mesh.
In Leveque [15] the source term is integrated into the wave propagation algorithm in order to propose a quasi-steady state wave propagation algorithm. But this method is only valid when the solution is near the steady state, because of the quasi-steady approximations and it shows difficulties when the flow is transcritical with a shock.

The Surface Gradient Method (SGM) suggested by Zhou et al. [26] takes into consideration the variation of the bed slope for data reconstruction, in particular the intercell water depth is computed starting from a MUSCL reconstruction of the water surface level (instead of the flow depth). Anyway this approach can't be considered strictly devoted to source terms evaluation, indeed no special treatment is proposed for the source terms that are calculated with a simple centered discretization. This method is very simple and provides an accurate reconstruction of the variable flows at cell interfaces, but can result in very small water depths that have to be modified to avoid unphysical results.
Audusse and Bristeau [5] proposed a general strategy based on a local hydrostatic reconstruction that allows the derivation of a well-balanced scheme from any solver for the homogeneous problem (Godunov, Roe, kinetic...). This technique yields a simple and fast well-balanced scheme that presents the advantage of preserving the non-negativity of the water height.
Valiani and Begnudelli [24] presented an approach characterized by simplicity and that takes its inspiration from the idea that the simplest way towards numerical closure of physical balances is the divergence form of physical laws, which leads to conservation of physical properties such as mass, momentum, energy and so on. The bed slope source term is strictly linked to a physical meaning, indeed it represents the static force due to the bed slope. This method is combined with a SGM variable reconstruction and allows the preservation of the quiescent water over irregular domains and steady flows. On the other hand a strong and restrictive hypothesis is made : the continuity of the bottom profile. To overcome this assumption, Caleffi and Valiani [9] presented another work where difficulties in the treatment of the bed slope source term arising from possible discontinuities of the bottom profiles are taken into account with a flux correction. Among these techniques found in the literature we choose to analyze and apply the hydrostatic reconstruction (Audusse) and the divergence form bed (Valiani), that seem simple with good numerical properties at the same time.

3.2.1 Hydrostatic reconstruction

Audusse [5] started from the assumption that cell-centered evaluations of the source term don't usually maintain steady states of a lake at rest in time, which are characterized by

$$h_i + z_i = const, \qquad u_i = 0 \tag{3.8}$$

He considers that in finite volume schemes we calculate the flux at the cell interface as

$$F_{i+1/2} = F(U_{i+1/2-}, U_{i+1/2+}) \tag{3.9}$$

where $U_{i+1/2}$ is the state at the interface of the cell, characterized by a value at the lef (-) and at the right (+).
His idea consists in deriving the two states at the right and at the left, from a local hydrostatic reconstruction, able to maintain steady states of a lake at rest and also to guarantee the non-negativity of water heights. The source term is discretized as

$$\mathbf{S}_i = \begin{pmatrix} 0 \\ (\frac{g}{2}h_{ij}^2 - \frac{g}{2}h_i^2)\mathbf{n}_{ij} \end{pmatrix} \tag{3.10}$$

where ij is a general interface between the vertex i and j, $\mathbf{n}_{ij}$ represents the normal in direction i-j and h_{ij} is the water depth evaluated as

$$h_{ij} = max(0, h_{ij}^*) \tag{3.11}$$

The water depth h_{ij}^* is the reconstructed value derived as

$$h_{ij}^* = (h_i + z_i - z_{ij}^*) \tag{3.12}$$

where $z_{ij}^* = max(z_i, z_j)$ is the reconstructed topography at the interface. This is a biased evaluation that guarantees non-negativity of the water height even when cells begin to dry out. The final finite volume discretization becomes

$$\mathbf{U}_i^{n+1} = \mathbf{U}_i^n - \sum_{j \in K} \sigma_{ij} F(\mathbf{U}_{ij}^{*n}, \mathbf{U}_{ji}^{*n}, \mathbf{n}_{ij}) - \sigma_i F(\mathbf{U}_i^n, \mathbf{U}_{ie}^n, \mathbf{n}_i) + \sum_{j \in K} \sigma_{ij} \mathbf{S}(\mathbf{U}_i^n, \mathbf{U}_{ij}^{*n}, \mathbf{n}_{ij}) \quad (3.13)$$

We can see that with a few and simple steps Audusse proposed a source term treatment that gives a stable and well-balanced scheme.
This drives us to test the application of this technique to our schemes.

3.2.2 Divergence Form for Bed slope source

This technique is based on the divergence form for the bed slope source and its main advantage is the independence of the numerical method used to solve the shallow water equations, in addition to its stability and simplicity. It has been presented by Valiani and Begnudelli [24] in 2008.
The bed slope source term for the one-dimensional shallow water equations (in x-direction) is $gh(-\partial z_b/\partial x)$. The authors demonstrate that this term can be written as

$$gh\left(-\frac{\partial z_b}{\partial x}\right) = \frac{\partial}{\partial x}\left(\frac{1}{2}gh^2\right)|_{\eta=const} \quad (3.14)$$

where $|_{\eta=const}$ means that the quantity is evaluated taking as a constant (with respect to x) the free surface elevation η. It's important to underline that the quantity η is taken as constant and so it can be moved inside or outside the spatial derivative. This means that we can write the source term $gh(-\partial z_b/\partial x)$ as the partial derivative with respect to x of the quantity $gh^2/2$ evaluated for a constant value of the free surface elevation η.
Moreover we can also interpret the equation (3.14) as

$$gh^*\left(-\frac{\partial z_b}{\partial x}\right) = \frac{\partial}{\partial x}\left(\frac{1}{2}gh^2\right)|_{\eta=const=\eta^*} \quad (3.15)$$

where η^*=average water surface level, evaluated over the same interval as for the average flow depth $h*$. In fact, the term on the right-hand side can be evaluated from the limit for vanishing Δx of

$$\frac{\partial}{\partial x}\left(\frac{1}{2}gh^2\right)|_{\eta=const=\eta^*} = \lim_{\Delta x \to 0} -g\frac{\Delta z_b}{\Delta x}\left(\eta * - \frac{z_{b2} + z_{b1}}{2}\right) \quad (3.16)$$

where $\Delta z_b = z_{b2} - z_{b1}$. Recalling that h^* and η^* have been defined as the average flow depth and water surface elevation, respectively, at a second-order approximation we have $\eta^* = h^* + (z_{b1} + z_{b2})/2$. For $\Delta x \to 0, \Delta z_b/\Delta x$ tends to $\partial z_b/\partial x$, so we obtain equation (3.15). This approximation is consistent with the overall second-order accuracy of the numerical model that has been used in the present study. The achievement of the second-order accuracy has been verified by the authors by an error norm analysis.
Concerning the values of η^* and h^*, that are constant and depending from the grid discretization, we specify that in the case of the finite volumes models they are constant within each computational cell.
We can now extend the source term treatment to the 2D SWEs, so we obtain:

$$\mathbf{S_0} = \begin{bmatrix} -gh\frac{\partial z_b}{\partial x} = \frac{\partial}{\partial x}\left(\frac{1}{2}gh^2\right)|_{\eta=\eta^*} \\ -gh\frac{\partial z_b}{\partial y} = \frac{\partial}{\partial y}\left(\frac{1}{2}gh^2\right)|_{\eta=\eta^*} \end{bmatrix} = -gh\nabla z_b = \nabla\left(\frac{1}{2}gh^2\right)|_{\eta=\eta^*} \quad (3.17)$$

If we introduce now the following matrix $\mathbf{H}$:

$$\mathbf{H} = [\mathbf{E}_b \qquad \mathbf{G}_b] = \begin{bmatrix} 0 & 0 \\ \frac{1}{2}gh^2 & 0 \\ 0 & \frac{1}{2}gh^2 \end{bmatrix} \tag{3.18}$$

Finally we rewrite the source term $\mathbf{S_0}$ in the divergence form

$$\mathbf{S_0} = \nabla \cdot \mathbf{H}|_{\eta=\eta^*} \tag{3.19}$$

Hence, we get the following compact form for the shallow water equations:

$$\frac{\partial \mathbf{U}}{\partial t} + \nabla \cdot \mathbf{F} = \nabla \cdot \mathbf{H}|_{\eta=\eta*} + \mathbf{S_f} \tag{3.20}$$

In [24], the authors prove also that the divergence form for bed slope source term is a suitable interpretation, demonstrating it for three important cases:

- Quiescent fluid over irregular bottom
- Hydraulic jump
- Uniform flow

We remark that we can apply this source term treatment to any mathematical models, but two important estimations are required: η^* and h^*.
So now we can formulate the DFB technique for a finite volume framework, as Valiani et al. did, but we consider a vertex-centred finite volume approach in which the domain is composed of an unstructured mesh made with triangles cells. We can integrate eq (3.20) in space over an arbitrary cell and applying the Gauss theorem we obtain:

$$\int_{K_i} \frac{\partial \mathbf{U}}{\partial t}\, \mathrm{d}V + \int_{\Gamma_i} \mathbf{F}(\mathbf{U}) \cdot \mathbf{n}_i d\Gamma = \int_{\Gamma_i} \mathbf{H}|_{\eta=\eta^*} \cdot \mathbf{n}_i d\Gamma + \int_{K_i} \mathbf{S_f}(\mathbf{U})\, \mathrm{d}V \tag{3.21}$$

So we can evaluate $\mathbf{H}$ as :

$$\int_{\Gamma_i} \mathbf{H}|_{\eta=\eta^*} \cdot \mathbf{n}_i d\Gamma = \begin{bmatrix} 0 \\ \int_{\Gamma_i} \frac{1}{2}gh^2|_{\eta=\eta^*} \mathbf{n}_x d\Gamma \\ \int_{\Gamma_i} \frac{1}{2}gh^2|_{\eta=\eta^*} \mathbf{n}_y d\Gamma \end{bmatrix} \tag{3.22}$$

The source term can be now discretized with the same procedure adopted for the flux term. The bed slope source term becomes:

$$\frac{\Delta t L_{ij}}{|K_i|} \mathbf{S}_0 = \begin{bmatrix} 0 \\ \sum_{j=1}^{m_i} \frac{1}{2}gh_r^2|_{\eta=\eta^*} \mathbf{n}_{xr} \\ \sum_{j=1}^{m_i} \frac{1}{2}gh_r^2|_{\eta=\eta^*} \mathbf{n}_{yr} \end{bmatrix} \tag{3.23}$$

where $\mathbf{n}_{xr}$ and $\mathbf{n}_{yr}$ are the Cartesian components of outward pointing normal unit vector, corresponding to the rth side of the cell; and h_r is the numerical flow depth related to this side (see 3.2). Finally, free surface elevation η^* and h_r are estimated as:

- $\eta^* = \eta_i$ where i is the index of the control volume
- $h_r(r = 1, ..., m) = \eta^* - z_r$ where z_r is evaluated as the average of the elevations of the two vertex of the side r.

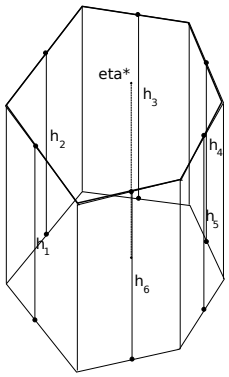

Figure 3.2: $\eta*$ and h_r for a control volume

The final finite volume discretization becomes:

$$\mathbf{U}_i^{n+1} = \mathbf{U}_i^n - \sum_{j \in K} \sigma_{ij} F(\mathbf{U}_{ij}^{*n}, \mathbf{U}_{ji}^{*n}, \mathbf{n}_{ij}) - \sigma_i F(\mathbf{U}_i^n, \mathbf{U}_{ie}^n, \mathbf{n}_i) + \sum_{j \in K} \sigma_{ij} \mathbf{S}(\mathbf{U}_i^n, \mathbf{U}_{ij}^{*n}, \mathbf{n}_{ij}) \quad (3.24)$$

If we compare this technique with the hydrostatic reconstruction, we remark that the DFB guarantees the well-balanceness as the HR (hydrostatic reconstruction), but in addition it guarantees the conservation of the total force across the hydraulic jump (that isn't true for the HR). Finally, the DFB technique is of second order accuracy.
From a computational point of view we also remark that the water depths ($h*$) is evaluated starting from a constant value of the free surface over the cell ($\eta*$). At the same time, in terms of flux calculation, when we use the DFB technique, we need a flux correction in order to take into account the discontinuity of the bed.
This flux correction is presented by Caleffi in [9]. The values at the interfaces are reconstructed starting from the results of the study of a steady flow over a step, based on a local total energy conservation.
On one hand, the DFB technique is based on a simple idea (the hydrostatic reconstruction too), but on the other hand, its application seems to be less easy then the hydrostatic reconstruction. As we will see in the next chapter, it will be also interesting to compare these explicit techniques with two schemes (Zokagoa and Tchamen) which have a different discretization of the source term.

Chapter 4

Finite volumes schemes in Telemac-2D

Telemac-2D is part of a bigger system, called TELEMAC, which is a software package initially built at the Electricite de France (EDF) and now managed by a consortium of core users (BudesAnstalt fur Wasserbau, Centre d'Etudes Techniques Maritimes et Fluviales, Daresbury Laboratory, EDF, HR Wallingford, Sogreah). The system TELEMAC is an integrated set of models in the domain of hydro environmental problems. TELEMAC is used mostly for dimensioning and impact studies, where safety issues are critical and, for this reason, reliability, validation and worldwide recognition of its capabilities are of utmost importance. This software includes different modules for different domains of application. We resume here its structure [29]:

- Hydrodynamic
  - Telemac-2D: 2D flows (Saint Venant equations)
  - Telemac-3D: 3D flows (Navier-Stokes equations)
  - Artemis: port agitation
  - Tomawac: wave propagation in costal areas
- Transport/Dispersion
  - Sisyphe: 2D Sedimentary transport
  - Sedi-3D: 3D Sedimentary transport in suspension
- Pre-/post processors
  - Rubens: graphic post-processor
  - Matisse: mesh generator
  - Stbtel: mesher interface
  - Postel-3D: extractor 2D from the 3D results
- SPH
  - Spartacus-2D: 2D Flows (Smoothed Particle Hydrodynamics)
- Underground flows

– Estel-2D

– Estel-3D

Historically TELEMAC was developed using the finite element method in the 1990s. The spatial domain is discretized with an unstructured mesh of triangular elements, which allows the refining of the mesh in the most interesting zones .
All the numerical algorithms have a common library that is called BIEF that guarantees coherence of the system. The mesh can be created with the generator integrated in the system (Matisse), but in our case we have used another software package, Janet.
In our work we focus on the Telemac-2D module in order to develop and to validate a stiff finite volume kernel. We note that three finite volume schemes were already present in the software package, which are Roe and the kinetic scheme of first and second order accuracy (2004), while the other four schemes are new and they are still considered a work in progress. Some specific targets have been reached, but we will speak about this in the next chapter.
We make some preliminary remarks about the input and output files used or created by Telemac-2D. In particular we will list what we have mostly used in this work. The input files are the following:

- the steering file (obligatory), containing the configuration of the computation
- the geometry file (obligatory), containing the mesh
- the boundary conditions file (obligatory), containing the description of the type of each boundary
- the Fortran file, containing the specific programming
- the liquid boundary file, containing information about the prescribed values at the open boundaries (elevations, flowrates...)
- the reference file, containing the "reference" results, which are used in the model validation
- the sections input file, containing the description of the control sections of the model (sections across which the flowrate is computed)

The output files are the following:

- the result file, containing the graphical results
- the listing printout, which is the "log file" of the computation
- the section output file, containing the results of the control section computations

Telemac-2D stores information in the results file during the computation. It contains first of all information about the mesh geometry, then the names of the stored variables. It also contains the time for of time step and the values of the different variables at all mesh points.

Finally, before starting with the detailed description of the finite volume schemes, we make some specifications about the scheme names used herein. In order to be coherent with the software package, we leave the same names present in Telemac-2D to call a scheme, but we specify that these names are used to identify a complete model, which has a specific way to calculate the numerical flux, with a specific source term treatment. Indeed the models presented have common aspects, including the time integration and the treatment of boundary conditions, but they differ in the source term treatment and in the flux calculation. This means that when we

describe the "HLLC scheme" it's important to know how is the source term is treated because HLLC refers only to a typical way to calculate the flux. For example, in the "Zokagoa scheme" we will not have a specific source term discretization because the bathymetry is already included in the flux term.

This chapter aims to present the schemes implemented in Telemac-2D, focusing on the new schemes. We will analyze the fundamental features of the new finite volume schemes (such as the source term treatment, the numerical flux calculation...) and we will provide an overview of the schemes existing in Telemac-2D.

4.1 Zokagoa and Tchamen scheme

Even if they are two different schemes, we treat them together because they make similar assumptions and have similar formulations of numerical flux.
The peculiarity of these schemes is that the numerical flux is calculated assuming a new set of unknowns values, where the first component is η and not h. This simplifies the fulfillment of certain properties but at the same time it complicates the treatment of other aspects, as we will see in the following paragraphs.
We apply to our framework what Zokagoa and Soulaimani proposed in [27], considering also the proposition of Tchamen [20], specifically for the bathymetry source term and the numerical flux.

4.1.1 Source terms

We can separate the source term in the bathymetry and in the friction term, as seen in (3.1).

4.1.1.1 Bathymetry

The treatment of this term is very important for simulations with complex beds which includes cases that are close to reality. The method proposed by Zokagoa and Tchamen is based on a divergent form of the bathymetry related integral term: $g\int_{K_i} h\nabla z \,\mathrm{d}\Omega$. Substituting z by $\eta - h$ we find:

$$\int_{K_i} h\nabla z \,\mathrm{d}\Omega = \int_{K_i} h\nabla\eta \,\mathrm{d}\Omega - \int_{K_i} \frac{1}{2}\nabla h^2 \,\mathrm{d}\Omega, \tag{4.1}$$

but the term $\int_{K_i} g\nabla h^2 \,\mathrm{d}\Omega$ is also present in the convection flux in equations (3.2) and (3.4), which becomes:

$$\mathbf{S}_{b_i} = \int_{K_i} gh\nabla\eta \,\mathrm{d}\Omega. \tag{4.2}$$

With this simplification, the convection flux h and the source term will be modified as we can see in the next sections.

Tchamen : proposed a local linearization of $\mathbf{S}_{b_i}$,
$\mathbf{S}_{b_i} = \bar{h}\int_{K_i} gh\nabla\eta \,\mathrm{d}\Omega$
The value of $\bar{h}$ is defined in accordance with the conservation properties and interface states (wet or dry cells).
The vectors $\mathbf{G}$ and $\mathbf{H}$ in equation (3.2) are rewritten as:

$$\mathbf{G}(\mathbf{V}) = \begin{bmatrix} hu \\ hu^2 + \bar{h}g\eta \\ huv \end{bmatrix}, \mathbf{H}(\mathbf{V}) = \begin{bmatrix} hu \\ huv \\ hv^2 + \bar{h}g\eta \end{bmatrix} \tag{4.3}$$

where $\mathbf{V} = [\eta \quad hu \quad hv]^T$ is the new set of unknowns.

Zokagoa : proposed a non linear model, derived in order to compute more accurately the propagation of discontinuities. The water depth in equation 4.2 is substituted by the difference between the free surface and the bottom levels: $h = \eta - z$, but with the constraint $h = \eta - z > 0$, so:
$\mathbf{S}_{b_i} = \int_{K_i} gh\nabla \,\mathrm{d}\Omega = \int_{K_i} g\nabla(\frac{\eta^2}{2})\,\mathrm{d}\Omega - \int_{K_i} gz\nabla\eta \,\mathrm{d}\Omega$
Evaluating the term $\int_{K_i} gz\nabla\eta \,\mathrm{d}\Omega$ as $g\bar{z}\int_{K_i} \nabla\eta \,\mathrm{d}\Omega$, he approximated
$\mathbf{S}_{b_i} \approx g\int_{K_i} \nabla(\frac{\eta^2}{2} - \bar{z}\eta)\,\mathrm{d}\Omega$
where $\bar{z}$ is an averaged value of the bed level, defined in accordance with the conservation properties.
The vectors $\mathbf{G}$ and $\mathbf{H}$ are rewritten as:

$$\mathbf{G}(\mathbf{V}) = \begin{bmatrix} hu \\ hu^2 + g\frac{\eta^2}{2} - \bar{z}g\eta \\ huv \end{bmatrix}, \mathbf{H}(\mathbf{V}) = \begin{bmatrix} hu \\ huv \\ hv^2 + g\frac{\eta^2}{2} - \bar{z}g\eta \end{bmatrix} \tag{4.4}$$

The Tchamen model is very robust but less accurate than Zokagoa model, which shows better resolution of discontinuities. These two simplifications of the bathymetry source term will be significant for the flux calculation and the wet/dry treatment.

4.1.1.2 Friction

Following the simplifications in section 4.1.1.1, the global source term is reduced to the friction source term, or:

$$\mathbf{S}(\mathbf{U}) = \begin{bmatrix} 0 & -gh\dfrac{u\sqrt{u^2+v^2}}{k^2h^{\frac{4}{3}}} & -gh\dfrac{v\sqrt{u^2+v^2}}{k^2h^{\frac{4}{3}}} \end{bmatrix}^T, \tag{4.5}$$

which can be integrated over a control volume, through the expressions:

$$\begin{cases} \int_{K_i} ghS_{f_x} d\Omega \approx |K_i| gh_i S_{f_x} = |K_i| gh_i \frac{u\sqrt{u^2+v^2}}{k^2h^{\frac{4}{3}}} \\ \int_{K_i} ghS_{f_y} d\Omega \approx |K_i| gh_i S_{f_y} = |K_i| gh_i \frac{v\sqrt{u^2+v^2}}{k^2h^{\frac{4}{3}}}, \end{cases} \tag{4.6}$$

where k is the Strickler coefficient. The contribution of the friction term in time will be calculated with a semi-implicit scheme, explained in section 4.5.

4.1.2 Numerical flux

Due to the rotational invariance property, the flux can be approximated as a solution of a Riemann problem defined by solutions on the left and right sides of the interface Γ_{ij} corresponding to the states $(\mathbf{U_i}, \mathbf{U_j})$. In this case, we will consider the new set of unknown variables:

$$\mathbf{V} = [\eta \quad hu \quad hv]^T \tag{4.7}$$

for each cell K_i, which allows us to consider a 1D Riemann problem with the states $(\mathbf{V_i}, \mathbf{V_j})$. η is calculated as $\eta = h + z$ and u and v are given by $\frac{(hu)_i}{h_i}$ and $\frac{(hv)_i}{h_i}$.
The scheme used for the flux calculation is a simple centered type, with an artificial dissipative

term introduced in order to avoid instabilities. The numerical flux at each interface Γ_{ij} is defined as:

$$\tilde{\mathbf{F}}_{\mathbf{ij}}(\mathbf{V_i}, \mathbf{V_j}, \mathbf{n_{ij}}) = \frac{1}{2}\left[\mathbf{G}(\mathbf{T}_{\mathbf{n_{ij}}} \cdot \mathbf{V_i}) + \mathbf{G}(\mathbf{T}_{\mathbf{n_{ji}}} \cdot \mathbf{V_j})\right] - \frac{1}{2} D_{ij}(\mathbf{V_j} - \mathbf{V_i}), \tag{4.8}$$

where $\mathbf{G}$ depends on the use of the Zokagoa or Tchamen scheme, and D_{ij} is a stabilizing parameter, such a viscosity, that must be defined.

Tchamen : supposed that the averaged water depth $\bar{h}$ was equal to the water depth of the current cell h_i, so $\bar{h} = h_i$ and we have:

$$\tilde{\mathbf{F}}_{\mathbf{ij}}(\mathbf{V_i}, \mathbf{V_j}, \mathbf{n_{ij}}) = \frac{1}{2}\begin{bmatrix} h_i, u_{i,n} + h_j, u_{j,n} \\ h_i, u_{j,n}^2 + g h_i(\eta_i + \eta_j) \\ h_i, u_{i,n} v_{i,n} + h_j, u_{j,n} v_{j,n} \end{bmatrix} - \frac{1}{2} D_{ij} \begin{bmatrix} \eta_j - \eta_i \\ h_j u_{j,n} - h_i u_{i,n} \\ h_j v_{j,n} - h_i v_{i,n}, \end{bmatrix} \tag{4.9}$$

where $u_{k,n} = u_k n_{ij}^x + v_k n_{ij}^y$ and $v_{k,n} = v_k n_{ij}^x + u_k n_{ij}^y$ (k=ij)

Zokagoa : supposed that $\bar{z} = z_i$ and therefore the flux becomes:

$$\tilde{\mathbf{F}}_{\mathbf{ij}}(\mathbf{V_i}, \mathbf{V_j}, \mathbf{n_{ij}}) = \frac{1}{2}\begin{bmatrix} h_i, u_{i,n} + h_j, u_{j,n} \\ h_i, u_{j,n}^2 + \frac{1}{2} g(\eta_i^2 + \eta_j^2) - g z_i(\eta_i + \eta_j) \\ h_i, u_{i,n} v_{i,n} + h_j, u_{j,n} v_{j,n} \end{bmatrix} - \frac{1}{2} D_{ij} \begin{bmatrix} \eta_j - \eta_i \\ h_j u_{j,n} - h_i u_{i,n} \\ h_j v_{j,n} - h_i v_{i,n}, \end{bmatrix} \tag{4.10}$$

where $u_{k,n} = u_k n_{ij}^x + v_k n_{ij}^y$ and $v_{k,n} = v_k n_{ij}^x + u_k n_{ij}^y$ (k=ij).

We have tested two possible expressions for D_{ij}:

- Toro's choice : $D_{ij} = max|u_{i,n}| + \sqrt{g h_i}, |u_{j,n} + \sqrt{g h_j}|$
- Zokagoa's choice : $D_{ij} = \Lambda_{ij} = \alpha max|\bar{u}_{ij,n} - \bar{c}_{ij,n}| \cdot |\bar{u}_{ij,n}| \cdot |\bar{u}_{ij,n} + \bar{c}_{ij,n}|$
  where $0 \leq \alpha \leq 1$, $\bar{u}_{ij,n} = \frac{u_{i,n} + u_{j,n}}{2}$ and $\bar{c_{ij}}_{,n} = \sqrt{g \frac{h_i + h_j}{2}}$.

In our simulations, we will use the expression given by Zokagoa because it allows us to manipulate the parameter α, which influences the diffusion. Additionally, we note that we compute the numerical fluxes only if one of the two cells is wet.
This flux formulation, which includes the bed terms, verifies two important properties: the global mass conservation and the exact C-property (demonstrated in [27]).

4.1.3 Wet/dry interface treatment

A particular section is dedicated to this problem due to the fact that a river can occasionally rise and flood surrounding plains. From a numerical point of view, this phenomenon creates instabilities due to water depths that tend to zero and can consequently generate large and non-physical velocities.
For these schemes, the new variable η in the flux calculation requires a different treatment at the wet/dry interface. Indeed the system of partial equation is valid only for positive water depths, or $h = \eta - z > 0$, which is why we must avoid a flux calculation when h is very small or zero. Furthermore, we need to compute fluxes at the interfaces only when it is physically possible. For instance, at an interface Γ_{ij} between a wet cell (where $h_i > \varepsilon$) and a dry cell (where $h_j < \varepsilon$), when $z_j \leq \eta_i$ gravity and inertia forces make it possible for water to flow from

the upper wet to the dry cell.
For a water front advancing over an adverse steep slope $z_j > \eta_i$ (or $z_i > \eta_j$), a free surface correction (FSC) is enforced. The aim is to avoid the creation of a free surface gradient ($\nabla\eta \neq 0$) which is resposable for an unphysical flux across the edge Γ_{ij} leading to numerical spurious oscillations. The threshold value chosen for this calculation is very important and after several tests we set $\varepsilon = 10^{-6}m$ in order to have the highest quality results in the test cases (see 5). The imposed conditions are the followings:

$$\text{if} \begin{cases} \eta_i < z_j \\ h_i > \varepsilon \geq h_j \\ u_{i,n} \geq 0 \\ \frac{u_i^2}{2g} + h_i + z_i \geq 0 \end{cases} \quad \text{then} \begin{cases} \eta_i = \eta_j \\ z_j = \eta_i \\ h_j = 0 \\ u_j = v_j = 0 \end{cases} \tag{4.11}$$

The velocity condition implies that the water flows from the wet cell to the dry cell and the energy condition assures that the fluid has the minimum energy to make the possible passage from the wet to the dry cell. The condition imposed ensures that the flux computation at the interface should avoid this motion during the time step.
We impose the same conditions, changing the index, for a flow with $u_{j,n} \leq 0$.

4.2 Harten, Lax, van Leer, Contact (HLLC) scheme

4.2.1 The HLLC flux

The HLLC (C standing for Contact, the missing wave) is a modification proposed by Toro [22] of the basic HLL (Harten, Lax, van Leer) scheme that is correct for purely one dimensional problems without extra species-like equations. Indeed the HLL approach requires estimates of the wave speeds S_L and S_R for the smallest and largest signal velocities in the solution of the Riemann problem with data $\mathbf{U}_L = \mathbf{U}_i^n$, $\mathbf{U}_R = \mathbf{U}_{i+1}^n$ and corresponding fluxes $\mathbf{F}_L = \mathbf{F}(\mathbf{U}_L)$, $\mathbf{F}_R = \mathbf{F}(\mathbf{U}_R)$. This approach ignores the influence of the intermediate waves, such as shear weaves and contact discontinuities. To account for the influence of intermediate waves, we need consider another intermediate speed, called S_*.
To analyze the HLLC scheme, we start considering a general initial boundary value problem, where we know the intercell numerical flux

$$\mathbf{F}_{i+\frac{1}{2}} = \mathbf{F}(\mathbf{U}_{i+\frac{1}{2}}(0)), \tag{4.12}$$

in which $\mathbf{U}_{i+\frac{1}{2}}(0)$ is the exact similarity solution $\mathbf{U}_{i+\frac{1}{2}}(x/t)$ of the Riemann problem

$$\text{PDE:} \quad \frac{\partial \mathbf{U}}{\partial t} + \frac{\partial \mathbf{F}(\mathbf{U})}{\partial x} = 0 \tag{4.13}$$

$$\text{IC:} \quad \mathbf{U}(\mathbf{x}, \mathbf{0}) = \begin{cases} \mathbf{U_L} & \text{if} \quad x < 0 \\ \mathbf{U_R} & \text{if} \quad x > 0 \end{cases} \tag{4.14}$$

evaluated at $x/t = 0$. The structure of the exact solution of the Riemann problem for the x-split is presented in the figure 4.1.

The solution in the star region consists of two constant states separated from each other by a middle wave of speed S_*
With HLLC, we want to find direct approximations of the flux function $\mathbf{F}_{i+\frac{1}{2}}$. The HLLC

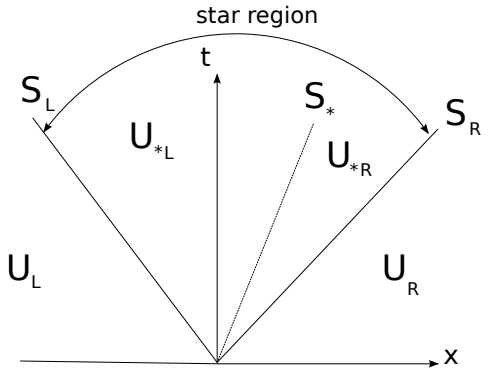

Figure 4.1: Structure of the exact solution for the Riemann problem

approximate Riemann solver is as follows:

$$\tilde{\mathbf{U}}(x,t) = \begin{cases} \mathbf{U_L}, & \text{if} \quad \frac{x}{t} \leq S_L \\ \mathbf{U_{*L}}, & \text{if} \quad S_L \leq \frac{x}{t} \leq S_* \\ \mathbf{U_{*R}}, & \text{if} \quad S_* \leq \frac{x}{t} \leq S_R \\ \mathbf{U_R}, & \text{if} \quad \frac{x}{t} \geq S_R \end{cases} \tag{4.15}$$

The three star states are

$$\mathbf{U}_{*K} = h_K \left(\frac{S_K - \mathbf{U}_K}{S_K - S_*} \right) \begin{bmatrix} 1 \\ S_* \\ v_K \end{bmatrix}, \tag{4.16}$$

with $k = L, R$. We seek a corresponding HLLC numerical flux defined as

$$\mathbf{F}^{hllc}_{i+\frac{1}{2}} = \begin{cases} \mathbf{F_L}, & \text{if} \quad 0 \leq S_L \\ \mathbf{F_{*L}}, & \text{if} \quad S_L \leq 0 \leq S_* \\ \mathbf{F_{*R}}, & \text{if} \quad S_* \leq 0 \leq S_R \\ \mathbf{F_R}, & \text{if} \quad 0 \geq S_R \end{cases}, \tag{4.17}$$

with the intermediate fluxes $\mathbf{F_{*L}}$ and $\mathbf{F_{*R}}$ still to be determined. Figure 4.2 shows the of the HLLC approximate Riemann solver.

By integrating over appropriate control volumes, or more directly, by applying the Rankine-Hugoniot condition for each of the waves speeds S_L, S_*, S_R, we obtain

$$\mathbf{F}_{*L} = \mathbf{F}_L + S_L(\mathbf{U_{*L}} - \mathbf{U}_L) \tag{4.18}$$

$$\mathbf{F}_{*R} = \mathbf{F}_{*L} + S_L(\mathbf{U_{*R}} - \mathbf{U}_{*L}) \tag{4.19}$$

$$\mathbf{F}_{*R} = \mathbf{F}_R + S_R(\mathbf{U_{*R}} - \mathbf{U}_R) \tag{4.20}$$

These conditions are sufficient to ensure consistency, as demonstrated by Toro and they are the three equations for the four unknowns vectors $\mathbf{U}_{*L}, \mathbf{F}_{*L}, \mathbf{U}_{*R}, \mathbf{F}_{*R}$. Before a summary of the steps required to estimate the wave speeds, which allow us to find the four unknowns values, we note some basic conditions that we need to impose in order to satisfy the exact solution of the problem. For water depth and normal component of velocity we have:

$$\begin{aligned} h_{*L} &= h_{*R} = h_* \\ u_{*L} &= u_{*R} = u_* \end{aligned} \tag{4.21}$$

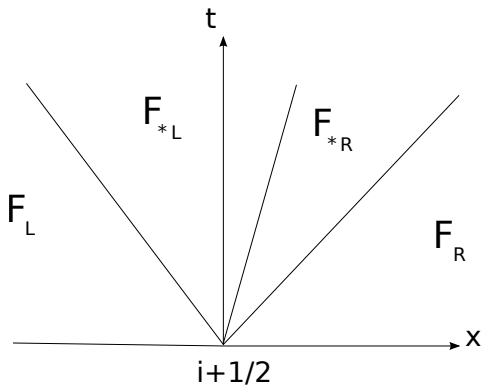

Figure 4.2: Evaluation of the HLLC flux related to the Riemann problem of figure 4.1

and for tangential velocity component we have:

$$\begin{aligned} v_{*L} &= v_L \\ v_{*R} &= v_R \end{aligned} \tag{4.22}$$

Thus the wave speed estimates are based on depth and particle velocity in the star region, so

- we evaluate h_* and u_*

$$h_* = \frac{(h_L + h_R)}{2} - \frac{1}{4}\frac{(u_R - u_L)(h_L + h_R)}{c_L + c_R} \tag{4.23}$$

$$u_* = \frac{(u_L + u_R)}{2} - \frac{1}{4}\frac{(h_R - h_L)(c_L + c_R)}{h_L + h_R} \tag{4.24}$$

  with $c = \sqrt{gh}$

- we set
  - $S_L = u_L - c_L q_L$
  - $S_* = u_*$
  - $S_R = u_R - c_R q_R$

- we detect if we are in presence of a shock or a refracted wave through a comparison between the values $h_{L,R}$ with h_*. In this way we can calculate the coefficients q_L and q_R.

$$q_K = \begin{cases} 1 & \text{if} \quad h_* \leq h_K, \quad \text{rarefraction} \\ \sqrt{\frac{1}{2}\left[\frac{(h_* + h_K)h_*}{h_K^2}\right]} & \text{if} \quad h_* > h_K, \quad \text{shock} \end{cases} \tag{4.25}$$

In this way, we are able to define the HLLC numerical flux expressed by (4.17)

4.2.2 Source terms

4.2.2.1 Bathymetry

The discretization of the topography source term is crucial for the goodness of numerical properties of schemes. The chosen method has to guarantee the well-balanceness or the C-property.

This means that the final scheme has to conserve a lake at rest i.e. for a constant free surface $h + z = const$ and a zero velocity $\mathbf{u} = (0, 0)$, no artificial (spurious) movement of water is allowed to appear.
In [4], Audusse et al. have presented a general way to handle geometric source terms in order to ensure the well-balanceness. The hydrostatic reconstruction can be applied with any consistent scheme. The main steps are the following:

- Define an interface topography, starting with a piecewise constant approximation of the bottom topography. For the interface between vertex i and j, we define $z_{ij} = z_{ji} = max(z_i, z_j)$
- Define the interface water depth: considering the previous definition of interface topography, a water depth at the interface (hydrostatic reconstructed water depth) can be obtained as : $h^*_{ij} = (h_i + z_i - z_{ij})_+$ and thus a new variable set at the interface, is obtained:
$$\mathbf{U}^*_{ij} = (h^*_{ij}, h^*_{ij}u, h^*_{ij}v)^T \tag{4.26}$$
It's important to note that $h^*_{ij} \leq h_i$ ensures the positivity property of the scheme.
- From the hydrostatic balance, $\nabla(gh^2/2) = -gh\nabla z$, the new discretization of geometric source term is written as:
$$\mathbf{S}(\mathbf{U}_i, \mathbf{U}^*_{ij}, \mathbf{n}_{ij}) = \begin{pmatrix} 0 \\ \frac{g}{2}(h^{*2}_{ij} - h^2_i)\mathbf{n}_{ij} \end{pmatrix} \tag{4.27}$$
- The final finite volume solution of the shallow water system is found by combining equation (4.26) into the classical incell values flux expression (3.4), which gives:
$$\mathbf{U}^{n+1}_i = \mathbf{U}^n_i - \sum_{j\in K} \sigma_{ij} F(\mathbf{U}^{*n}_{ij}, \mathbf{U}^{*n}_{ji}, \mathbf{n}_{ij}) - \sigma_i F(\mathbf{U}^n_i, \mathbf{U}^n_{ie}, \mathbf{n}_i) + \sum_{j\in K} \sigma_{ij} \mathbf{S}(\mathbf{U}^n_i, \mathbf{U}^{*n}_{ij}, \mathbf{n}_{ij}) \tag{4.28}$$

4.2.2.2 Friction

The friction term is evaluated as described in section 4.1.1.2.

4.3 Weighted average flux (WAF) scheme

4.3.1 The WAF approach

The WAF method was suggested first by Toro (1989) in [23]. It is assumed to guarantee second order accuracy in time and space. Second order accuracy in space is obtained with no need of data reconstruction. We first present the method in the one dimensional case and later we generalize it to two dimensions. Two versions of the WAF method can be considered:

4.3.1.1 Original version of the WAF scheme: a weighted average flux

The original version of the WAF scheme is a weighted sum of the fluxes in all regions of the solution of the piecewise constant data Riemann problem[23], namely:

$$\mathbf{F}_{\mathbf{i}+\frac{1}{2}} = \frac{\mathbf{1}}{\mathbf{\Delta x}} \int_{-\frac{\mathbf{\Delta x}}{\mathbf{2}}}^{\frac{\mathbf{\Delta x}}{\mathbf{2}}} \mathbf{F}\left(\mathbf{U}_{\mathbf{i}+\frac{1}{2}}(\mathbf{x}, \frac{\mathbf{\Delta t}}{\mathbf{2}})\right) \mathbf{dx}, \tag{4.29}$$

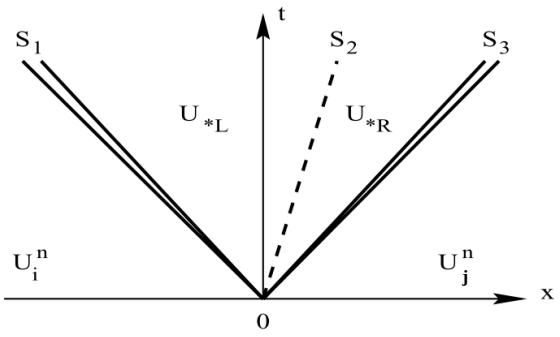

Figure 4.3: x-t diagram for the solution of the Riemann problem defined by left ($\mathbf{U_i}$) and right ($\mathbf{U_j}$) states [23].

where $\mathbf{U}_{\mathbf{i}+\frac{\mathbf{1}}{\mathbf{2}}}(\mathbf{x},\mathbf{t})$ is the solution of the following Riemann problem:

$$\text{PDE:} \quad \frac{\partial \mathbf{U}}{\partial t} + \frac{\partial \mathbf{F}(\mathbf{U})}{\partial x} = 0, \tag{4.30}$$

$$\text{IC:} \quad \mathbf{U}(\mathbf{x},\mathbf{0}) = \begin{cases} \mathbf{U_i^n} & \text{if} \quad x < 0 \\ \mathbf{U_i^{n+1}} & \text{if} \quad x > 0 \end{cases} \tag{4.31}$$

$\mathbf{U}_{\mathbf{i}+\frac{\mathbf{1}}{\mathbf{2}}}(\mathbf{x},\mathbf{t})$ can be obtained by an exact resolution of the Riemann problem (4.30,4.31), which is the case with first-order Godunov scheme. Approximate Riemann solver could be also used. For the shallow water equations, (x,t) diagram contains four constant states separated by three wave speeds (see figure 4.3). We will denote the wave speeds by S_1, S_2 and S_3 and the four (different) constant states by $\mathbf{U_i^n}$, $\mathbf{U_L^*}$, $\mathbf{U_R^*}$ and $\mathbf{U_{i+1}^n}$. Depending on the nature of the shock, additional intermediate states can appear inside fan of rarefaction waves. We will consider here the cases with no rarefaction shocks. These cases need special treatment if an exact Riemann solver is used. However, if an approximate Riemann solver (which provides a complete flux) is used, this special treatment is not required. This is the case for this work while we use the HLLC flux.
To evaluate the integral (4.29), we can easily deduce from figure (4.4), that:

$$\mathbf{F}_{\mathbf{i}+\frac{\mathbf{1}}{\mathbf{2}}} = \sum_{\mathbf{k=1}}^{\mathbf{N+1}} \beta_{\mathbf{k}} \mathbf{F}^{(\mathbf{k})}_{\mathbf{i}+\frac{\mathbf{1}}{\mathbf{2}}} \tag{4.32}$$

where:

- $\mathbf{F}^{(\mathbf{k})}_{\mathbf{i}+\frac{\mathbf{1}}{\mathbf{2}}} = \mathbf{F}(\mathbf{U}^{(\mathbf{k})})$,
- $\mathbf{U}^{(\mathbf{1})} = \mathbf{U_i^n}$, $\mathbf{U}^{(\mathbf{2})} = \mathbf{U_L^*}$, $\mathbf{U}^{(\mathbf{3})} = \mathbf{U_R^*}$ and $\mathbf{U}^{(\mathbf{4})} = \mathbf{U_{i+1}^n}$,
- N is the number of waves in the solution of the Riemann problem,

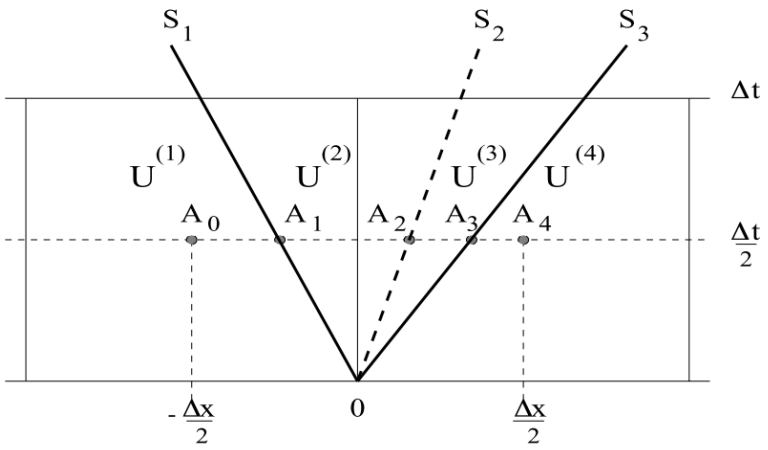

Figure 4.4: WAF diagram [23]

- β_k $(k = 1, \ldots, N+1)$ are the normalized lengths of the segments $A_k A_{k+1}$, which correspond to the difference between the Courant numbers c_k for successive wave speeds S_k:

$$\beta_k = \frac{|A_k A_{k+1}|}{\Delta x} = \frac{1}{2}(c_k - c_{k-1}) \tag{4.33}$$

$$c_k = \frac{\Delta t S_k}{\Delta x}; \quad c_0 = -1 \text{ and } c_{N+1} = 1 \tag{4.34}$$

We can see that equation (4.32) is the weighted average of the flux $\mathbf{F}$.

4.3.1.2 A weighted average state version

An alternative way to obtain a weighted average flux is to compute the flux over a weighted average state $\overline{\mathbf{W}}_{i+\frac{1}{2}}$. First, we define

$$\overline{\mathbf{W}}_{i+\frac{1}{2}} = \frac{1}{\Delta x} \int_{-\frac{\Delta x}{2}}^{\frac{\Delta x}{2}} \mathbf{W}_{\mathbf{i+\frac{1}{2}}}(\mathbf{x}, \frac{\mathbf{\Delta t}}{\mathbf{2}}) \mathbf{dx}, \tag{4.35}$$

which can be discretized using the notation of figure (4.4) as:

$$\overline{\mathbf{W}}_{i+\frac{1}{2}} = \sum_{k=1}^{N+1} \beta_k \overline{\mathbf{W}}^{(k)}_{i+\frac{1}{2}} \tag{4.36}$$

where β_k are the same as defined before. Then, the flux is evaluated over this weighted state such as:

$$\mathbf{F}_{\mathbf{i+\frac{1}{2}}} = \mathbf{F}(\overline{\mathbf{W}}_{\mathbf{i+\frac{1}{2}}}) \tag{4.37}$$

For the 2D shallow water equations, one can use $\overline{\mathbf{W}} = (h, u, v)$, where u and v are the x and y components of the velocity. If one or many tracers are present, these could be added to $\overline{\mathbf{W}}$. The numerical treatment of tracers is similar to the y-component of the velocity.
As for the computational cost, equation (4.37) is more advantageous than (4.32) because the flux is evaluated once.

4.3.2 The WAF scheme on unstructured meshes

In spite of the good numerical aspects of the WAF scheme, the literature dedicated to this scheme is not rich. Moreover, the rare 2D applications use structured meshes through the dimensional splitting approach (see for example [7] and [8]). Loukili and Soulaimani [17] gave the only application of the WAF scheme on unstructured mesh. Here we will try to follow and improve this application to handle more efficiently the aspects related to wetting/drying, stabilization, well-balanceness, etc. in order to give a general framework for the use of the WAF scheme with the shallow water equations on unstructured meshes and with real topography.
In this section, we will apply the WAF approach to the shallow water equations in 2D on unstructured meshes with variable topography. Following the suggestion of Loukili [17], the two first components of the flux are taken as a weighted average of the HLLC scheme. The third component is a weighted average of the WAF flux itself. These assumptions give:

$$\widetilde{\mathbf{F}}_i^{WAF}(\mathbf{U_L}, \mathbf{U_R}) = \omega_{\mathbf{L}}\mathbf{F_i}(\mathbf{U_L}) \; + \; \omega_{\mathbf{LR}}\widetilde{\mathbf{F}}^{\mathbf{HLLC}}(\mathbf{U_L}, \mathbf{U_R}) \; + \; \omega_R\mathbf{F_i}(\mathbf{U_R}) \qquad \text{for i = 1,2} \tag{4.38}$$

$$\widetilde{\mathbf{F}}_3^{WAF}(\mathbf{U_L}, \mathbf{U_R}) = (\omega_{\mathbf{L}*}\,\mathbf{v_L} \; + \; \omega_{\mathbf{R}*}\mathbf{v_R}) \; \widetilde{\mathbf{F}}_{\mathbf{1}}^{\mathbf{WAF}}(\mathbf{U_L}, \mathbf{U_R}) \tag{4.39}$$

where the weights are given as:
$\omega_L = (1 + c_L)/2$, $\omega_R = (1 - c_R)/2$, $\omega_{LR} = (c_R - c_L)/2$, $\omega_{L*} = (1 + c_*)/2$ and $\omega_{R*} = (1 - c_*)/2$
$c_L = S_L\Delta t/\Delta x$, $c_R = S_R\Delta t/\Delta x$ and $c_* = S_*\Delta t/\Delta x$ are local Courant numbers for the left, right and star waves respectively. In our case, we have chosen $\Delta x = D$, where D is the diameter of the largest circle belonging to the control volume (the encircled). It is given by $D_i = min(d_{ij})$, where d_{ij} is the distance between node i and the surrounding vertex j of the polygonal control volume.

4.3.3 A TVD version of the scheme

The WAF scheme is second order in time and space. According to Godunov theorem, spurious oscillation could appear in areas with large gradients or in the vicinity of shock waves. Toro [22] extended the original version of the WAF scheme to satisfy the Total Variation Diminishing (TVD) version of the scheme. He clearly noted that this extension is empirical in a strict theoretical point of view; however, in practice, the TVD WAF scheme works well. We will see later that this TVD extension performs well for the case of shallow water equations.
The TVD extension of the WAF scheme applied to the shallow water equations, is an empirical generalization of the procedure rigorously applied to the scalar case, in which there is one conservation law and one wave. For our case, where we are in presence of three waves, we can assume that the solution of the entire system is characterized by *a jump in a single quantity q* across each wave [22]. The use of limiter functions (one for each intercell edge) is necessary to evaluate the flux and more specifically the weighting coefficients. These coefficients become:

$$\omega_L = (1 + sign(c_L)A(r_L, c_L))/2$$

$$\omega_R = (1 - sign(c_R)A(r_R, c_R))/2$$

$$\omega_{LR} = (sign(c_R)A(r_R, c_R) - sign(c_L)A(r_L, c_L))/2$$
$$\omega_{L*} = (1 + sign(c_*)A(r_*, c_*))/2$$
$$\omega_{R*} = (1 - sign(c_*)A(r_*, c_*))/2$$

where $A(r, c) = 1-(1-|c|)\phi(r)$ and $\phi(r)$ are the well-known limiter functions such as Superbee, van Albada, minmod etc. We refer to the excellent paper of Kemm [12] for a comparative study of these limiters. The flow parameter $r^{(k)}(q)$, for each wave k is given by:

$$r^{(k)} = \begin{cases} \frac{\Delta q^{(k)}_{i-\frac{1}{2}}}{\Delta q^{(k)}_{i+\frac{1}{2}}}, & \text{if } c_k > 0 \\ \frac{\Delta q^{(k)}_{i+\frac{3}{2}}}{\Delta q^{(k)}_{i+\frac{1}{2}}}, & \text{if } c_k < 0 \end{cases} \tag{4.40}$$

As recommended by Toro [22] and Loukili [17], q is chosen as h (water depth) for left (L) and right (R) waves and as the tangential velocity component v for the star wave.
$\Delta q^{(k)}_{i-\frac{1}{2}}$ denotes the jump of the quantity q across the wave k in the solution $\mathbf{U}_{i-\frac{1}{2}}$ of the Riemann problem defined with data ($\mathbf{U}^n_{i-1}$,$\mathbf{U}^n_i$). $\Delta q^{(k)}_{i+\frac{1}{2}}$ is the jump of the quantity q across the wave k in the local Riemann problem solution $\mathbf{U}_{i+\frac{1}{2}}$ with data ($\mathbf{U}^n_i$,$\mathbf{U}^n_{i+1}$); and finally $\Delta q^{(k)}_{i+\frac{3}{2}}$ is the jump across the wave k in the solution $\mathbf{U}_{i+\frac{3}{2}}$ in the Riemann problem solution with data ($\mathbf{U}^n_{i+1}$,$\mathbf{U}^n_{i+2}$) (see figure 4.6).

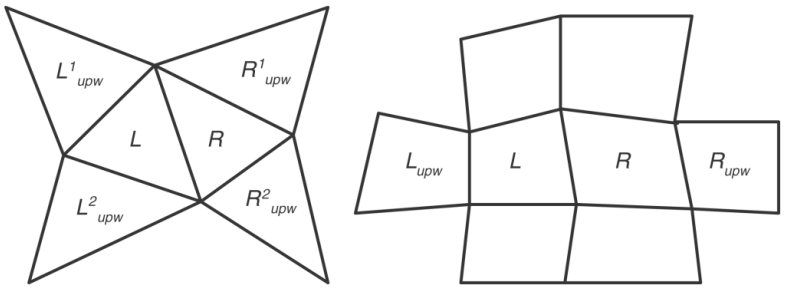

Figure 4.5: Choice for upwinding volumes for the case of cell-centered case, figure from [17]

For the 1D or 2D structured meshes, as well as, for quadrangular meshes, the choice of neighboring nodes (i-1, i+1 and i+2) is obvious. However, it is not the case for the unstructured mesh. This choice is less trivial for vertex-centered than for cell-centered finite volume description. Loukili [17] proposed the choice illustrated by figure 4.5 for the cell-centered case. For our vertex centered case, the choice is less obvious and we need to define the upwinding volumes [3]. For a node i, the immediate neighbor is denoted i+1 (see figure 4.6). The next

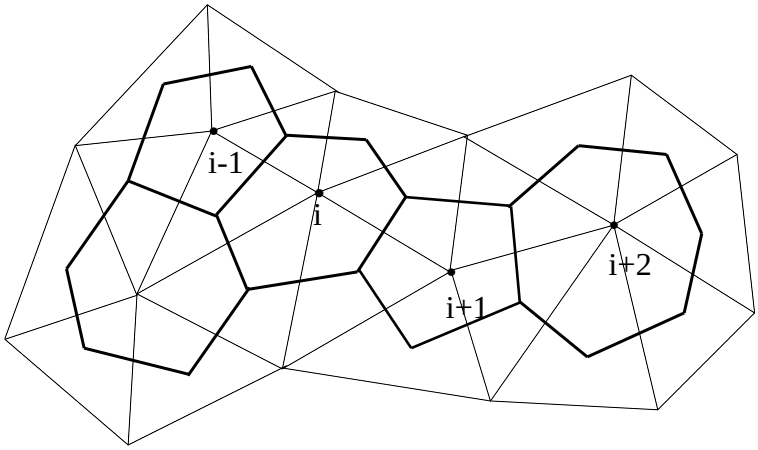

Figure 4.6: How to chose the upwinding for the TVD version of the WAF scheme

neighbor (in the direction of i+1) can be chosen as the closest vertex to the segment [i,i+1]. One can also chose the two closest nodes (indicated later by the superscripts 1 and 2) to [i,i+1] and use their mean values weighted by the distance to [i,i+1] as $q_{i+2} = 1/(d^1 + d^2)(d^2 q^1_{i+2} + d^1 q^2_{i+2})$. The identification of the neighbors and the neighbors of the neighbors is achieved once at the preprocessing step at the beginning of the computation.

4.3.4 Source terms

4.3.4.1 Bathymetry

Even with this scheme we use the discretization of topography source term presented by Audusse [4] and described in section 4.2.2.1 for the HLLC scheme.

4.3.4.2 Friction

The friction term is evaluated as described in section 4.1.1.2.

4.4 Boundary conditions

In this work we consider only two types of boundaries: solid walls and liquid boundaries. Referring to equation (3.4), we need to define the status U_e, which represents the values in a fictitious cell adjacent to the boundary. In the case of a solid wall, we impose a perfect slip condition in order to obtain the continuity of the tangential component. In mathematical terms,

this means imposing $\mathbf{u} \cdot \mathbf{n} = 0$.
On the other hand, in the case of a fluid boundary, we need to distinguish two subcases: the torrential case and the fluvial case. It will be necessary to specify for every point along the boundary, a number of conditions equal to the number of characteristics, which depends on the regime.
We recall that a torrential regime is characterized by $|\mathbf{u}| > c$ or $Fr > 1$ (where c is the celerity and Fr is the Froude number), while in a fluvial regime, $|\mathbf{u}| > c$ or $Fr < 1$. Following the theory of the characteristics, for a fluvial boundary we will prescribe one condition at the inlet and one condition at the outlet because for every point there is one incoming and one ingoing characteristic. For a torrential inlet we will prescribe two upstream conditions because we have two ingoing characteristics.

4.5 Time discretization

The user can choose two types of time discretizations in Telemac-2D.
The first one, which is also the first one implemented, is the Euler explicit scheme of first order. The formulation is:

$$\mathbf{U}_i^{n+1} = \mathbf{U}_i^n + \frac{\Delta t}{K_i}\mathbf{N}^n \tag{4.41}$$

where $\mathbf{N}^n = \mathbf{F}^n + \mathbf{S}^n$. In order to be stable, an explicit scheme needs to satisfy the Courant-Friedrichs and Lewy condition ([10])

$$0 < CFL < 1, \tag{4.42}$$

where CFL represents the so called Courant number. The CFL is effectively the fraction of the cell width Δx, traveled by a signal with a propagation speed λ in one time step of size Δt, the stability condition says that the scheme will allow time steps Δt such that the fastest signals/waves do not traverse more than a single cell of width Δx in time Δt. A generalization of this condition reads

$$\Delta t = \frac{CFL\Delta x}{S_{max}^n}, \tag{4.43}$$

where S_{max}^n is the magnitude of the maximum propagation speed, in the differential equation. In our case, $S_{max}^n = Max(\varepsilon, \sqrt{gh_i} + \sqrt{u_i^2 + v_i^2})$ where ε is a threshold value.
The second choice is the Newmark scheme

$$\mathbf{U}_i^{n+1} = \mathbf{U}_i^n + \frac{\Delta t}{K_i}\left((1-\gamma)\mathbf{N}^n + \gamma\mathbf{N}^{n+1}\right) \tag{4.44}$$

which is second order accurate and unconditionally stable when $\gamma = 0.5$.
In this work, we used only the Eueler explicit scheme, for all of the test cases. We note that the Zokagoa, Tchamen and HLLC scheme are all first order accurate in space, so we ask if it's necessary to increase the order in time. Considering that we can write the global error as

$$E = o(\Delta x) + o(\Delta t) \tag{4.45}$$

we find that increasing the accuracy in time for these scheme is not necessary.
On the other hand, the WAF scheme is already intrinsically second order accuracy in time (and also in space).

It is then necessary to include the friction term, that we decide to apply with a semi-implicit scheme. We note that this term only influences the momentum equations because it doesn't appear in the continuity equation. We manipulate equation 3.4 to find:

$$\mathbf{q}_i^{n+1} + g\Delta t \frac{|\mathbf{q}_i^n|\mathbf{q}_i^{n+1}}{k^2 h_i^n (h_i^{n+1})^{\frac{4}{3}}} = \mathbf{q}_i^n - \sum_{j\in K_i} \left(\frac{\Delta t L_{ij}}{|C_i|}\right) F_{ij}(\mathbf{U}_i^n, \mathbf{U}_j^n, \mathbf{n}_{ij}) - \left(\frac{\Delta t L_i}{|C_i|}\right) F_q(\mathbf{U}_i^n, \mathbf{U}_{e,i}^n, \mathbf{n}_i) \tag{4.46}$$

where C_i is the area of the cell, L_{ij} is the length of the edge between cells and F is the numerical flux at the interfaces (cells or boundaries). Consequently we have, if $\tilde{\mathbf{q}}_i^{n+1}$ is the right hand side term of equation (4.46):

$$\mathbf{q}_i^{n+1} = \frac{\tilde{\mathbf{q}}_i^{n+1}}{1 + g\Delta t \frac{|\mathbf{q}_i^n|}{k^2 h_i^n (h_i^{n+1})^{\frac{4}{3}}}} \tag{4.47}$$

The semi-implicit discretization is used in order to handle instabilities caused by possible abrupt changes in water depths and velocities.

4.6 Roe scheme - kinetic first and second order accurate scheme

The Roe scheme and the first/second order kinetic schemes were already present in Telemac-2D. In particular, the Roe scheme was chronologically the first FV scheme implemented in the system. Thus the three schemes were already validated and we will use them as a reference in the comparison between the test cases because they have good numerical properties and for the kinetic scheme we also have a second order extension. Here, we will limit our description of theses schemes, to a discussion of some of the basic elements that constitute them.

In the Roe scheme (Goutal,1996) the linearized technique of Roe (1981) is used to solve the Riemann problem at the interface. The main idea is that for every couple Q_R, Q_L two particular matrices (called Roe's linearized) exist and satisfy certain important relations. This allows us to write the Riemann problem as a linearized problem:

$$\frac{\partial \bar{Q}}{\partial t} + \tilde{A}\frac{\partial \bar{Q}}{\partial x} \tag{4.48}$$

$$\bar{Q}(x,0) = \begin{cases} Q_L & \text{if} \quad x < 0 \\ Q_R & \text{if} \quad x \geq 0 \end{cases} \tag{4.49}$$

The flux is calculated through the expression

$$f_{i+\frac{1}{2}}^{Roe} = \frac{1}{2}(f(Q_R) + f(Q_L)) - \frac{1}{2}\left|\tilde{A}\right|(Q_R - Q_L) \tag{4.50}$$

where $\tilde{A}$ is the Roe matrix. This procedure results in a first order scheme, stable under the Courant-Friedrichs-Lax condition. The inconvenience is that the Roe flux needs an entropic correction in order to avoid steady non-entropic discontinuities in proximity of the sonic points. The bed source terms are treated using a centered discretization that needs a decentralization, applied following the technique proposed by Vasquez-Cendon [6].
An implicit scheme is implemented for the friction source terms.
The major disadvantage of the Roe scheme is the possible presence of negative water depths, especially in cases where there are strong wet/dry passages. We will discuss this aspect in the

validation tests, chapter 5.

In the kinetic schemes (Audusse, 2004) the bathymetry source term is treated with the hydrostatic reconstruction, presented in the previous sections, that guarantees the positivity of the water depths. The friction term, as in the other new schemes, is discretized with a semi-implicit scheme, which is highly stable. On the contrary, the kinetic schemes have a constraint in the discretization of time, which is dictated by the CFL condition. For the flux calculation, we summarize here the main expressions:

$$\mathcal{F}(U_i^n, U_j^n, \mathbf{n}_{ij}) = F^+(U_i, \mathbf{n}_{ij}) + F^-(U_j, \mathbf{n}_{ij}) \tag{4.51}$$

with

$$F^+(U_i, \mathbf{n}_{ij}) = \int \xi \cdot \mathbf{n}_{ij} \geq 0 \xi \cdot \mathbf{n}_{ij} \begin{pmatrix} 1 \\ \xi \end{pmatrix} M_i(\xi)\, \mathrm{d}\xi \tag{4.52}$$

$$F^-(U_j, \mathbf{n}_{ij}) = \int \xi \cdot \mathbf{n}_{ij} \leq 0 \xi \cdot \mathbf{n}_{ij} \begin{pmatrix} 1 \\ \xi \end{pmatrix} M_j(\xi)\, \mathrm{d}\xi \tag{4.53}$$

where these expressions are defined according to the kinetic theory.
For the second order kinetic scheme a MUSCL (Monotone Upstream-centered Schemes for Conservation Laws) reconstruction has been used.

Chapter 5

Validation cases in Telemac-2D

This chapter provides a serie of validation tests for the new finite volumes schemes implemented in Telemac-2D, that are compared with the existing schemes. Firstly, for each case, we will present the objective of the test and we will show the geometry, highlighting which are the boundary conditions and the initial conditions of the problem. Secondly we will give to the reader the main characteristics (in terms of duration, Courant number...) used for the solution of the case. Finally we will show the results through graphics, doing a comparison between analytical or physical solutions where possible, in order to get a critical conclusion. In the cases that present an irregular topography, we firstly compare the two techniques for the source term discretization, so the Hydrostatic Reconstruction and the Divergence Form Bed, applied to the HLLC scheme. Then, we will present a graphic with seven solutions, computed used the schemes described in chapter 3. So in this last comparison we consider for the HLLC the best source term discretization, which is always the Hydrostatic Reconstruction.
Almost of test cases is part of the official series of test used for the validation of the finite elements in Telemac-2D [29][25]. We will introduce some new test cases and we will modify or change the original mesh where necessary.
We specify that all the results are treated with some appropriate post-processor, as FUDAA-PREPRO or TECPLOT, that allow to produce graphical outputs and statistics. In addition there are also graphics generated by GNUPLOT, a portable command-line driven graphing utility for Linux, opportune also because it supports many different types of output.

5.1 Lake at rest - CADAM1 problem

This test is useful to verify the ability of the model to maintain quiescent flow over an irregular bottom. The purpose is too validate the consistence of the discretization of the source terms and to demonstrate the well-balanceness of the scheme.
The computational domain is rectangular and it is made up with irregular triangles. Its topography varies sharply between 0 and 20 m (see figure 5.1) and the bathymetry data at 24 points of the channel are given in the table 5.1. The free surface level at the initial time is 21

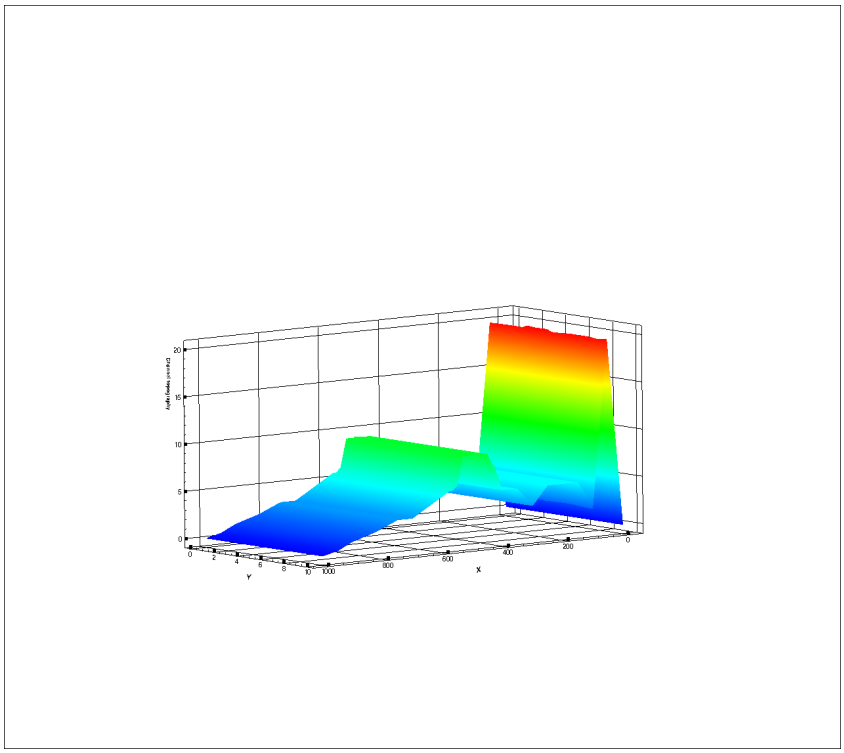

Figure 5.1: Lake at rest - Bathymetry of the channel

m. To validate the test, neither inflow nor outflow are imposed. Even though a duration of 200 s is sufficient to confirm the well balanceness of the scheme, we present here the results for a duration of 1000 s. We expect any variation neither in the free surface level nor in the velocity ($u = 0m/s$). Herein we resume the main characteristics of the problem.

Geometry

- size of the basin: rectangular 1000 m X 10 m;
- free surface at rest: 21 m

Mesh

- Triangle elements : 38506
- Nodes : 20516

- Average size range : 0.8 m

Boundaries

- solid wall with slip condition in the domain

Bottom

- no bottom friction

Time data

- time step is variable
- CFL number = 0.9
- simulation duration = 1000 s

x(m)	0	50	100	150	250	300	350	400	425	435	450	475	500	505
z(m)	0	20	2.5	5	5	3	5	5	7.5	8	9	9	9.1	9
x(m)	530	550	565	575	600	650	700	750	800	820	900	950	1000	1500
z(m)	9	6	5.5	5.5	5	4	3	3	2.3	2	1.2	0.4	0	0

Table 5.1: Lake at rest test - Bathymetry data

The figure 5.2 shows the results for the new schemes, after 1000 s along the x direction, for $y = 5$ m. We can see that our schemes are really well-balanced and that there isn't any spurious effects generated until the final time. In terms of velocity we can see that we have null velocities for all schemes except for the Roe; anyway the values are really low (order of $10^{-13} m/s$) so we can consider that it simulates well this case.

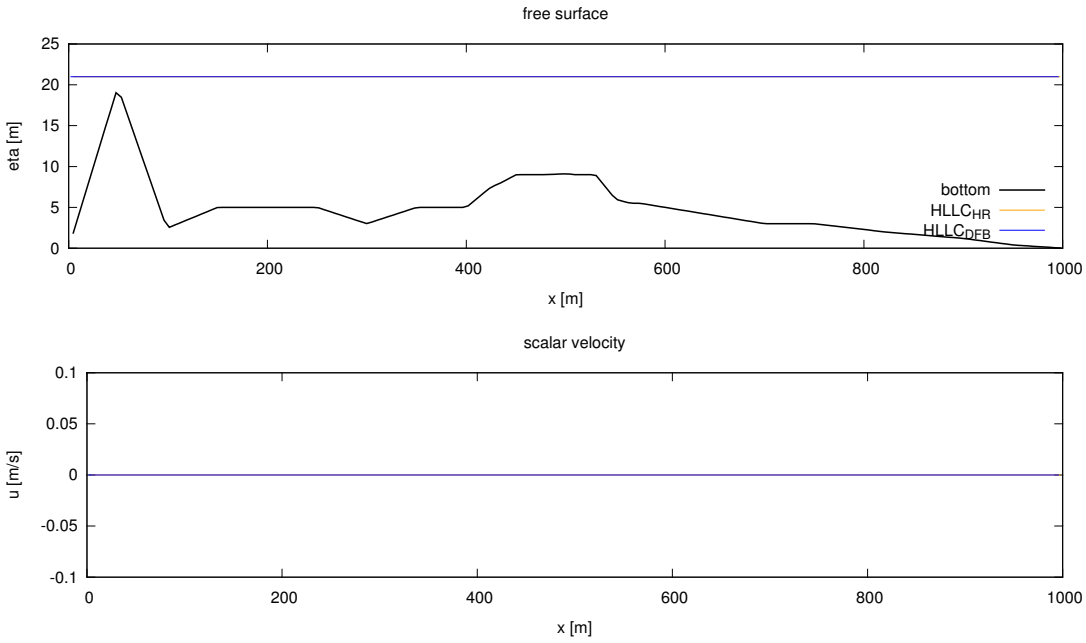

(a) HLLC scheme with HR and DFB

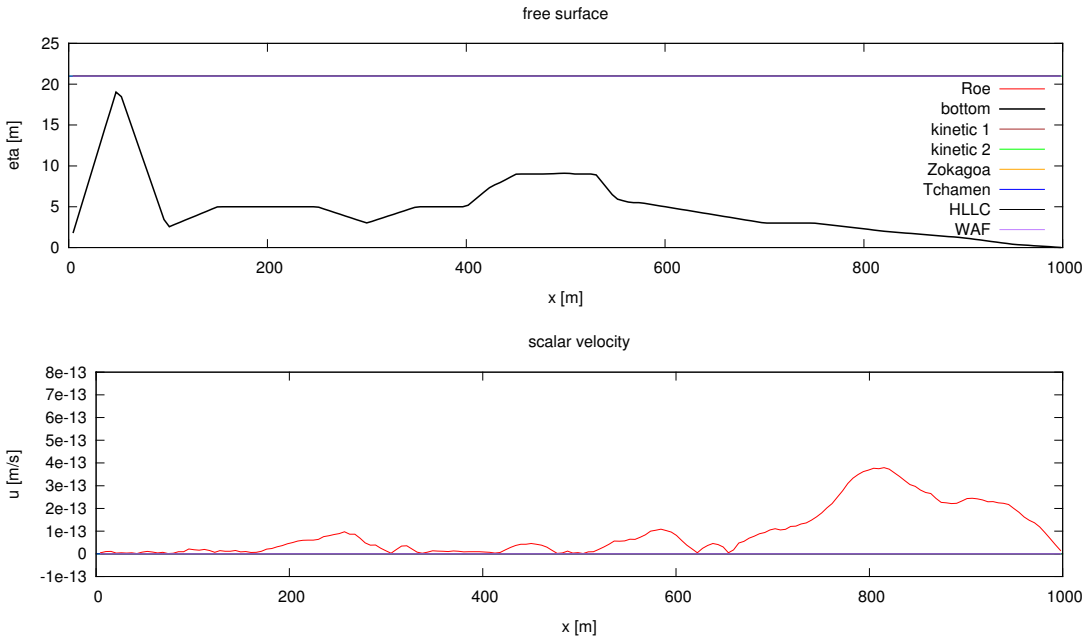

(b) schemes comparison

Figure 5.2: Lake at rest - Free surface and scalar velocity (t=1000 s)

5.2 Dam break - Stoker problem

This type of test is suited when we evaluate the shock capturing ability of the scheme. We present the problem analyzed according to two different type of mesh in order to evaluate the mesh influence. The purpose of the test is to demonstrate that Telemac-2D can solve the problem of a dam break wave propagating on an initially wet bed and to compare the water depth evolution as computed by Telemac-2D with the analytic solution to this problem.
We choose a rectangular computational domain, made up with irregular triangles. The bottom of the channel is flat and the free surface presents a discontinuity at x = 500, that is the dam location. The water depth is 6 m in the left side and 2 m in the right side. The flow is sub-critical and it will rest as such, both in the left side and in the right side, during all the time of simulation. This means that the Froude number remains lower than 1. In terms of refraction and shock waves, we will expect a refraction wave that will travel at the left side and a shock wave that will travel at the right side. We resume here the main data problem.

Geometry

- size of the basin: rectangular 1000 m X 10 m;
- water depth at rest:$0 \leq x \leq 500$ $H = 6m$; $x \geq 500$, $H = 2m$

The geometry and the initial state are shown on the figure 5.3(a) and 5.3(b).

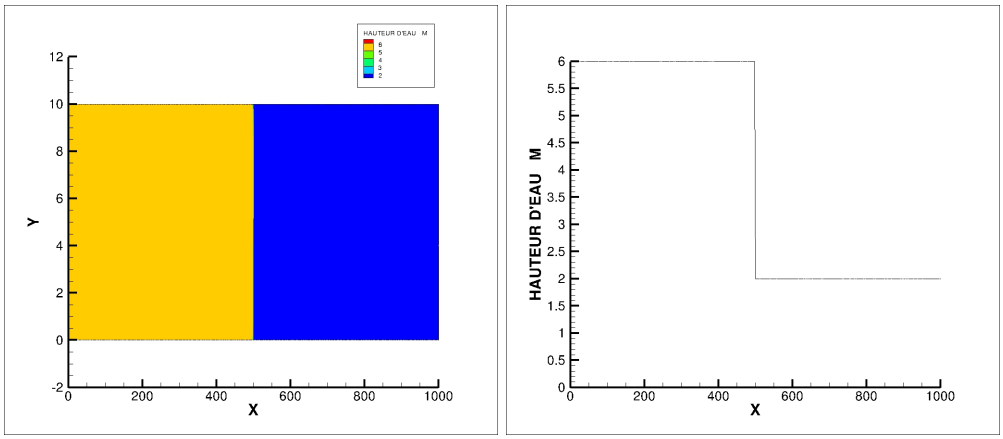

(a) Geometry (b) Initial condition

Figure 5.3: Wet bed case

Mesh

	triangles elements	nodes	average size range
coarse	6754	3883	2 m
refined	38506	20516	0.8 m

Boundaries

- solid wall with slip condition in the domain

Bottom

- no bottom friction

Time data

- time step is variable
- CFL number = 0.8
- simulation duration = 50 s

In 1957 Stoker [19] presented an analytical solution to a dam-break flood wave on horizontal, initially wet bed. We compare this solution with the finite volumes solutions. The schemes used in Telemac-2D show a good agreement with the analytical solution as shown in the figure 5.4(a) and 5.4(b), where all courses match well except the negative and positive wave fronts. All graphics are extrapolated at t = 50 s, for $y = 5$ m (middle point along the y direction).

We conclude that Telemac-2D reproduces well the dam break phenomenon, in terms of front wave and velocity as shown in the figures. We get better results when the mesh is more refined, but the time calculation is longer as shown in the table 5.2. Anyway, the results computed over a coarse mesh are already fully satisfying that we can conclude that a mesh coarse mesh (formed by about 3900 nodes) is enough to have a good simulation.
Concerning numerical diffusion, after a zoom on the refraction wave, we see that the WAF scheme and the kinetic second order accuracy scheme are less diffusive than the others. We find the same results when we make a zoom on the shock wave. Any scheme presents spurious oscillations near the shock, as expected.

	Roe	Kinetic 1	Kinetic 2	Zokagoa	Tchamen	HLLC	WAF
coarse	13 s	9 s	30 s	7 s	6 s	8 s	15 s
refined	4 min 21 s	4 min 19 s	9 min 38 s	3 min 17 s	2 min 15 s	3 min 41 s	4 min 37 s

Table 5.2: Stoker problem - CPU times

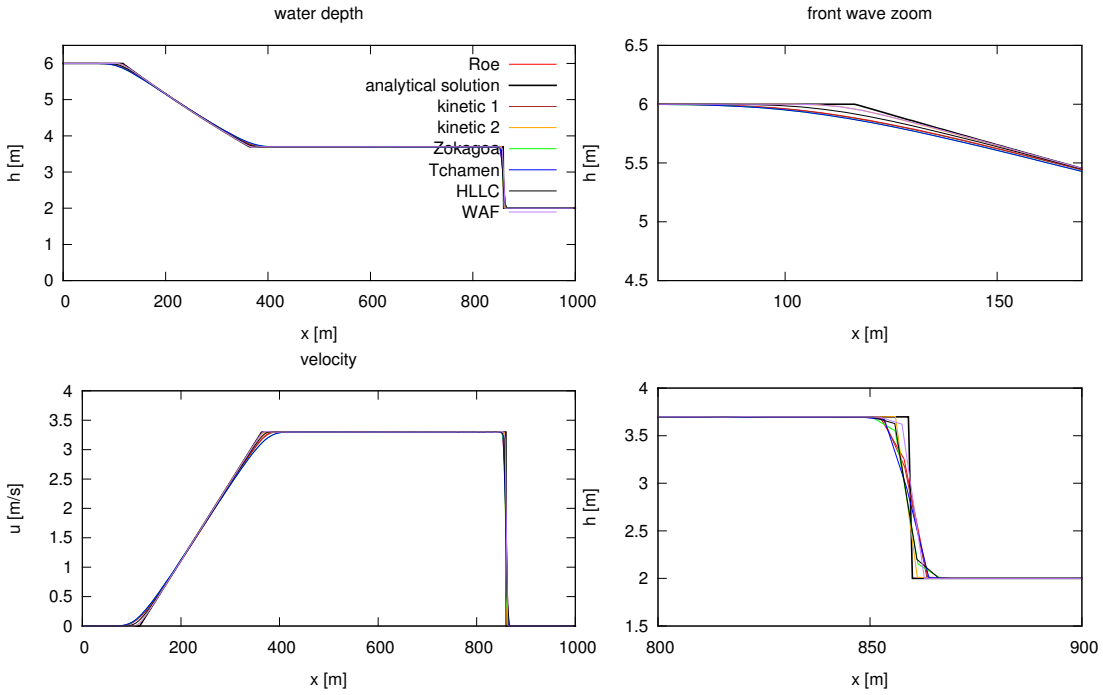

(a) Refined mesh

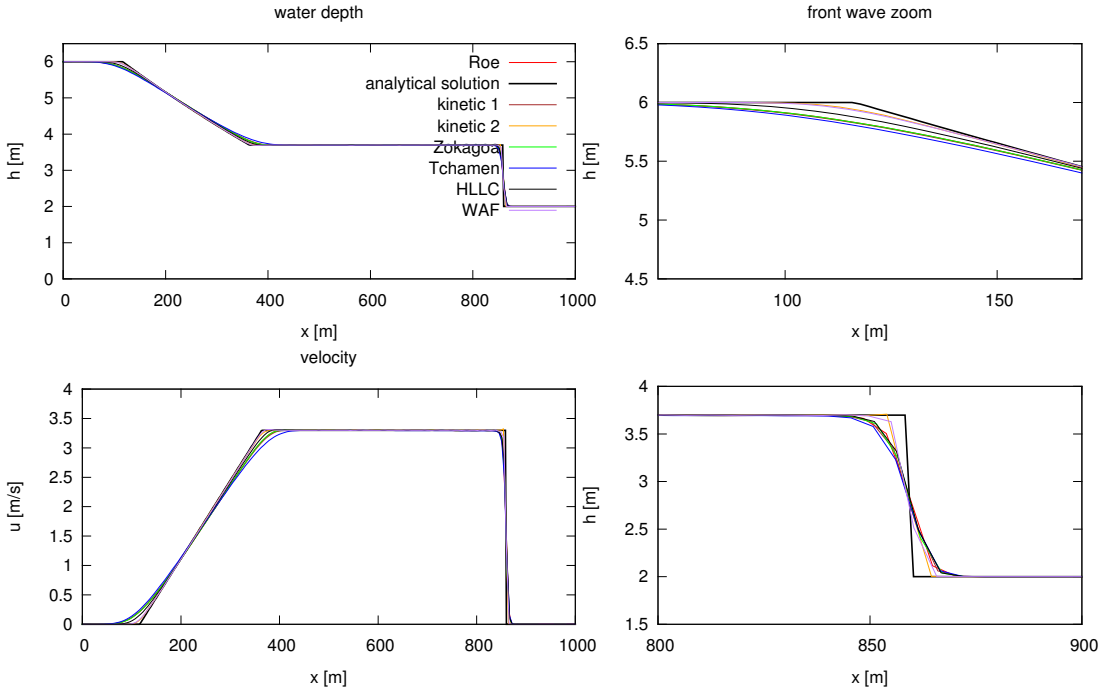

(b) Coarse mesh

Figure 5.4: Solutions for the Stoker problem (t=50 s)

5.3 Dam break - Ritter problem

This test is helpful to evaluate the correct speed of propagation of the front. Also in this case we will test two different type of mesh (refined and coarse). The aim is to demonstrate that Telemac-2D can solve the problem of a dam break wave propagating on an initially dry and to compare the water depth evolution as computed by Telemac-2D with the analytic solution to this problem.
The computational domain is rectangular and it is made up with irregular triangles. The bottom of the channel is flat and the free surface presents a discontinuity at x = 500, that is the dam location. In the dry case the water depth in the left side is 3 m, at rest, while in the right side the basin is dry. The flow is subcritical in the upstream part and it becomes supercritical in the downstream part, the Froude number is 1 in correspondence to the dam location. In this case we will expect a single left refraction wave.

Geometry

- size of the basin: rectangular 1000 m X 10 m;
- water depth at rest:$0 \leq x \leq 500$ $H = 3m$; $x \geq 500$, $H = 0m$

The geometry and the initial state are shown on the figure 5.5(a) and 5.5(b).

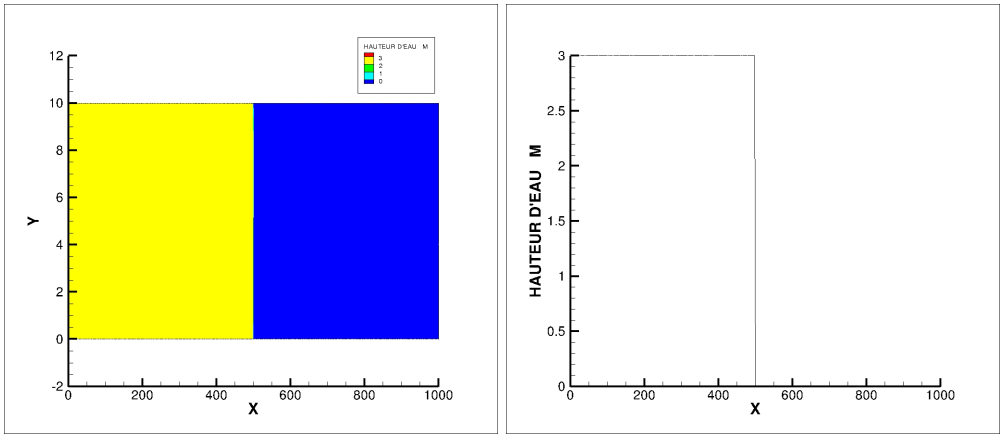

(a) Geometry (b) Initial conditions

Figure 5.5: Dry bed case

Mesh

	triangles elements	nodes	average size range
coarse	6754	3883	2 m
refined	38506	20516	0.8 m

Boundaries

- solid wall with slip condition in the domain

Bottom

- no bottom friction

Time data

- time step is variable
- CFL number = 0.8
- simulation duration = 50 s

We uses an analytical solution, calculated by Ritter [18], to compare the results of the finite volumes schemes.
Ritter considered a channel of horizontal bottom with smooth bed and walls and rectangular cross-section; the dam runs at right angle to bed and breaks outright. The initial conditions are given as

$$h(x, t = 0) = \begin{cases} h_0 & \text{if} \quad x < 0, \\ h = 0 & \text{if} \quad x > 0 \end{cases} \tag{5.1}$$

for the water height and

$$u(x, t = 0) = 0. \tag{5.2}$$

for the velocity. The solutions are

$$h(x, t) = \frac{(2\sqrt{gh_0} - \frac{x}{t})}{9g} \tag{5.3}$$

$$u(x, t) = \frac{2}{3}\left(\sqrt{gh_0} + \frac{x}{t}\right) \tag{5.4}$$

it is defined in the interval

$$-1 < \frac{x}{t\sqrt{gh_0}} < 2 \tag{5.5}$$

Outside of this interval the quantities h and u are not affected by the wave. The solution for the wave shows the following properties: its profile is parabolic with a tangent to the channel bottom at its front; at the dam site the water height is constant in time with $h(x = 0, t) = \frac{4}{9}h_0$. The velocity is linear along the channel with the values zero at the negative front and $2\sqrt{gh_0}$ at the positive front.This quantity, too, is independent of time at the location of the dam where $u(x = 0, t) = \frac{2}{3}\sqrt{gh_0}$ is hold. At this point the discharge thus follows as constantly $q(x = 0, t) = \frac{8}{27}h_0\sqrt{gh_0}$. The propagation of the wave takes place at the velocity $u(x = +front, t) = 2\sqrt{gh_0}$ in the downstream direction and upstream it is supercritical with $u > \sqrt{gh_0}$; at the dam site the flow is critical with Froude number $Fr = \frac{u}{\sqrt{gh}} = 1$.
The schemes used in Telemac-2D are in good agreement with the analytical solution as shown in the figure 5.6(a) and 5.6(b) ; low numerical diffusion is present in the refracted wave. The WAF scheme and the kinetic second order accuracy show solutions closer to the analytical one. The figures are extrapolated at the end of simulation, for $y = 5$ m, as in the previous case.

It results that Telemac-2D reproduces quite well the dam break with initially bed, in terms of water depths and velocity as shown in the figures 5.6(a) et 5.6(b). As in the previous case we get better results when the mesh is more refined, but not enough to justify the choice of a so refined mesh. In addition the time of calculation is very high for a refined mesh. We show in table 5.3 the CPU times for the two kinds of mesh.

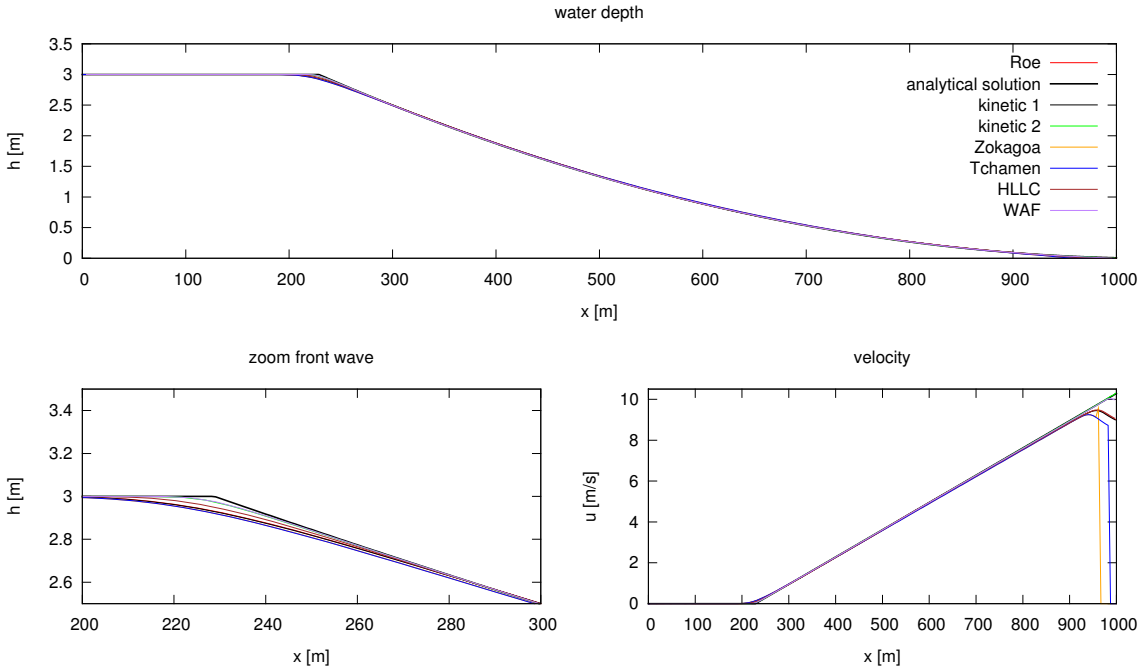

(a) Refined mesh

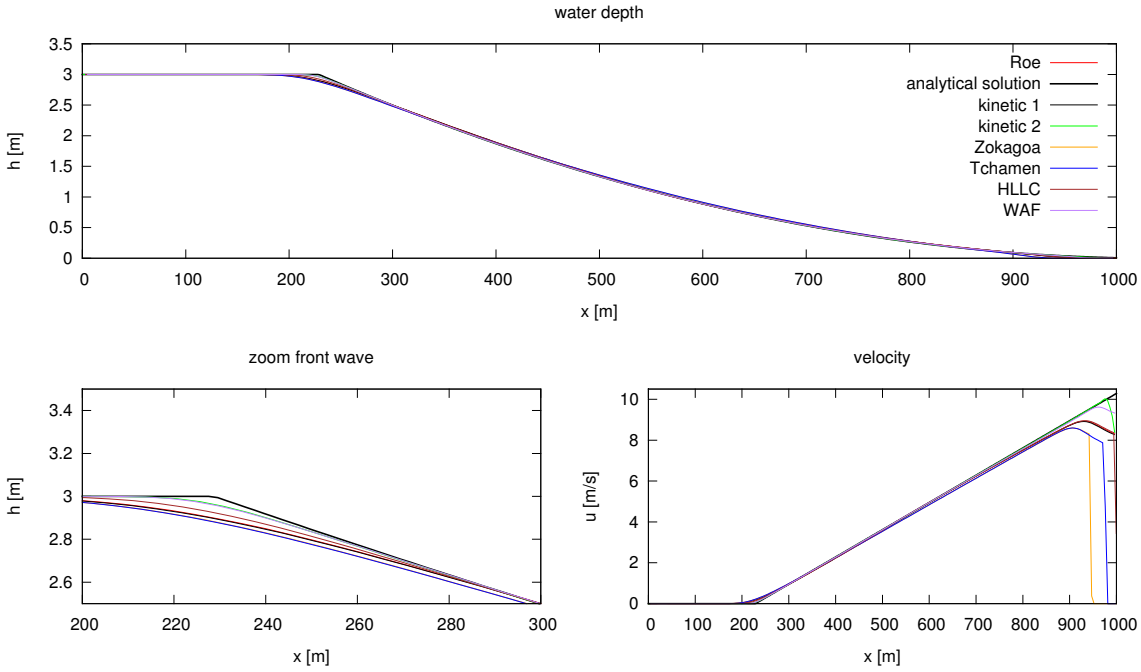

(b) Coarse mesh

Figure 5.6: Solutions for the Ritter problem (t=50 s)

	Roe	Kinetic 1	Kinetic 2	Zokagoa	Tchamen	HLLC	WAF
coarse	10 s	7 s	14 s	5 s	5 s	7 s	13 s
refined	3 min 57 s	3 min 49 s	7 min 59 s	2 min 51 s	2 min 48 s	3 min 3 s	2 min 51 s

Table 5.3: Ritter problem - CPU times

5.4 Drying of a basin - Balzano problem

This is a drying test simulation useful to check if the model can conserve the mass during flooding and drying and so its toughness during wet/dry passages. The aim in this case, is to demonstrate that Telemac-2D can solve the problem of flooding and drying in a basin and also to evaluate the different results of the finite volumes schemes in Telemac-2D.
The computational domain is rectangular and it is made up with irregular triangles. The bottom of the channel has a uniform slope and presents a reservoir formed by a relative maximum at x = 4800. At the beginning of the simulation the free surface is at rest, constant and equal to 2 m, as shown in the figure 5.7(a) and 5.7(b). Once simulation starts, the water level at the right boundary decreases until the free surface gets the value -2 m. This means that the water level in the reservoir will asymptotically reach the relative maximum bottom elevation.
This test has been first done by Balzano with several wetting and drying methods but with a very coarse mesh made up with 543 triangles having a characteristic length of 600 m. We prefer refine the geometry to improve the accuracy of the results.

Geometry

- size of the basin: rectangular 13500 m X 1200 m
- free surface at rest: 2 m

Mesh

- Triangle elements : 8000
- Nodes : 4161
- Average size range : 100 m

Boundaries

- lateral boundaries: solid wall with slip condition
- outflow boundary: open with prescribed depth and free velocity

Bottom

- no bottom friction

Time data

- time step is variable
- CFL number = 0.8
- simulation duration = 80 000 s

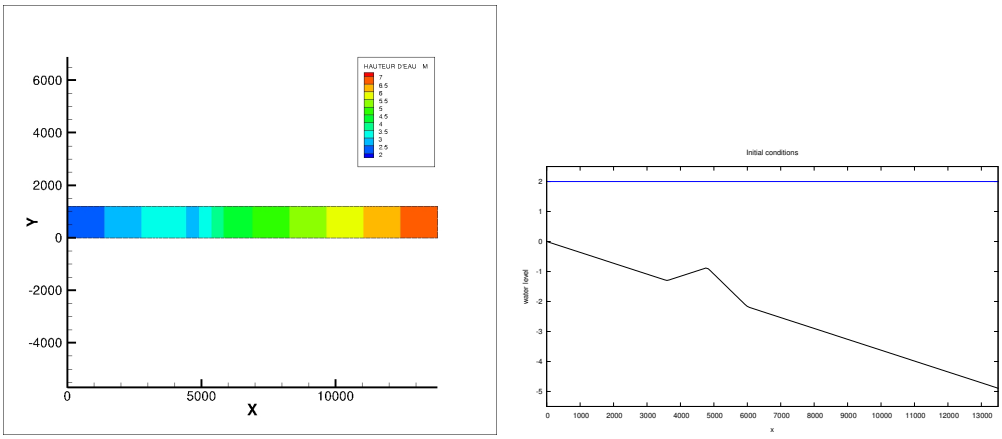

(a) Geometry (b) Initial conditions

Figure 5.7: Drying of a basin

Normally the flow should reach a steady regime with a free surface elevation of -2 m in the domain, except in the reservoir. Velocity should be null in all the domain.

In this case we don't present the comparison between the HR and the DFB because the DFB don't allow us to find good solutions because of the difficulty of this test for the wet/dry passages.
The figure 5.8 (extrapolated at $t = 80000$ s and $y = 6000$ m) shows good solutions in terms of water depth except for the kinetic schemes. Indeed these schemes present oscillations that prevent the flow to reach the steady condition. This reveals that there are problems when there are brutal wet/dry passages, that is valid also for the Zokagoa scheme, which stops it before the end of the simulation. On the other side the Roe's scheme presents a problem of negative water depth, as expected.
The velocity tends to zero in the reservoir and in the part of the domain where the water is at rest.

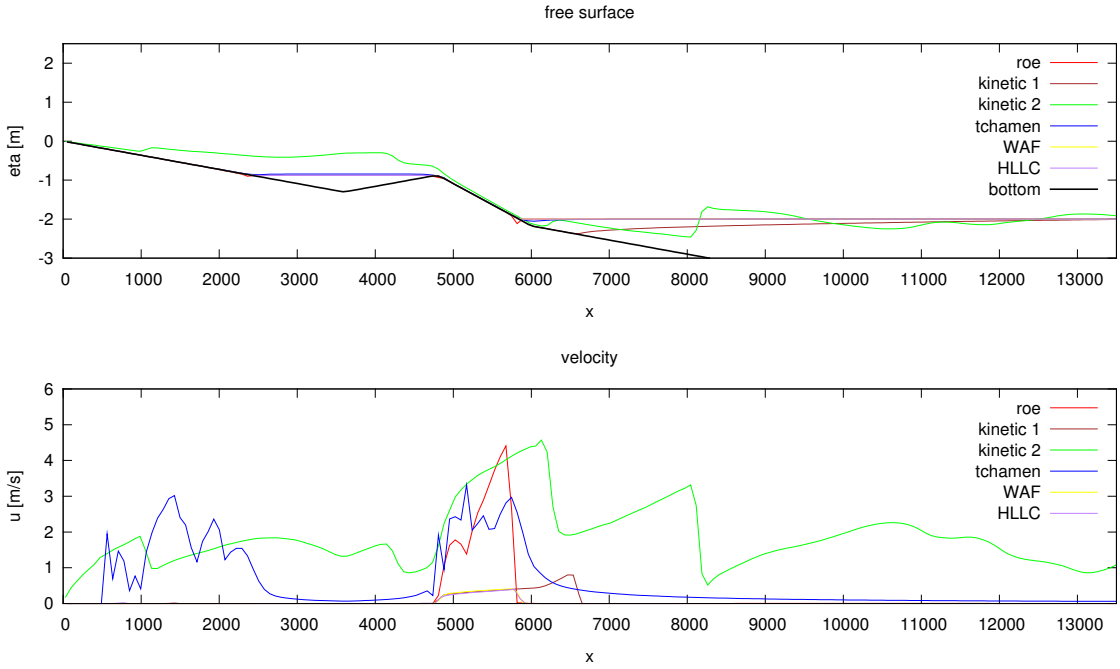

Figure 5.8: Drying of a basin - Water depth and velocity (t = 80000 s)

5.5 Flow over a bump - subcritical condition

The purpose of this test is to compare the different finite volume schemes with the analytical solution, evaluating the capacity to reproduce a steady condition. We impose a subcritical regime of the flow and we expect that after a transitory period it will reach an equilibrium state.
The computational domain is rectangular and it is made up with irregular triangles. The bottom of the channel is flat except in a central zone where there is a bump. At the beginning of the simulation the free surface is at rest and equal to 1,8 m, as shown in the figure 5.9(a) and 5.9(b).

Geometry

- size of the basin: rectangular 20,5 m X 2 m
- if $8 < x < 12$ m, $z_f = -0.05(x-10)^2$, $z_f = -0.20$ elsewhere
- free surface at rest: 1,8 m

Mesh

- Triangle elements : 6957
- Nodes : 3689
- Average size range : 0.14 m

Boundaries

- lateral boundaries: solid wall with slip condition
- channel entrance : discharge $Q = 8,86m^3/s$ imposed
- channel outlet: water depth imposed $h = 1,8m$

Bottom

- no bottom friction

Time data

- time step is variable
- CFL number = 0.8
- simulation duration = 150 s

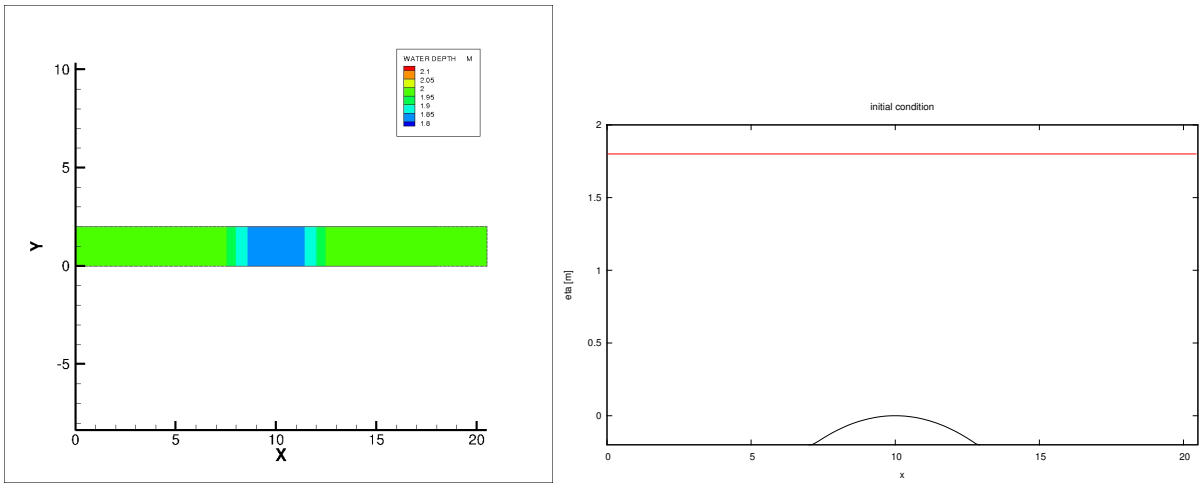

(a) Geometry

(b) Initial conditions

Figure 5.9: Subcritical case

No friction on the bottom allows to wite the Bernoulli equation between the entrance of the channel E (where $q_E = 4,43m^2/s$ and $h_E = 2m$) and a point A of abscissa x_A:

$$z_{fA} + h_A + \frac{q^2}{2gh_A^2} = z_{fE} + h_E + \frac{q^2}{2gh_E^2} = z_{fE} + 2,25m \tag{5.6}$$

Therefore we can calculate the water depth from $h_A^3 + (z_{fA} - 2,05)h_A^2 + \frac{q^2}{2g} = 0$.
The solutions calculated by Telemac-2D are very similar to the exact solution, as we can see in the graph. The steady condition is reached and the flow is subcritical. We remark that for this test case we didn't use the mesh proposed in the official tests series of Telemac-2D, because it was too coarse (1452 nodes - 2620 elements). In this way the results are very excellent (see figure 5.11); we remark only that Zokagoa and Tchamen schemes less accurate in terms of free surface ($+0,02m$) than the others and that the kinetic second order scheme underestimates the velocity because also the initial scalar flowrate is underestimated ($-0,1m^2/s$). These figures are extrapolated at $t = 150$ s and $y = 1$ m.

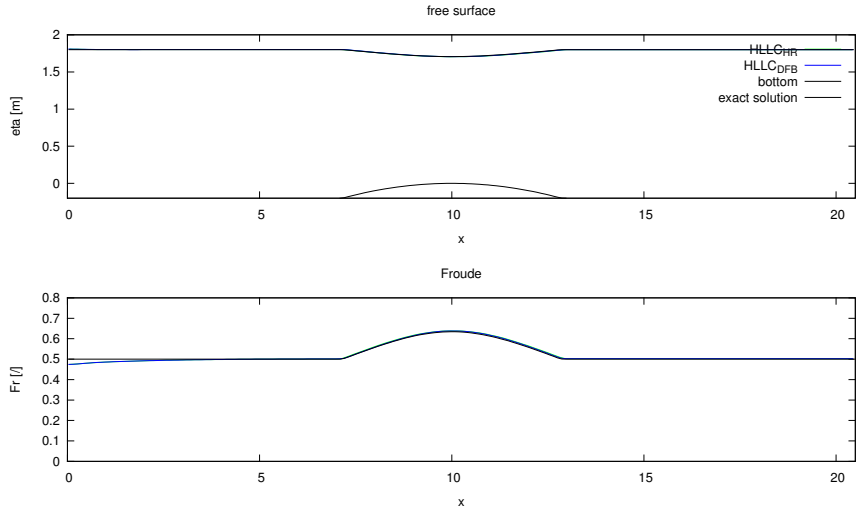

(a) Free surface and Froude number

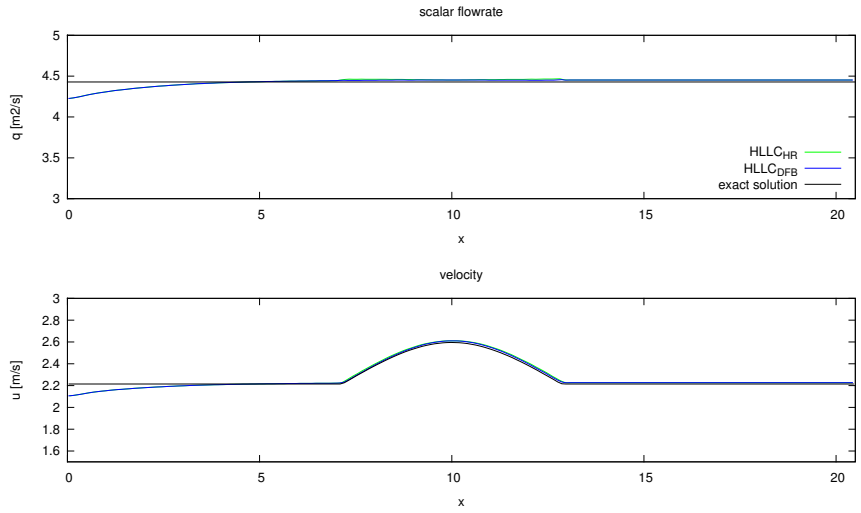

(b) Scalar flowrate and velocity

Figure 5.10: Subcritical condition - HLLC scheme with the HR and the DFB (t=150 s)

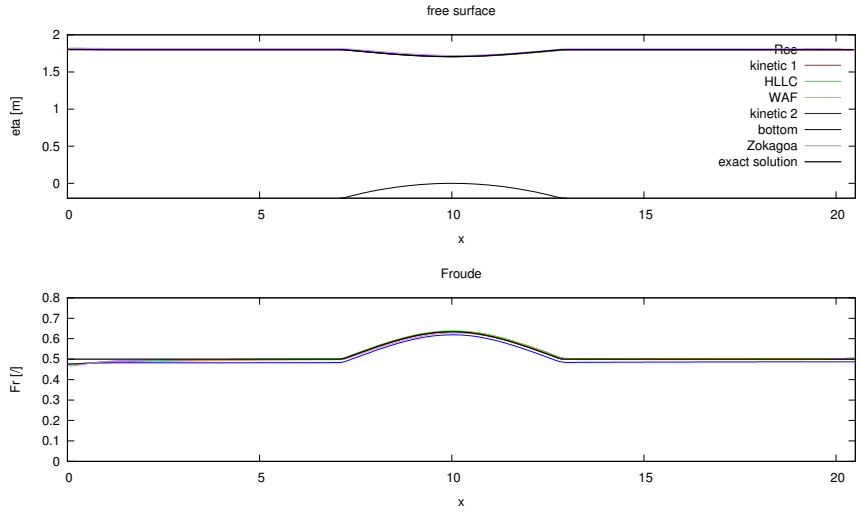

(a) Free surface and Froude number

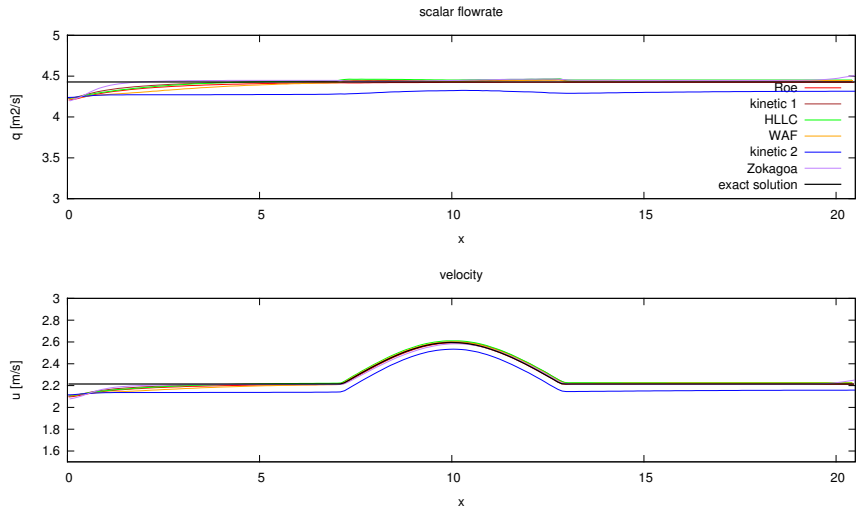

(b) Scalar flowrate and velocity

Figure 5.11: Subcritical condition - Schemes comparison (t=150 s)

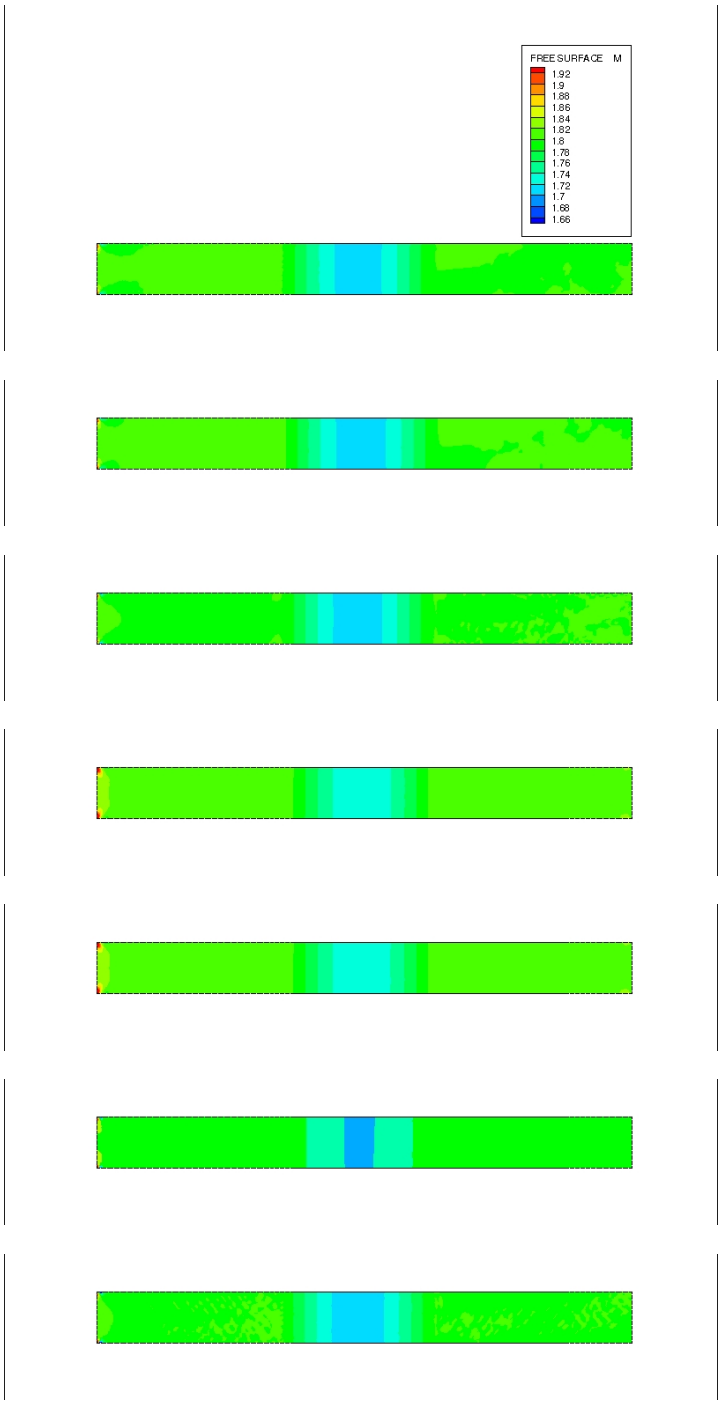

Figure 5.12: Subcritical condition - Free surface in x-y plane for Roe, Kinetic 1, Kinetic 2, Zokagoa, Tchamen, HLLC, WAF scheme (t=150 s)

5.6 Flow over a bump - transcritical condition

The purpose of this test is to compare the different finite volume schemes with the analytical solution, in a transcritical case. We impose at the inlet of the channel a flowrate but we leave a free water depth condition at the outlet. So we expect a transition from a subcritical regime to a supercritical one, passing for a transcritical state (where $Fr = 1$) in correspondence of the middle of the bump.
The computational domain is rectangular and it is made up with irregular triangles. The bottom of the channel is flat except in a central zone where the bump is located. At the beginning of the simulation the free surface is at rest and equal to 1,8 m, as in the previous case.

Geometry

- size of the basin: rectangular 20,5 m X 2 m
- if $8 < x < 12$ m, $z_f = -0.05(x-10)^2$ m, $z_f = -0.20$ m elsewhere
- free surface at rest: 1,8 m

Mesh

- Triangle elements : 6957
- Nodes : 3689
- Average size range : 0.14 m

Boundaries

- lateral boundaries: solid wall with slip condition
- channel entrance : discharge $Q = 0.6m^3/s$ imposed

Bottom

- no bottom friction

Time data

- time step is variable
- CFL number = 0.8
- simulation duration = 150 s

For the analytical solution we calculate the critical depth over the bump with the equation $h_c = \left(\frac{q^2}{g}\right)^{1/3}$. The corresponding specific energy is $E_c = h_c + \frac{q^2}{2gh_c^2} = \frac{3}{2}h_c$. We can then write the Bernoulli equation between the bump and any point A located in the domain, so we have

$$z_{fA} + h_A + \frac{q^2}{2gh_A^2} = z_c + E_c h_A^3 + (z_{fA} - z_{fc} - E_c)h_A^2 + \frac{q^2}{2g} = 0$$

At point C, we have $(h_A - h_C)^2(h_A + \frac{1}{2}h_c) = 0$, that has as positive double solution $h_A = h_c$. At the foot of the bump, we find two positive solutions, for the subcritical and supercritical case: $h_{upstream} = 0.49535m$ and $h_{downstream} = 0.106m$. The corresponding surface elevation

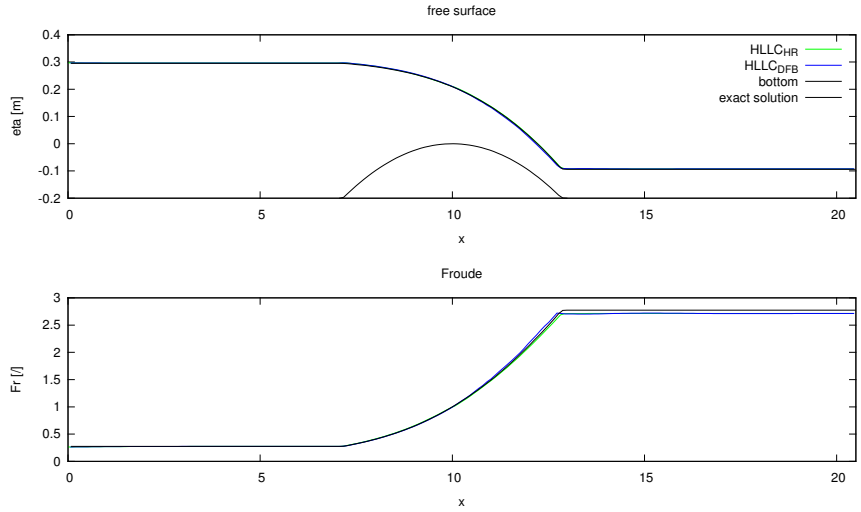

(a) Free surface and Froude number

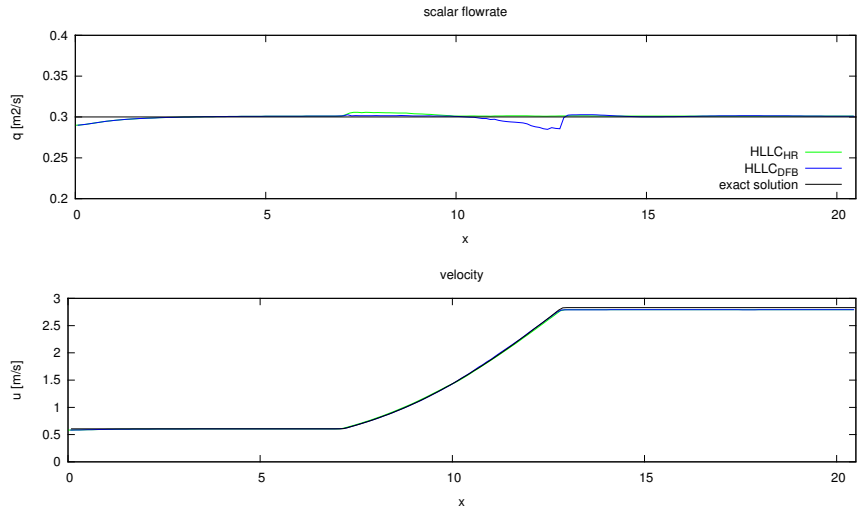

(b) Scalar flowrate and velocity

Figure 5.13: Transcritical condition - HLLC scheme with the HR and the DFB (t=150 s)

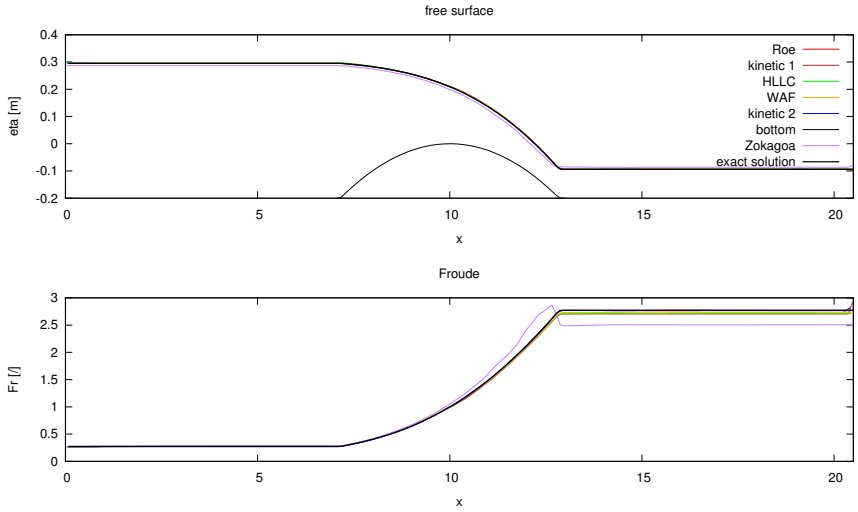

(a) Free surface and Froude number

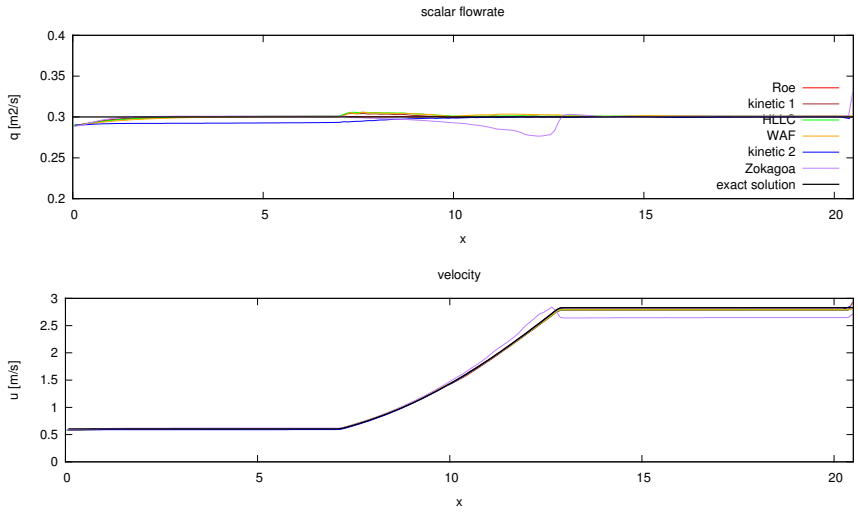

(b) Scalar flowrate and velocity

Figure 5.14: Transcritical condition - Schemes comparison (t=150 s)

are so $\eta_{upstream} = 0.29535m$ and $\eta_{downstream} = -0.094m$.
The solutions calculated by Telemac-2D are really excellent if compared to the analytical solution. The steady condition is reached and the flow is subcritical before the bump and supercritical after it. The Froude number is equal to 1 in the middle of the bump, as we can see in the graph herein. In terms of accuracy the Zokagoa and Tchamen solutions are less exact, in particular if we look at the Froude number we see that these schemes have difficulties to reproduce the results after the transcritical passage. In the $x-y$ plane all solution are coherent and don't present boundary effects in the y direction.
Also for this test we use a different mesh from that proposed in the official test of Telemac-2D.

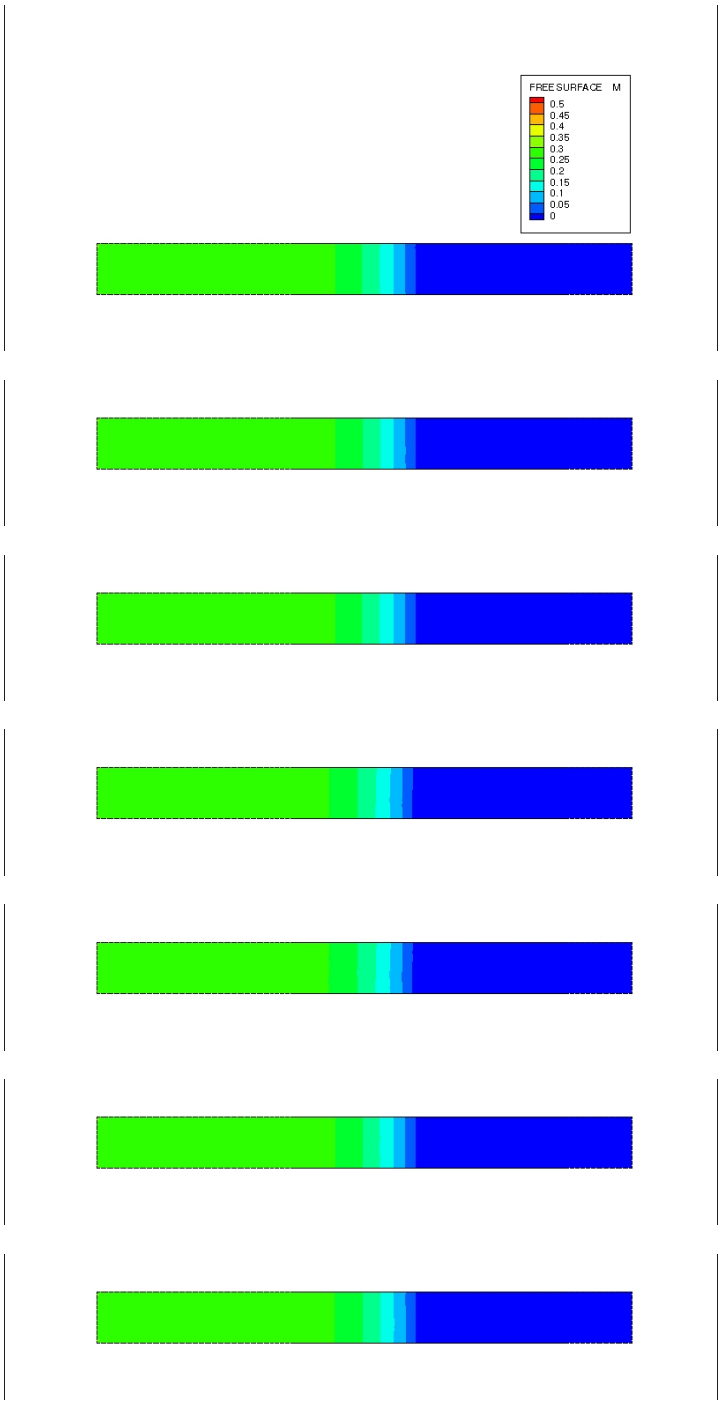

Figure 5.15: Transcritical condition - Free surface in x-y plane for Roe, Kinetic 1, Kinetic 2, Zokagoa, Tchamen, HLLC, WAF scheme (t=150 s)

5.7 Flow over a bump - transcritical condition with hydraulic jump

This test is interesting to see how the FV schemes capture the hydraulic jump. This is a very important target for a numerical scheme, indeed the hydraulic jump represents a shock where the major difficulty is to conserve the momentum. To simulate this case it's necessary imposing a flowrate at the entrance of the channel but also a water depth at the outlet. This creates an hydraulic jump over the bump, that involve a loss of energy in the flow.
The computational domain is rectangular and it is made up with regular triangles. The bottom of the channel is flat except in a central zone where there is a bump. At the beginning of the simulation the free surface is at rest, constant and equal to 1,8 m, as for the subcritical case and the transcritical one.

Geometry

- size of the basin: rectangular 20,5 m X 2 m
- if $8 < x < 12$ m, $z_f = -0.2 - 0.05(x - 10)^2$, $z_f = -0$ elsewhere
- free surface at rest: 0,33 m

Mesh

- Triangle elements : 2620
- Nodes : 1452
- Average size range : 0.16 m

Boundaries

- lateral boundaries: solid wall with slip condition
- channel entrance : discharge $Q = 0,36m^3/s$ imposed
- channel outlet: water depth imposed $h = 0,33m$

Bottom

- no bottom friction

Time data

- time step is variable
- CFL number = 0.8
- simulation duration = 150 s

The solutions produced by Telemac-2D reproduce quite well the hydraulic jump. As in the previous steady cases over a bump, the Zokagoa and Tchamen schemes are the most approximate and the shock is not so precise respect to the other schemes. For this test case we are also interested to the scalar flowrate along the x direction. Indeed for a numerical scheme is really hard to conserve this quantity when we are in presence of a hydraulic jump. We remark that the schemes that show less scalar flow rate variation are the HLLC and the Roe scheme.

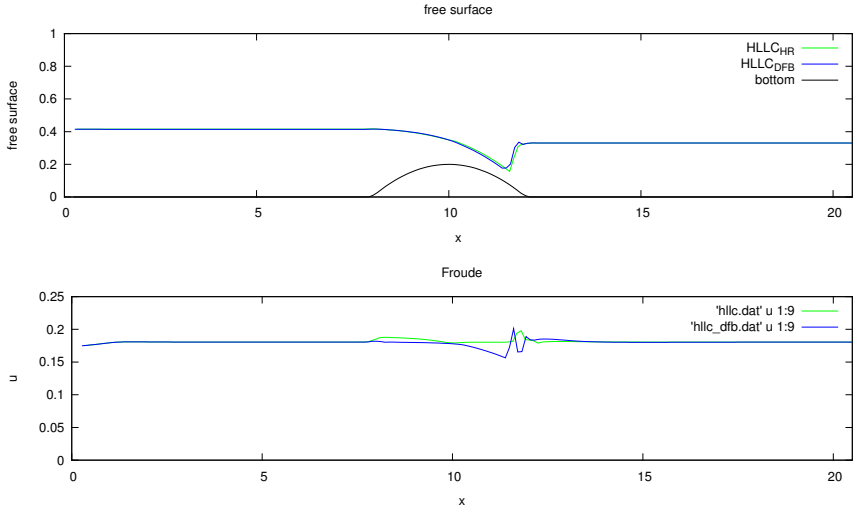

(a) Free surface and Froude number

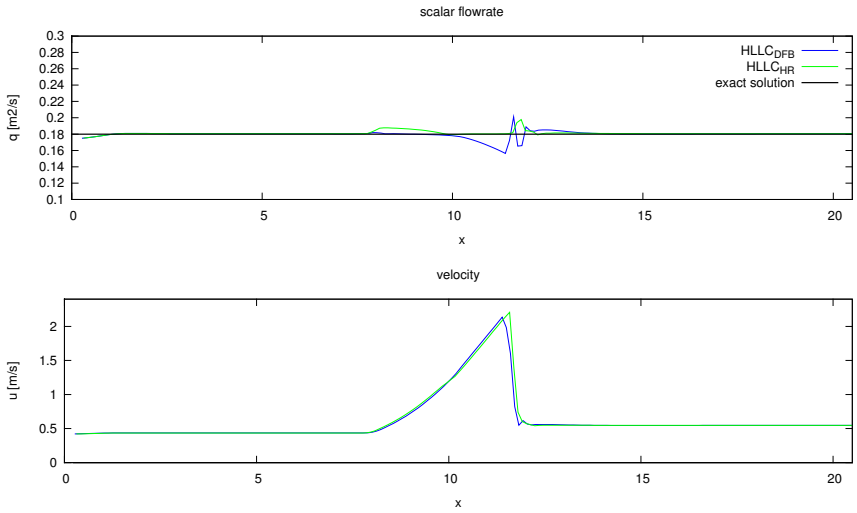

(b) Scalar flowrate and velocity

Figure 5.16: Transcritical condition with hydraulic jump - HLLC scheme with the HR and the DFB (t=150 s)

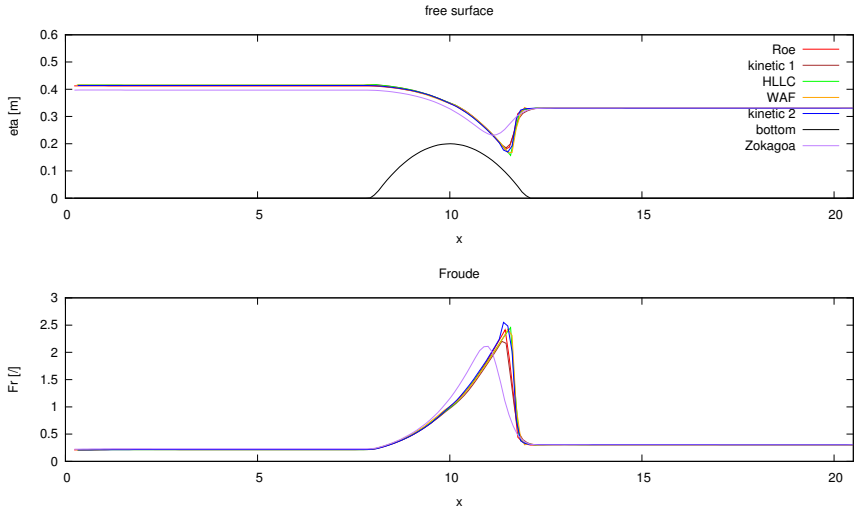

(a) Free surface and Froude number

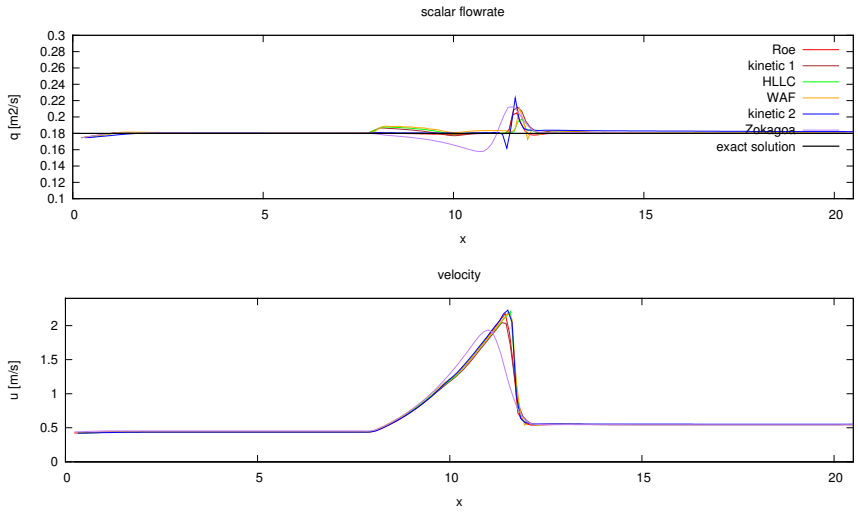

(b) Scalar flowrate and velocity

Figure 5.17: Transcritical condition with hydraulic jump - Schemes comparison (t=150 s)

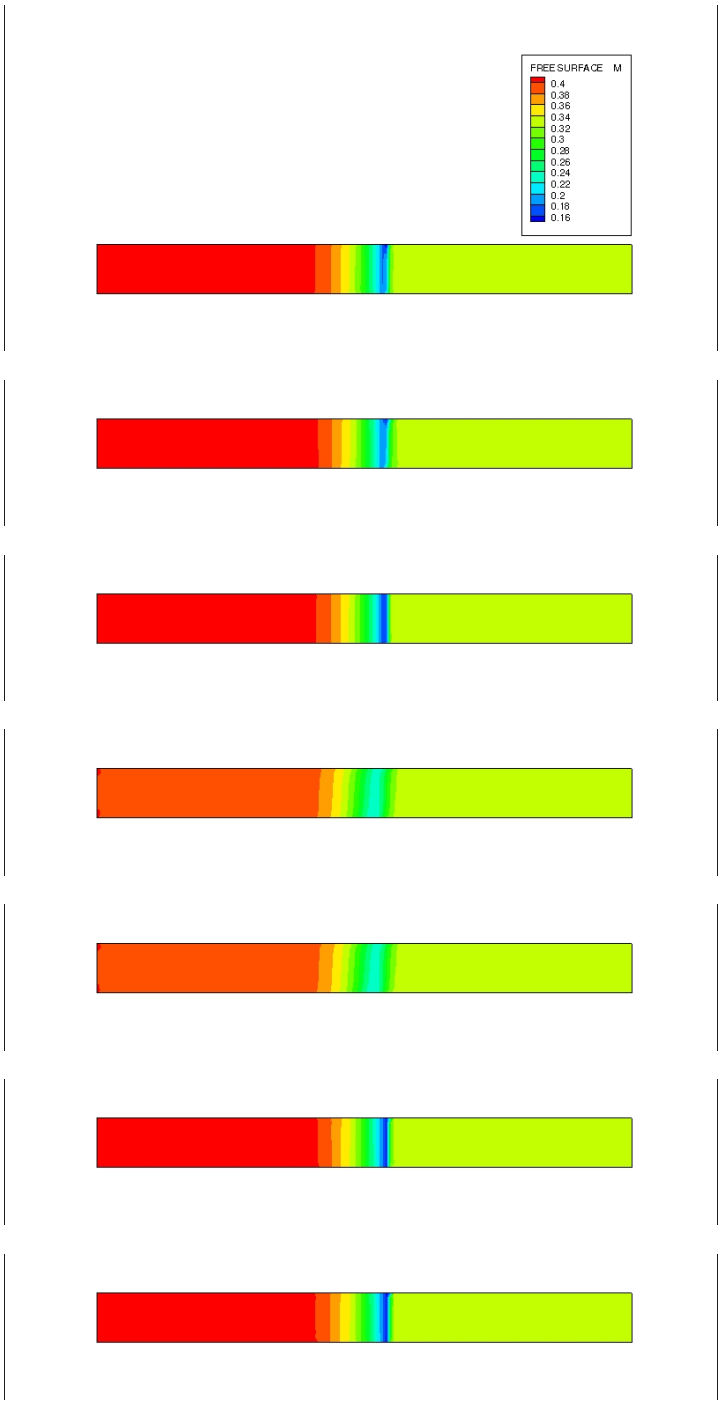

Figure 5.18: Transcritical condition with hydraulic jump - Free surface in x-y plane for Roe, Kinetic 1, Kinetic 2, Zokagoa, Tchamen, HLLC, WAF scheme (t=150 s)

5.8 River confluence

The river confluence is not a simple case to reproduce from a numerical point of view, indeed we don't have an analytical solution of reference. In spite of this we can look at physical model experiments (see [13]) to compare our solutions.
The model represents the junction between two rectilinear laboratory channel with rectangular cross-section and constant slop. The main channel is 0,8 m broad whereas its influent is 0,5 m broad, both channels have a slope of 10^{-3}. The angle between the two channel is 55°.
The free surface is at rest at the beginning of the simulation. We impose a flowrate at the inlet for the two channel and we impose a water depth at the outlet. In this way we will expect that the free surface increases and the water depths should be convergent in the junction area.

Geometry

- size of the basin
  - main channel: 10,8 m X 0,8 m
  - influent: 3,2 m X 0,5 m
- free surface at rest: 0,2852 m

Mesh

- Triangle elements : 6168
- Nodes : 3303
- Average size range : 0,06 m

Boundaries

- main channel
  - inflow: $Q = 0,07m^3/s$
  - outflow: $h = 0,2852$ m
- influent
  - inflow: $Q = 0,035m^3/s$
- lateral boundaries : solid walls with slip condition

Bottom

- $k_s = 62m^{1/3}/s$

Time data

- time step is variable
- CFL number = 0.8
- simulation duration = 100 s

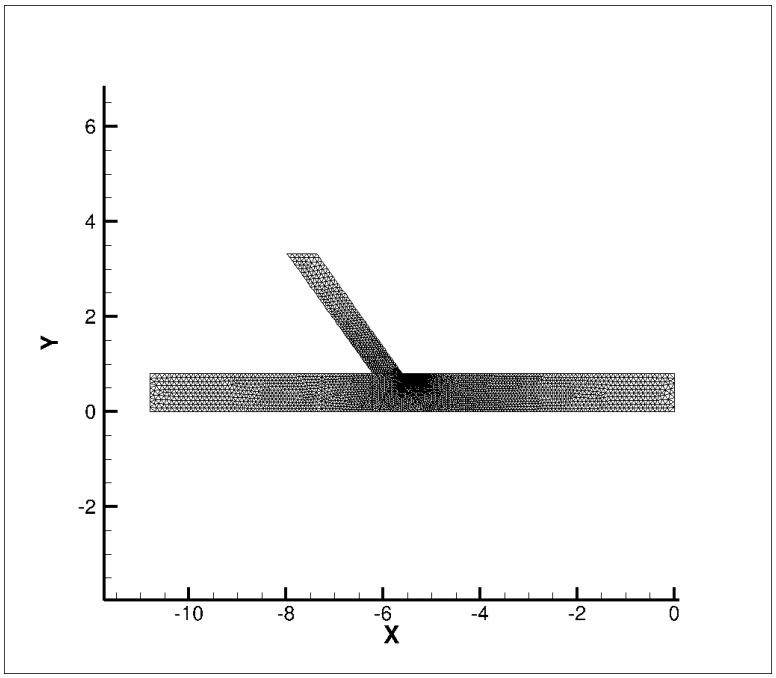

Figure 5.19: River confluence - Mesh

The results calculated by Telemac-2D are good and coherent between them and also with the experimental solution. Indeed the water depths in both channels (upstream and downstream) tends to be uniform. In the junction area the free surface is rapidly varying but any back eddy is founded with the finite volumes schemes, despite the mesh refinement in this zone. A back eddy is instead visible in the experimental solution.
For this test case we choose to compare solutions reproduced with different finite volumes schemes, examining the free surface values in four critical points that are shown in figure 5.20(a).

We group data in table 5.4, where the coordinates of the points are in table 5.5.

	P1	P2	P3	P4
Roe	0,285 m	0,317 m	0,276 m	0,291 m
Kinetic 1	0,329 m	0,318 m	0,271 m	0,291 m
Kinetic 2	0,327 m	0,314 m	0,275 m	0,291 m
Zokagoa	0,333 m	0,321 m	0,271 m	0,292 m
Tchamen	0,333 m	0,321 m	0,271 m	0,292 m
HLLC	0,328 m	0,316 m	0,273 m	0,291 m
WAF	0,327 m	0,314 m	0,272 m	0,291 m

Table 5.4: River confluence - Free surface measures in four critical points

The table and the 2D images show that the results are all coherent and physically acceptable. We remark that also in this test case the Zokagoa and Tchamen schemes overestimate the free surface value.

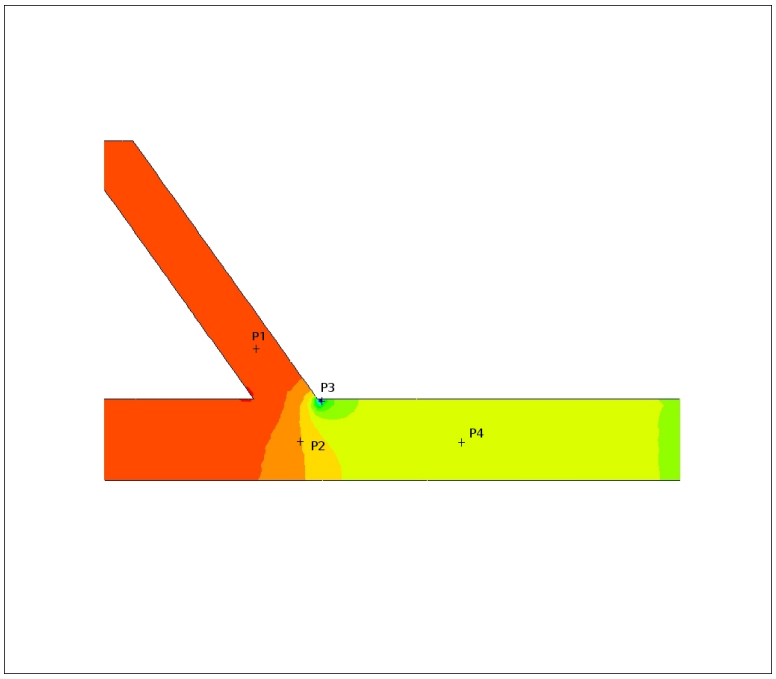

(a) Point of measure

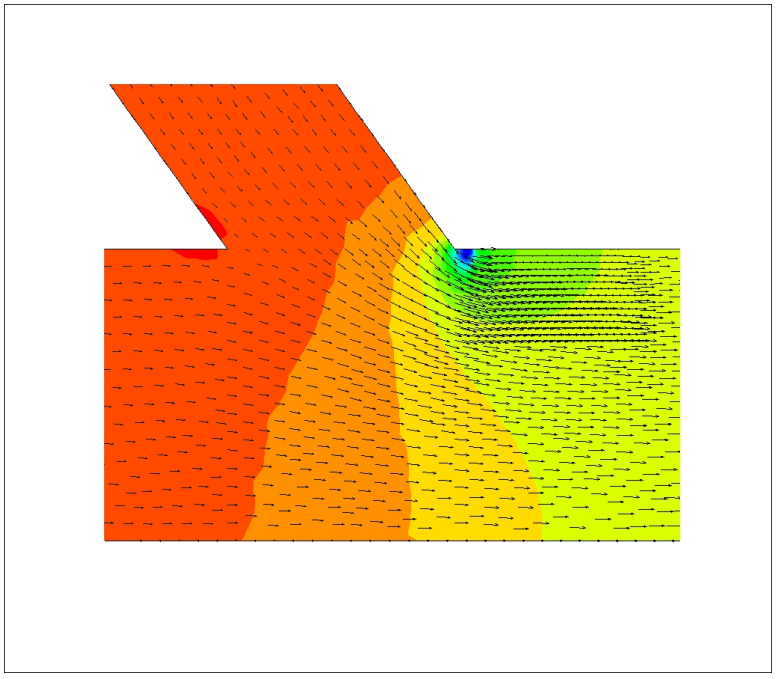

(b) Vectors

Figure 5.20: River confluence - zoom in the junction zone

P1 = (−6, 19; 1, 27)
P2 = (−5, 86; 0, 43)
P3 = (−5, 50; 0, 75)
P4 = (−2, 92; 0, 44)

Table 5.5: River confluence - Coordinates of the measure points

5.9 Simulation of a real case - Malpasset dam break

In several cases the Malpasset dam break represents a benchmark in the validation of numerical models. Its main characteristic is the real bathymetry, that is complex enough to cause instabilities in the numerical simulations.

The Malpasset dam is located in the south-est of the France, approximately 7 km north of Frejus, on the Cote d'Azur. It was an arch dam on the Reyran river, constructed between the 1952 and the 1954, 66 meters high and 223 meters long (the vault). On the 2 December 1959 the dam collapsed, moving about 48 millions of cubic meters of water and killing about 423 people. The water velocity reached 70 km/h and firstly overwhelmed the two villages of Malpasset and Bozon, arriving after 20 minutes until Frejus and letting off in the sea. The cause of the rupture was associated to an insufficient geological study, indeed the rocks under the dam weren't stout enough to support the weight of the structure and the water.

The purpose of this test is to validate the finite volume schemes for a real case. The maximum values of water depths and the arriving times of the wave, will be the parameters characteristic for this test. These parameters are also the most useful in the ahead planning and for the protection activities.

Geometry
The geometry is presented in the figure 5.21. The dam is located between the points M(4701.18m, 4143.41m) and N(4655.5m, 4392.10m). The location of the voltage transformers is given by the table 5.6.

Transformers	x (m)	y (m)
A	5550	4400
B	11900	3250
C	13000	2700

Table 5.6: Malpasset dam-break - Locations of the voltage transformers

In the 60's, a physical model has been constructed at LNH (Laboratoire National d'Hydraulique)to reproduce the scenario of Malpasset dam break. Some gauges were posed in this physical model. Their coordinates are listed in the table 5.7. In addition, the police provided to make some measure of heights in situ after the wave passage, but we will limit to compare our results with that of the physical model, more reliable.

At the beginning of the simulation the free surface is set to 100 m at the upstream, in the reservoir, and it is null at the downstream (see figure 5.22). Obviously the velocity is null at the initial condition.

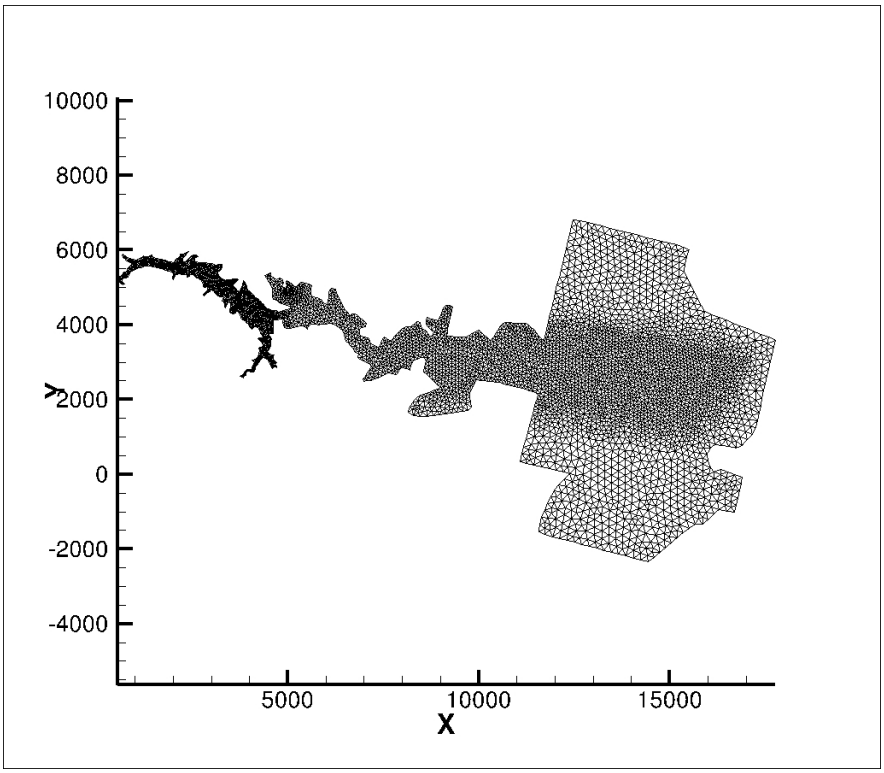

Figure 5.21: Malpasset dam-break - Geometry and mesh

Mesh
We use a mesh that is different respect to the one used in Telemac-2D for the finite elements simulations. Indeed we don't need a too refined mesh for the simulation, that cause an extension of the calculation time without bringing more accuracy, as reported in [1].

- Triangle elements : 10049
- Nodes : 5435

Boundaries
Each frontiers is assumed as solid wall with slip condition because the wave doesn't reach the outlet border during the time simulation.

Bottom
We impose a Strickler friction law with a coefficient of 30 $m^3 s^{-1}$. It is an average value, defined in according to the kind of vegetation existing in the basin.

Time data

- time step is variable
- CFL number = 0.8
- simulation duration = 4000 s

number of gauges	x (m)	y (m)
6	4947.46	4289.71
7	5717.30	4407.61
8	6775.14	3869.23
9	7128.20	3162.00
10	8585.30	3443.08
11	9674.97	3085.89
12	10939.15	3044.78
13	11724.37	2810.41
14	12723.70	2485.08

Table 5.7: Malpasset dam-break - Location of gauges

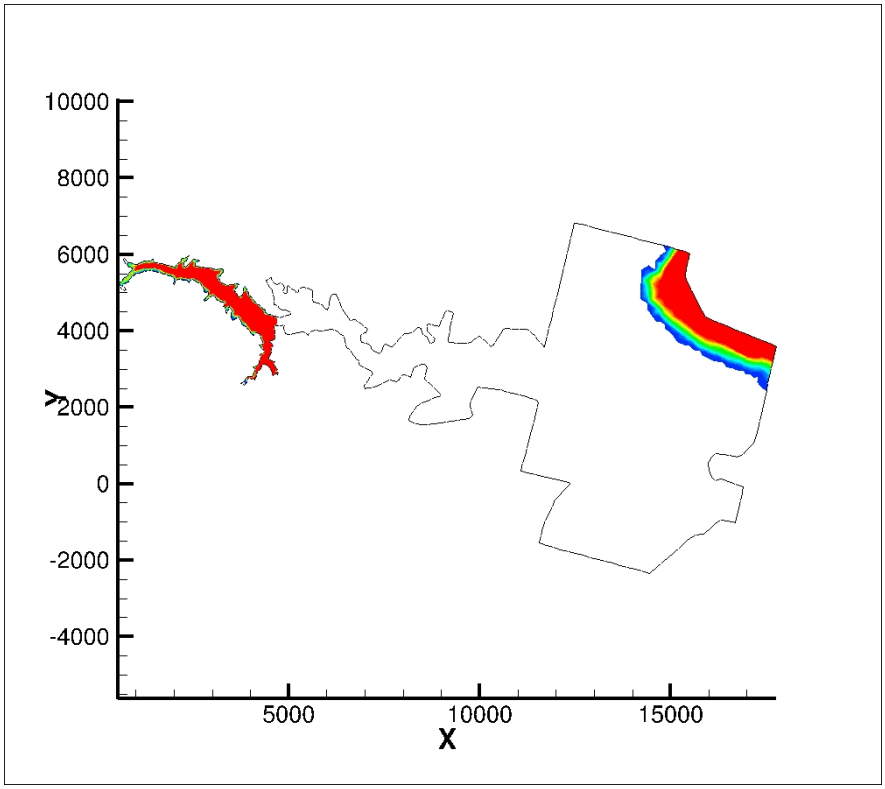

Figure 5.22: Malpasset dam-break - Initial condition

This real case is well simulated by the HLLC and the WAF schemes, as well as with the Kinetic of first and second order accuracy. We make a comparison between the free surfaces computed in the points of the dipstick and we calculate the error respect to the measure obtained with the physical model (see table 5.8):

$$e_{FVS} = \frac{max(\eta_{FVS} - \eta_{gauge})}{\eta_{gauge}}$$

We find an error that is always less then 10% for all the schemes, except for the gauge number

6,7,9,12.
As regards the Zokagoa and the Tchamen scheme, their results are not so satisfying hence they are not reported here. The reasons could be of two types: the first one is the wet/dry treatment, that need further modifications to have an optimal result; the second one is related to the artificial dissipative term that is too diffusive. The good capacity of simulation for this real case by these schemes will be a future goal.

Points	gauge	Kinetic 1	Kinetic 2	HLLC	WAF	$err_{kin1(\%)}$	$err_{kin2(\%)}$	$err_{HLLC(\%)}$	$err_{WAF(\%)}$
6	84,20	76,87	81,46	73,63	72,58	-8,70	-3,25	-12,56	-13,80
7	49,10	56,39	55,35 m	55,76	55,77	14,86	12,73	13,57	13,58
8	54,00	52,29	52,69 m	52,50	52,36	-3,17	-2,43	-2,78	-3,03
9	40,20	46,73	49,18 m	47,65	47,34	16,24	22,34	18,52	17,75
10	34,90	36,12	37,00 m	36,38	36,24	3,48	6,02	4,24	3,83
11	27,40	24,95	25,48 m	25,18	25,11	-8,93	-7,01	-8,12	-8,34
12	21,50	18,98	18,78	18,88	19,02	-11,72	-12,65	-12,19	-11,53
13	16,10	17,31	17,90 m	17,62	17,62	7,50	11,18	9,43	9,43
14	12,90	12,63	12,84 m	12,84	12,78	-2,11	-0,47	-0,50	-0,93

Table 5.8: Malpasset dam break - free surfaces comparison [m]

	nature	Kinetic 1	Kinetic 2	HLLC	WAF
A	100 s	71 s	62 s	67 s	66 s
B	1240 s	1389 s	1275 s	1396 s	1411 s
C	1420 s	1651 s	1500 s	1658 s	1653 s
sea	2160 s	2988 s	2728 s	2750 s	2753 s

Table 5.9: Malpasset dam-break - Wave arriving times

We can also compare the arriving times of the wave at the points where the voltage transformers are located. We consider that the water reaches a point when $h \geq 5cm$ (h = water depth). The results (see table 5.9) show a good agreement with the reality but the times are in general bigger. This can be caused by the parameter k_s that is uniform in all the domain and this is not realistic from a physical point of view.
Another comparison is related to the CPU times (see table 5.10) and we remark that between the WAF and the Kinetic 2, both second order accuracy scheme, the CPU for the WAF is more interesting that that for the Kinetic 2 scheme. The time for the first order accuracy scheme are similar.

	Kinetic 1	Kinetic 2	HLLC	WAF
CPU time	55 s	1 min 56 s	46 s	1 min 8 s

Table 5.10: Malpasset dam-break - CPU times

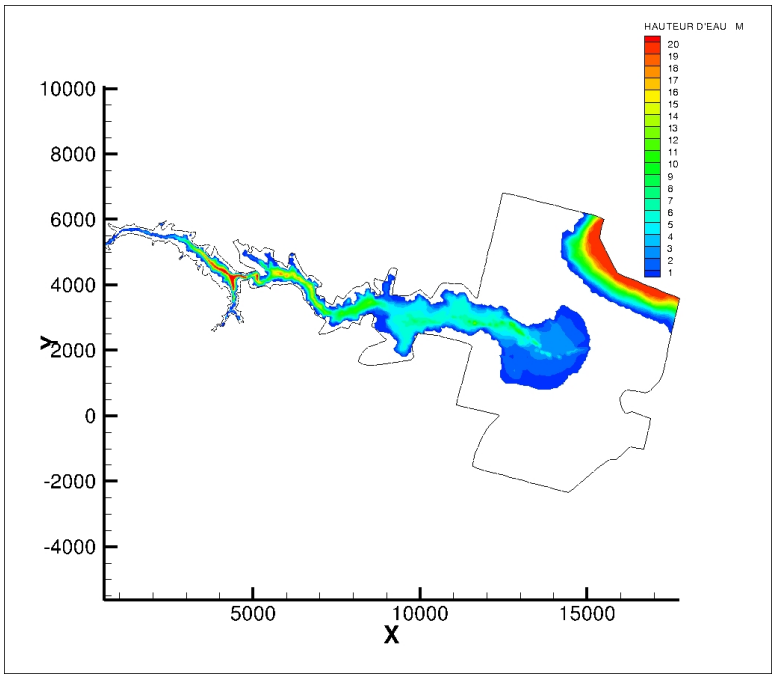

(a) t=2344 s

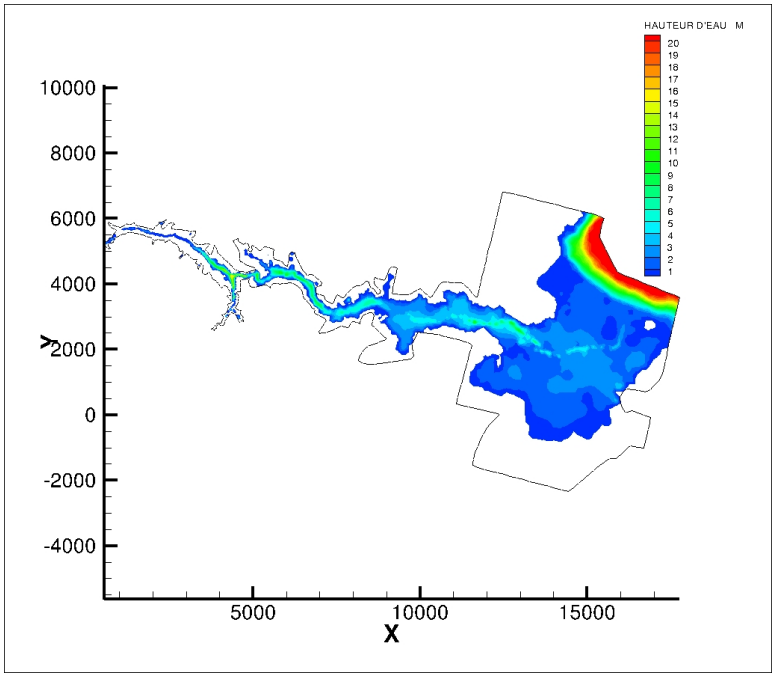

(b) t=4000 s

Figure 5.23: Malpasset dam-break - First order kinetic scheme

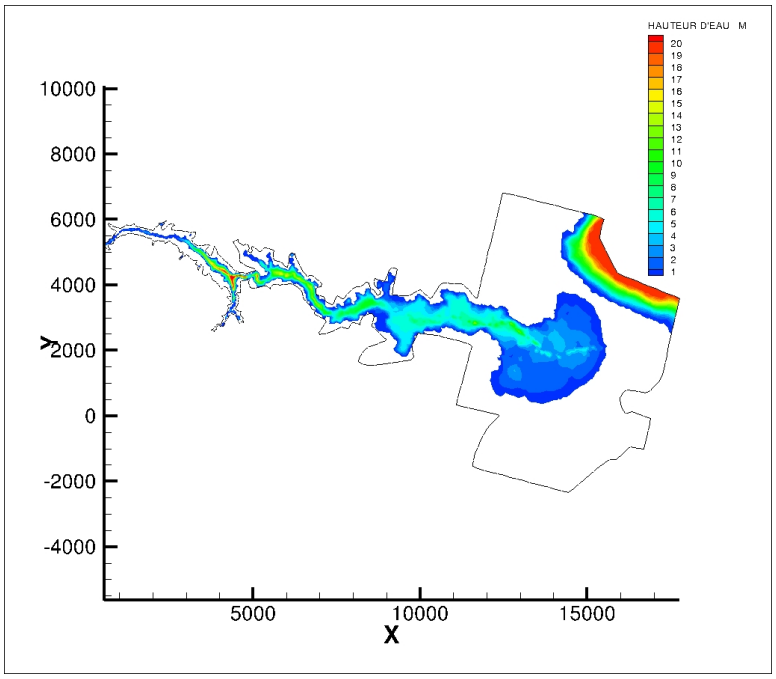

(a) t=2352 s

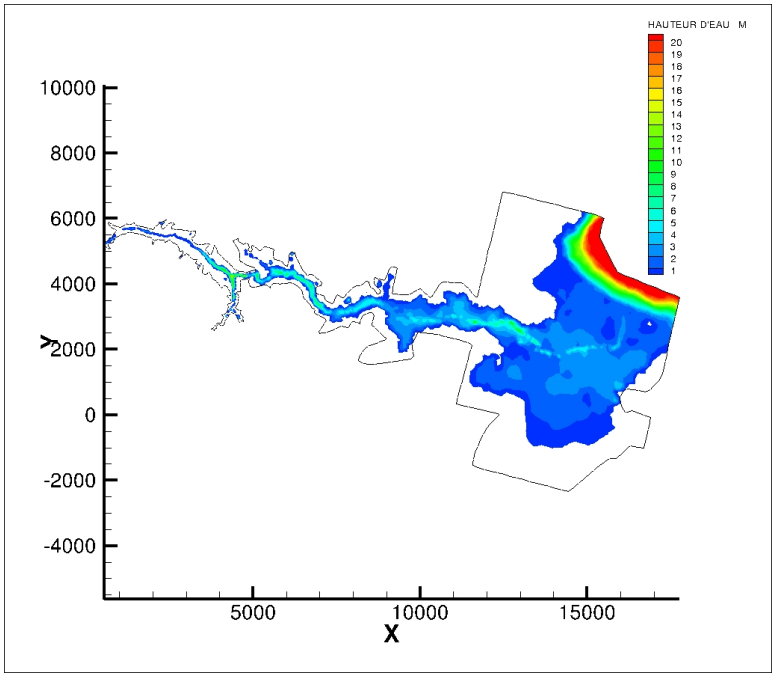

(b) t=4000 s

Figure 5.24: Malpasset dam-break - Second order kinetic scheme

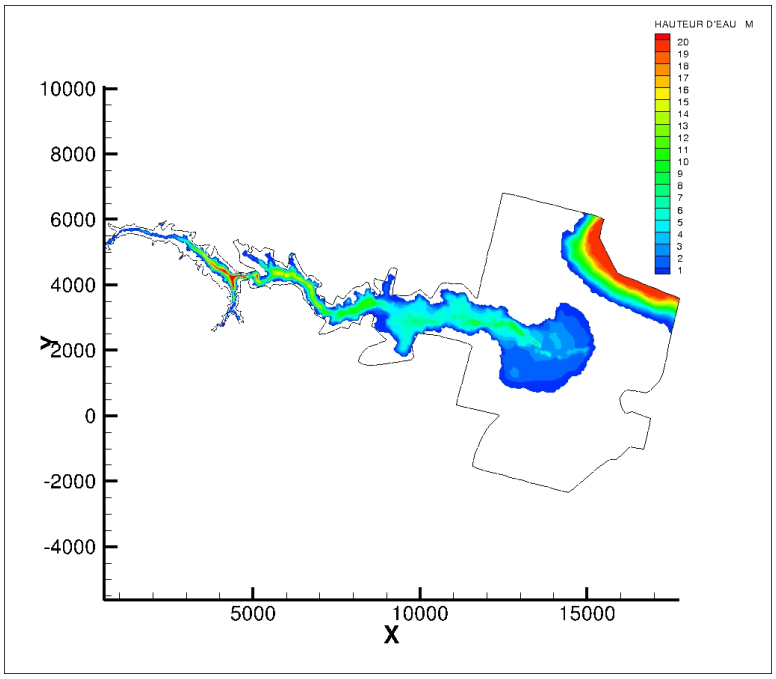

(a) t=2452 s

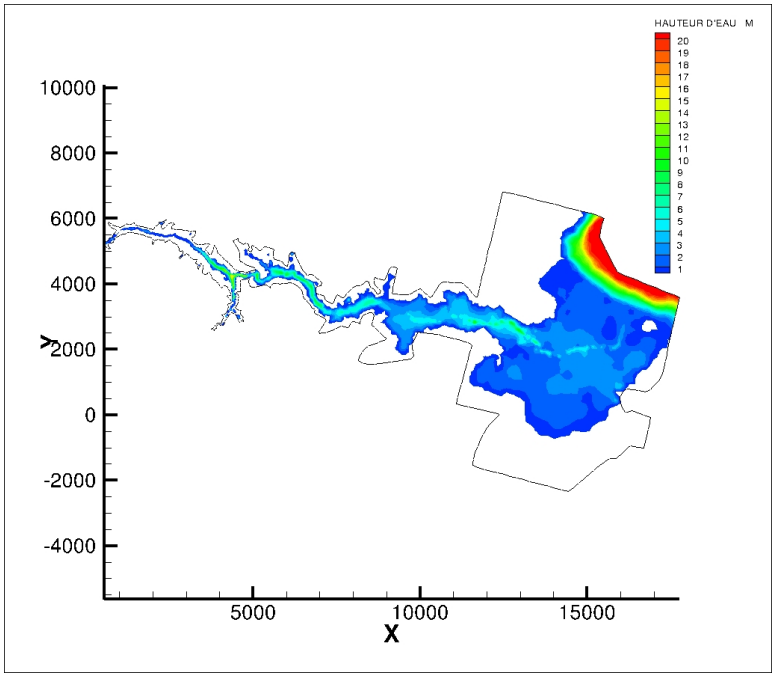

(b) t=4000 s

Figure 5.25: Malpasset dam-break - HLLC scheme

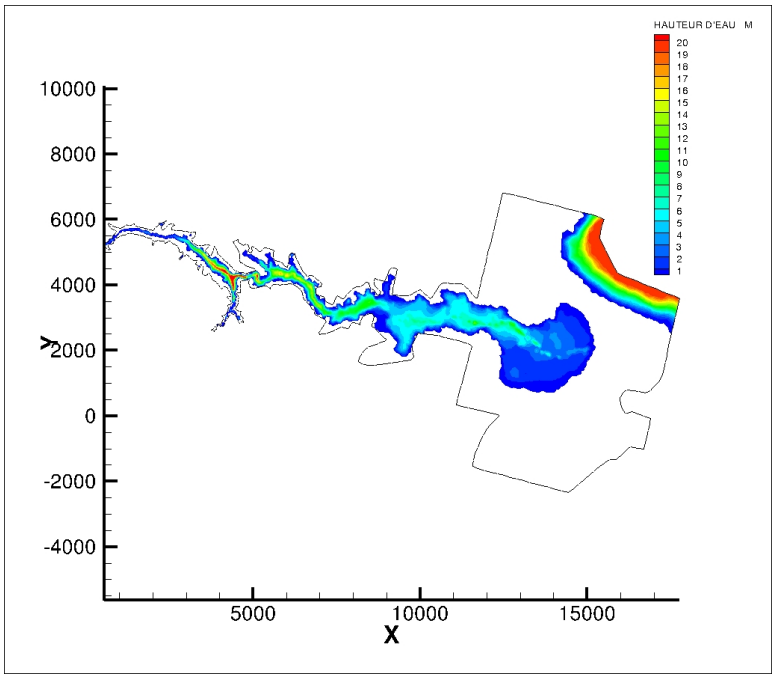

(a) t=2425 s

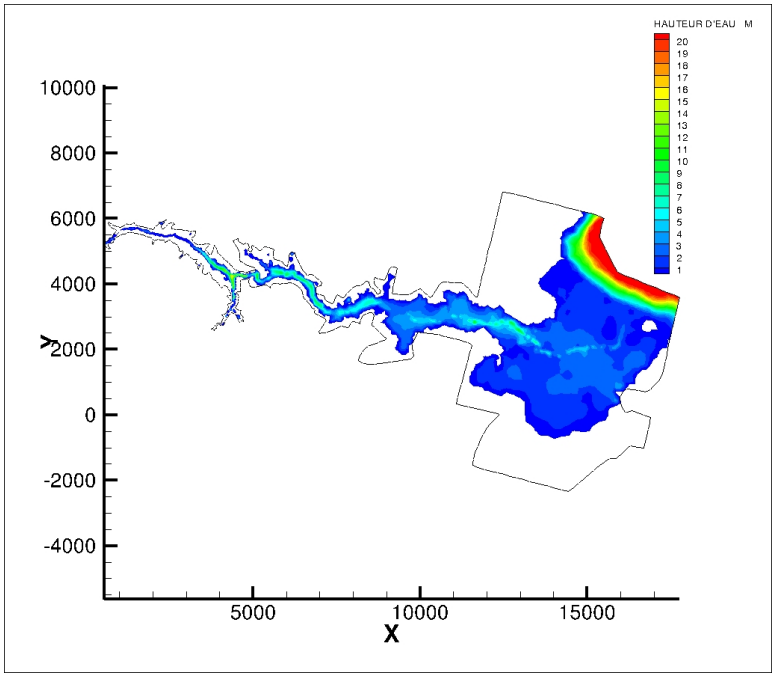

(b) t=4000 s

Figure 5.26: Malpasset dam-break - WAF scheme

Chapter 6

Conclusion

In this work we have demonstrated that finite volumes methods are very suitable and efficient to solve the Saint Venant equations. Indeed, this family of numerical method allows to capture the shocks at the correct speed without major computational efforts. Besides, applying a good discretization of the source term, as for the hydrostatic reconstruction, we can obtain well-balanced schemes. This means that the scheme is able, among the others, to reproduce steady states. Indeed it guarantees the mass conservation, the non-negativity of the water depth, the capability to retrieve dry states (where $h = 0$) and also to compute transcritical flows. The fulfillment of these properties permits to simulate real cases characterized by very complex and irregular topographies.

An indeed comparison of the finite volume schemes of Telemac-2D shows the capacity of each scheme in terms of shock-capturing and well-balanceness. Moreover an assessment of their accuracy and their needs in CPU times was achieved.
The tests presented in chapter 5 show that the WAF scheme is the most efficient, because it reproduces excellent solutions for all cases. Thanks to its second order accuracy in time and in space, the numerical diffusion is muffled near shocks. In addition, if we compare it with the second order kinetic scheme, we note that the CPU time is lower for the WAF scheme.
The WAF scheme demonstrates its robustness also in facing wet/dry problems, as the Balzano test presented in section 5.4. For this case, we point out the stability and the positivity of the water depth, that are instead critical points for the other models.
However we obtained satisfying results also for the HLLC scheme, that is a first order scheme, so less accurate than the WAF scheme.

As regards the Zokagoa and Tchamenn schemes, they reproduce good solutions but not especially for the real case and the Balzano problem. This shows that they need specific tricks for the wet/dry passages, but at the same time they present the advantage to not demand a specific source term treatment.
As regards the source term treatment, it will be desirable to apply the DFB with the flux correction proposed by Caleffi, moreover to test the conservation of the total force during the hydraulic jump.
Application of WAF scheme with tracers can be the subject of future works, indeed the numerical treatment of tracers is similar to the y-component of the velocity.
From the computational point of view the schemes presented are efficient and robust, so this finite volume kernel could be parellelized in order to simulate big real cases.

Bibliography

[1] Ata R., Goutal N., Zaoui F.. "Evaluation des performance des schemas cinetiques du code Telemac-2D". EDF internal report. H-P73-2010-00449-FR.

[2] Ata R., Soulaimani A., Chinesta F.. "The natural volume method (NVM) : Presentation and application to shallow water inviscid flows" (2009). *Int. J. Numer. Method. Fluids* (59) 19–45.

[3] Ata R., Toro E.F., Pavan S.. "WAF approximation for shallow water equations with friction and real topography". Submitted.

[4] Audusse E., Bristeau M.O., "A well balanced positivity preserving second order scheme for shallow water flows on unstructured meshes" (2005). *J. Comput. Physics* (206)311-333.

[5] Audusse E., Bristeau M.O.. "A fast and stable well-balanced scheme with hydrostatic reconstruction for shallow water flows"(2004). *SIAM J. Sci.Comput.*, Vol.25, no.6,2050-2065.

[6] Bermudez A., Vazquez M.E.. "Upwind methods for hyperbolic conservation laws with source terms". *Comput. Fluids*, 23:1043-1071, 1994.

[7] Billett S. J., Toro E. F.. "WAF-Type Schemes for Multidimensional Hyperbolic Conservation Laws"(1995).*J. Comput. Physics* Vol.130:1-24.

[8] Brocchini M., Bernetti R., Mancinelli A. and Albertini G., An efficient solver for nearshore flows based on the WAF method, *Coastal Engineering* (2001) 43, p. 105-129.

[9] Caleffi V., Valiani A. "Well-balanced bottom discontinuities treatment for High-Order Shallow Water Equations WENO Scheme"(2009). *Jorunal of engineering mechanichs*,135:7(684).

[10] Friedrichs KO., Lewy H., Courant R.. "On the partial differential equations of mathematical physics". *IBM Journal*, 11:215-234, 1967.

[11] Garcia-Navarro P., Vazquez M.E. "On numerical treatment of the source terms in shallow water equations". *Comput. Fluids*, 29:951-979,2000.

[12] Kemm F., A comparative study of TVD-limiters well-known limiters.

[13] Kumar Gurram S., Karki K.S., Hager W.H. (1997). "Subcritical junction flow". *Journal of Hydraulic Engineering*, May 1997, 447-455.

[14] Lax P.D. and Wendroff B.. "Systems of conservation laws". *Comm. Pure Appl. Math.*, 13:217-237, 1960.

[15] LeVeque R.J. "Balancing source terms and flux gradients in high-resolution methods: The quasi-steady wave-propagation algorithms". *J. Comp. Physics*,146:346-365, 1998.

[16] LeVeque R.J. *Finite Volume Methods for Hyperbolic Problems*. Cambridge texts in applied mathematics (2002).

[17] Loukili Y., Soulaimani A.. "Numerical tracking of shallow water waves by the unstructured finite volume WAF approximation (2007)". *Int. J. Comp. Meth. Engng. Scien. Mech.*(8)1-14.

[18] Ritter A. "Die fortpflanzung der wasserwellen". *Zeitshrift des Vereins Deutscher Ingenieure*,36:947-954, 1892.

[19] Stoker J.J. *Water Waves: The Mathematical Theory with Applications*. Interscience, London, 1957.

[20] Tchamen G.W. "L'utilisation des schemas de Riemann pour la solution des equations de Navier Stokes". Ecole Polytechnique de Montreal, Montreal, 2006.

[21] Toro Eleuterio F. *Shock-Capturing Methods for Free-Surface Shallow Flows*. John Wiley & sons, LTD, 2001.

[22] Toro E. F. *Riemann Solvers and Numerical Methods for Fluid Dynamics:A Practical Introduction. Third edition*. Berlin, Heidelberg:Springer Verlag,2009.

[23] Toro E. F. A Weighted Average Flux Method for Hyperbolic Conservation Laws (1989). Proc. Roy. Soc. London, (423) 401-418.

[24] Valiani A., and Begnudelli L. (2006). "Divergence Form for Bed Slope Source Term in Shallow Water Equations." *J.Hydraul.Eng.*,132:7(652).

[25] TELEMAC modelling system, Validation Document. 2D Hydrodynamics Telemac-2D Software Version 6.0.

[26] Zhou et all. "The Surface Gradient Method for the Treatment of Source Terms in the Shallow-Water Equations".*J. Comput. Physics*,168,1-25 (2001).

[27] Zokagoa J.M., Soulaimani A. "Modeling of wetting-drying transition in free surface flows over complex topographies." *Computer Methods in Applied Mechanics and Engineering* 199 (2010) 2281-2304.

[28] Methode des Volumes Finis pour les ecoulements compressibles. Arts et Metiers ParisTech.

[29] http://www.opentelemac.org/